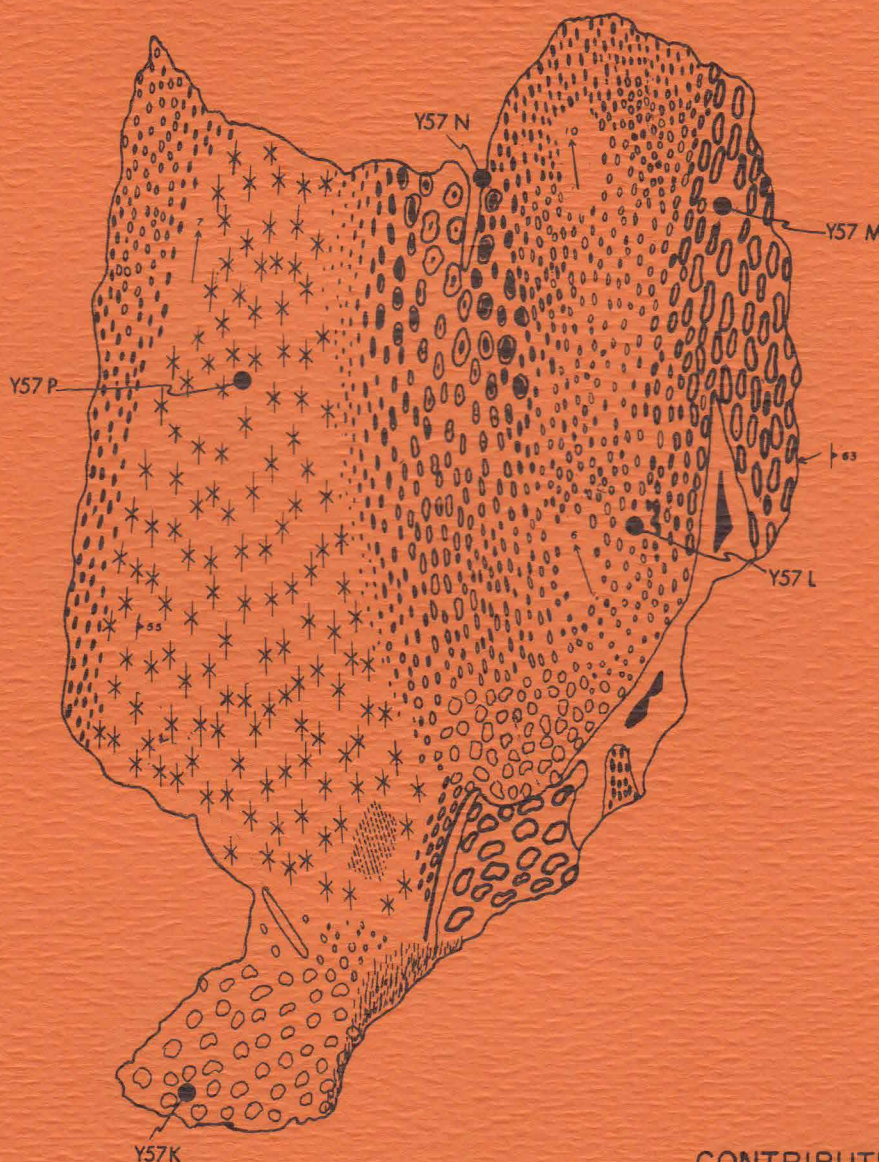


# ULTRAMAFIC LENSES IN THE MIDDLE ORDOVICIAN PARTRIDGE FORMATION, BRONSON HILL ANTICLINORIUM CENTRAL MASSACHUSETTS

BY ROBERT A. WOLFF



CONTRIBUTION NO. 34  
DEPARTMENT OF GEOLOGY & GEOGRAPHY  
UNIVERSITY OF MASSACHUSETTS  
AMHERST, MASSACHUSETTS

ULTRAMAFIC LENSES IN THE MIDDLE ORDOVICIAN PARTRIDGE FORMATION  
BRONSON HILL ANTICLINORIUM, CENTRAL MASSACHUSETTS

By

Robert A. Wolff

Contribution No. 34

Department of Geology and Geography

University of Massachusetts

Amherst, Massachusetts

December 1978



## TABLE OF CONTENTS

	Page
ABSTRACT . . . . .	1
INTRODUCTION . . . . .	3
Location and Geologic Setting . . . . .	3
Previous Work . . . . .	6
Purpose of Study. . . . .	7
Field Methods . . . . .	7
Laboratory Methods. . . . .	8
Microscopy . . . . .	8
X-ray diffraction. . . . .	9
Mineral separations. . . . .	9
Electron microprobe analyses . . . . .	9
Acknowledgments . . . . .	10
DESCRIPTIVE GEOLOGY OF ULTRAMAFIC LENSES AND SURROUNDING ROCKS. . . . .	12
Structural Setting and Regional History . . . . .	12
Geology of Ultramafic Lenses. . . . .	16
Y57 . . . . .	16
B65 . . . . .	20
500 . . . . .	21
018 . . . . .	26
N01/9Q9 . . . . .	28
OG2B . . . . .	35
5A5 . . . . .	36
Q222 . . . . .	38
K28 . . . . .	38



K34 . . . . .	46
J98 . . . . .	47
N45 . . . . .	53
DESCRIPTIVE PETROGRAPHY . . . . .	54
Orthopyroxene-Olivine Hornblendite . . . . .	54
Hybridized Ultramafic Rocks . . . . .	60
Two-amphibole rocks . . . . .	60
Plagioclase-bearing rocks . . . . .	61
Garnetiferous rocks . . . . .	61
Biotite rocks . . . . .	62
Retrograded Rocks . . . . .	63
Adjacent Country Rocks . . . . .	64
MINERALOGY . . . . .	65
Hornblende . . . . .	65
Cumingtonite . . . . .	79
Anthophyllite . . . . .	82
Orthopyroxene . . . . .	88
Olivine . . . . .	94
Spinel . . . . .	100
Chlorite . . . . .	110
Phlogopite and Biotite . . . . .	115
Plagioclase . . . . .	117
Garnet . . . . .	120
Serpentine . . . . .	121
Carbonate . . . . .	121
Ilmenite . . . . .	121
Graphite . . . . .	122
Sulfides . . . . .	123

Rutile and Sphene . . . . .	127
EMPLACEMENT OF BODIES. . . . .	128
Contact Data. . . . .	128
Bulk Chemistry. . . . .	130
Ultramafic lava flows. . . . .	130
Contact metamorphosed metasomatic margins of serpentinites . . . . .	134
METAMORPHISM . . . . .	139
Interrelationship Between Bulk Chemistry and Mineralogy . . . . .	139
Metamorphic Conditions. . . . .	142
Chlorite breakdown . . . . .	142
Aluminum content of orthopyroxene. . . . .	150
Hypothetical application of garnet composition to estimate minimum pressure . . . . .	152
SUMMARY. . . . .	154
REFERENCES . . . . .	156
APPENDIX 1 . . . . .	160
APPENDIX 2 . . . . .	162

## FIGURES

## Page

1. Generalized regional geologic map showing locations of ultramafic lenses within the Partridge Formation . . . . .	4
2. Generalized geologic map of north-central Massachusetts showing zones of metamorphic mineral assemblages and ultramafic lenses . . . . .	14
3. Equal area projection of structural features at locality Y57 . . . . .	20
4. Sketch map of locality B65 . . . . .	21
5. Outcrop map of locality 500 . . . . .	22
6. Equal area projection of structural features at locality 500 . . . . .	25
7. Sketch of easternmost outcrop at locality 018 . . . . .	27
8. Equal area projection of structural features at locality 018 . . . . .	28
9. Equal area projections of structural features at locality N01/9Q9 . . . . .	34
10. Outcrop map of locality 5A5 . . . . .	37
11. Sketch map of locality Q222 . . . . .	39
12. Outcrop map of locality K28N . . . . .	40
13. Outcrop map of locality K28S . . . . .	42
14. Equal area projection of structural features at localities K28N and K28S . . . . .	45
15. Outcrop map of locality K34 . . . . .	48
16. Equal area projection of structural features at locality K34 . . . . .	47
17. Outcrop map of locality J98 . . . . .	50
18. Equal area projection of structural features at locality J98 . . . . .	51
19. Modal analyses of Opx-Ol hornblendites plotted in terms of Ol, Opx, and Hb . . . . .	55
20. Orthopyroxene megacryst; specimen Y57I . . . . .	56
21. Sketch of orthopyroxene-olivine hornblendite showing mineral lineation; specimen Q222 . . . . .	57

22. Orthopyroxene megacryst and pargasite; specimen Y57I . . . . .	57
23. Sketch of specimen Y57I showing distribution of orthopyroxene megacrysts . . . . .	59
24. Orthopyroxene megacryst in pitted nodule; specimen Y57N . . . . .	59
25. Garnet-bearing hornblendite; specimen K34A . . . . .	62
26. Retrograded hornblendite; specimen Y57H . . . . .	63
27. A-site occupancy vs. tetrahedral Al plot of hornblende formulae . . .	70
28. ACF plot of amphiboles, garnet, and plagioclase . . . . .	78
29. A-site occupancy vs. tetrahedral Al plot of anthophyllite formulae . .	84
30. Tetrahedral Al vs. (Fe/Fe+Mg) plot of anthophyllite formulae . . . . .	85
31. Actinolite-hornblende-anthophyllite-gedrite ternary reciprocal system showing coexisting hornblende and anthophyllite . . . . .	87
32. Orthopyroxene analyses plotted in terms of Si, (Al+Cr+Fe <sup>3+</sup> ), and (Mg+Fe <sup>2+</sup> +Mn+Ca) . . . . .	94
33. Forsterite-fayalite-enstatite-ferrosilite ternary reciprocal diagram showing coexisting olivine and orthopyroxene . . . . .	100
34. Spinel analyses plotted in terms of Cr <sup>3+</sup> , Al <sup>3+</sup> , and (Fe <sup>3+</sup> +2Ti <sup>4+</sup> ) . .	108
35. Selected faces of spinel composition prism . . . . .	109
36. Chlorite analyses plotted in terms of Si, (Mg+Fe <sup>2+</sup> +Mn+Ca-Ti), and (Al+Cr+2Ti-Na-K) . . . . .	114
37. Chlorite analyses plotted in terms of Si, Mg, and (Fe+Mn). . . . .	114
38. Garnet analyses plotted in terms of Ca, Mg, and (Fe+Mn). . . . .	120
39. Ilmenite and magnetite compositions plotted in terms of TiO <sub>2</sub> , (MgO+MnO), and (Fe <sub>2</sub> O <sub>3</sub> +Cr <sub>2</sub> O <sub>3</sub> ) . . . . .	123
40. Sketch of ilmenite containing rutile inclusion . . . . .	127
41. Bulk compositions plotted in terms of A, (Al <sub>2</sub> O <sub>3</sub> -Na <sub>2</sub> O-K <sub>2</sub> O), CaO, (FeO+MnO+MgO), and B, SiO <sub>2</sub> , Al <sub>2</sub> O <sub>3</sub> , (FeO+MnO+MgO) . . . . .	132
42. Pargasite, anthophyllite, and garnet from specimen K34A plotted in terms of (Al <sub>2</sub> O <sub>3</sub> -CaO-Na <sub>2</sub> O), MgO, and (FeO+MnO) . . . . .	141
43. Chlorite breakdown assemblage plotted in terms of A; Si, (Al+Cr+2Ti-Na-K), (Mg+Fe <sup>2+</sup> +Mn+Ni+Ca-Ti), and B; Al <sub>2</sub> O <sub>3</sub> , MgO, (FeO+MnO). . . . .	144



44. Invariant point and univariant curves showing breakdown reaction of magnesian chlorite . . . . .	146
45. Effects on the reaction $Fo + Cord = En + Sp$ by A; substitution for Mg and B; substitution of Cr for Al . . . . .	146
46. T-X diagram showing effects of Fe substitution on chlorite breakdown . . . . .	148
47. Position of chlorite breakdown in P-T space . . . . .	148
48. $Al_2O_3$ isopleths of enstatite . . . . .	150
49. Sillimanite projection of the reaction: $Gar = Opx + Sp + Sill$ onto the $SiO_2$ - $MgAl_2O_4$ - $FeAl_2O_4$ plane in the $SiO_2$ - $Al_2O_3$ - $FeO$ - $MgO$ tetrahedron . . . . .	153

## PLATES

In pocket

1. Outcrop map of locality Y57I
2. Outcrop map of locality 018
3. Outcrop map of locality 9Q9/N01

## TABLES

	Page
1. Modal analyses and descriptions of samples from locality Y57 . . . . .	18
2. Estimated modes of ultramafic rock at locality B65 . . . . .	21
3. Estimated modes and sample descriptions from locality 500 . . . . .	24
4. Estimated modes and sample descriptions from locality 018 . . . . .	27
5. Estimated modes and sample descriptions from locality N01 . . . . .	30
6. Modal analyses and descriptions of samples from locality 9Q9 . . . . .	31
7. Point counted mode of specimen OG2B . . . . .	36
8. Estimated mode of specimen 5A5B . . . . .	36
9. Estimated mode of specimen Q222 . . . . .	38
10. Estimated modes and descriptions of samples from localities K28N and K28S . . . . .	44
11. Point counted mode of specimen K34A . . . . .	46
12. Estimated modes and descriptions of samples from locality J98 . . . . .	52
13. Point counted mode of specimen N45A . . . . .	53
14. Optical properties of pargasites and hornblende . . . . .	65
15. Electron probe and wet chemical analysis of pargasitic hornblende . . . . .	67
16. Optical properties of cummingtonite . . . . .	79
17. Electron probe analyses of cummingtonite and anthophyllite . . . . .	80
18. Optical properties of anthophyllite . . . . .	83
19. Optical properties of orthopyroxene . . . . .	88
20. Electron probe and wet chemical analyses of orthopyroxene . . . . .	90
21. Optical properties of olivine . . . . .	95
22. Electron probe analyses of olivine . . . . .	96
23. Electron probe analyses of aluminous spinels and magnetite . . . . .	102
24. Electron probe analyses of chromian spinels and chrome magnetite . . . . .	106

25.	Optical properties of chlorite . . . . .	111
26.	Electron microprobe analyses of chlorite . . . . .	113
27.	Electron microprobe analyses of phlogopite . . . . .	116
28.	Optical properties of plagioclase . . . . .	117
29.	Electron microprobe analyses of plagioclase, garnet, and serpentine	118
30.	Reflected light properties of ilmenite . . . . .	122
31.	Electron probe analyses of ilmenite and sphere . . . . .	124
32.	Reflected light properties of pyrrhotite . . . . .	126
33.	Bulk chemical analyses of orthopyroxene-olivine hornblendites and a hybridized ultramafic rock . . . . .	131
34.	Bulk compositions of selected ultramafic rocks from central Massachusetts and of four classes of komatiite . . . . .	135
35.	Bulk compositions of ultramafic rocks from central Massachusetts and New South Wales, Australia . . . . .	137
A-1	Bulk compositions determined by calculations and X-ray diffraction .	161
A-2	Calculation of $X_{Mg}$ for chlorite breakdown products . . . . .	163

## ABSTRACT

A small number of ultramafic lenses are disposed within a narrow stratigraphic horizon of the Middle Ordovician Partridge Formation, within the Bronson Hill Anticlinorium, in central Massachusetts. Geologic maps of 12 of these lenses have been constructed. There are very few exposed contacts and many of the maps are based upon mineralogical and textural variations across individual outcrops. All lenses lie within the sulfidic schist member of the Partridge Formation, predominantly metamorphosed marine black shale; except one lens that is within the augen gneiss member. Amphibolites derived from mafic lavas and tuffs are very common in the vicinity of the ultramafic rocks. Mica schists adjacent to the lenses contain assemblages typical of the sillimanite-staurolite through sillimanite-orthoclase zones.

The primary, prograde metamorphic assemblage of the ultramafic rocks: pargasite-orthopyroxene (Fs.<sub>20-26</sub>)-olivine (Fa.<sub>24-29</sub>)-spinel-chlorite ( $X_{Fe}$ .<sub>11-15</sub>)-ilmenite, is believed to have formed during the Devonian Acadian Orogeny from a protolith of uncertain derivation. Little is known of the pre-Devonian history of these rocks because of limited available contact data. Anthophyllite- or cummingtonite-hornblende-( $\pm$ plagioclase) assemblages occur at the outer margins of some lenses, and one small body (K34) is made up of a pargasite-anthophyllite-garnet( $Alm_{50-52}Pyr_{36-38}Gro_9Spe_2$ )-plagioclase( $An_{96}$ ) rock. Such assemblages are thought to be hybridization products formed from ultramafic or adjacent country rocks which were chemically altered prior to regional metamorphism, most probably by low-temperature metasomatic processes. This idea is supported by bulk chemical analyses which show a hybridized rock, K34, to be enriched in Si, Al, Na, and K with respect to the orthopyroxene-olivine hornblendites. Many rocks show retrograde effects with development of secondary chlorite, talc, and carbonate.

No single hypothesis easily explains the origin of these ultramafic lenses. The possibility that they are dismembered ultramafic lava flows is remote, on the basis of comparison with bulk chemistries of komatiites. Bulk compositions and mineral assemblages of orthopyroxene-olivine hornblendites are comparable with minor portions of metasomatized serpentinites in New South Wales, Australia, which, following metasomatism, were thermally metamorphosed by the intrusion of the Bogong Granite. Similar bulk compositions and assemblages are reported elsewhere but none in a regional setting comparable to central Massachusetts. A third, perhaps most plausible, hypothesis is that the ultramafic rocks of this study are "drop stones" from tectonically over-riding ultramafic masses, analogous to those in Newfoundland melange deposits, that may have been metasomatized subsequent to emplacement in their present setting of metamorphosed black shales.

Peak metamorphic conditions in the vicinity of these lenses during regional metamorphism have been estimated to range from 605-675°C at pressures between 5 and 7 kbars, on the basis of garnet-biotite equilibria (Tracy et al., 1976). Maximum possible temperatures within the ultramafic rocks in this pressure range were estimated to be between 730 and 765°C, in the presence of essentially pure H<sub>2</sub>O, on the basis of the experimentally explored reaction: chlorite = orthopyroxene+olivine+spinel+4H<sub>2</sub>O. The difference between this and the previous estimate is undoubtedly due to substantial reduction of a<sub>H<sub>2</sub>O</sub> in the natural situation. A temperature estimate of 650°C was derived from the Al<sub>2</sub>O<sub>3</sub> content of orthopyroxene(2.2-2.3 wt%) coexisting with olivine and spinel, which is broadly consistent with regional estimates in spite of impurities in the natural samples. The garnet composition in K34 can be used to estimate minimum pressure using garnet isopleths for the reaction: garnet = sillimanite + orthopyroxene + spinel, when such data become available.

## INTRODUCTION

### Location and Geologic Setting

A number of isolated, ultramafic lenses occurs within the Middle Ordovician Partridge Formation in north-central Massachusetts (Robinson, 1963). The Partridge Formation in this area consists predominantly of rusty-weathering, sulfidic and graphitic sillimanite-bearing schists and gneisses, and amphibolites. The schists represent metamorphosed marine shales and the amphibolites are interpreted as metamorphosed volcanics which locally make up more than half of the outcrops (Robinson, 1963, Thompson et al., 1968). The Partridge Formation constitutes a major part of the metamorphosed, Middle Ordovician sedimentary and volcanic rocks which unconformably mantle gneisses exposed in the en-echelon domes of the Bronson Hill Anticlinorium, a major structural feature extending from Long Island Sound to the Maine-New Hampshire boundary (Billings, 1956, Thompson et al., 1968).

Most of the lenses investigated are of one type and located within the sulfidic-schist member of the Partridge Formation (Robinson, 1963), along the eastern flank of the main body of Monson Gneiss in the vicinity of Orange, Massachusetts (Figure 1). The northernmost body, however, is located within the augen gneiss member of the Partridge Formation. The distance between the northernmost and southernmost outcrops is approximately 40 kilometers (Figure 1).

Individual lenses range in thickness from 3 meters to 60 meters and in exposed length from 3 meters to 210 meters. They appear to have behaved as relatively competent boudins within more plastic surrounding





Mesozoic sedimentary and volcanic rocks



Devonian intrusive rocks



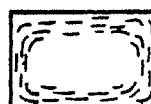
Lower Devonian Littleton and Erving Formations



Silurian Clough and Fitch Formations

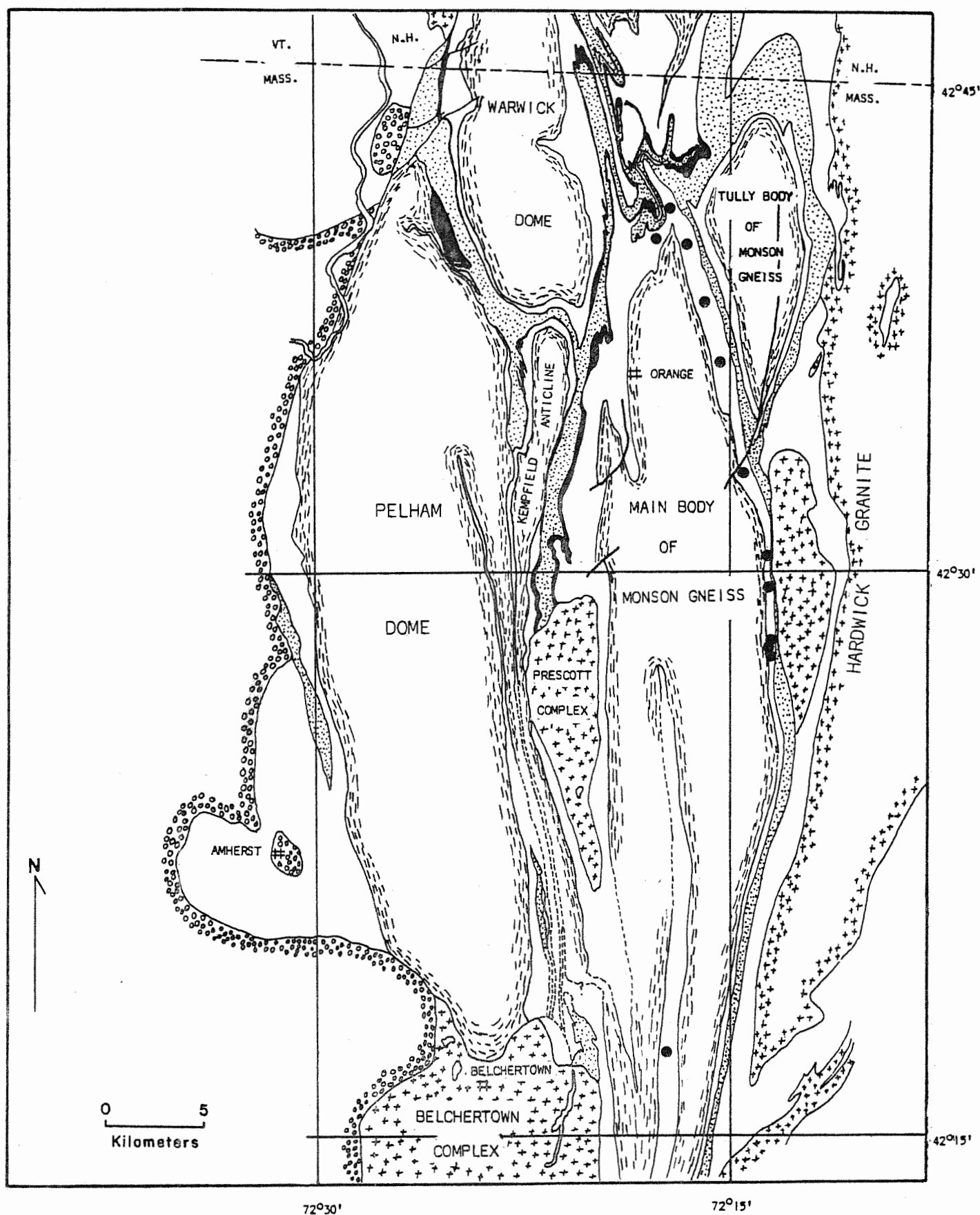


Middle Ordovician Ammonoosuc Volcanics and  
Partridge Formation. Ultramafic lenses indicated.



Gneisses exposed in cores of domes. Late  
Precambrian or uncertain age.

Figure 1. Generalized regional geologic map showing locations of ultramafic lenses occurring within the Middle Ordovician Partridge Formation. Map modified from Robinson (1967).



schist and amphibolite. Contact relations are cryptic due to poor exposure, multi-stage deformation, and late stage alteration. Textural evidence in thin section suggests equilibration under metamorphic conditions. The primary prograde metamorphic assemblage of the predominant rock-type is pargasite, orthopyroxene, olivine, colorless Mg-chlorite, and spinel. Accessory ilmenite and sulfides are ubiquitous. Graphite has been observed in selected specimens. Assemblages involving various combinations of pargasite, orthoamphibole, plagioclase, phlogopite, garnet, and apatite occur near the contacts and may be the result of metasomatic processes involving silica contamination and/or hydration. Extensive retrograde metamorphism, commonly localized on fractures in some of these rocks, has resulted in the production of green chlorite, talc, carbonate, serpentine, and magnetite.

#### Previous Work

Most of the bodies investigated have been located and discussed by Robinson (1963, 1967), who provided descriptions, locations, and estimated modes of many ultramafic rocks as well as the first reference to the spinel-bearing assemblage in this area. H.W. Jaffe carried out the initial detailed optical study of a sample from locality OG2 (sample OG2B) which, at the time, was the only known ultramafic body in the area containing the assemblage, pargasite-orthopyroxene-olivine-spinel-chlorite-ilmenite. Jaffe also prepared purified mineral separates of pargasite and orthopyroxene from this sample for wet chemical analyses. Wet chemical analyses were done by Mahito Kumanomido of the Japan Analytical Chemistry Research Institute. Initial electron microprobe analyses of primary and secondary phases from sample OG2B were performed by A.E. Bence of the State University of New York at Stony Brook at the request of Peter Robinson. Brown and Prewitt (1973) have refined the

structure and determined the site occupancy of Fe and Mg for an olivine crystal from sample OG2B using single crystal diffraction methods.

### Purpose of Study

A major objective of this study was to obtain detailed information on the size, shape, and internal variation of ultramafic lenses in the Partridge Formation in an attempt to delineate their mode and relative time of emplacement, and post-emplacement history. Particular attention was given to chemical information bearing on the primary origin of these bodies and on phase relations indicative of the pressure, temperature, and fluid activity under which they were metamorphosed.

Due to the number and variation in types of ultramafic rocks in north-central Massachusetts (Robinson, 1963, 1967), this study is restricted to those in the Partridge Formation (Fig. 1) on the basis of their proximity to each other and consistency in assemblage.

### Field Methods

The locations of most of the bodies were provided by Professor Robinson. Field work was carried out during the summers of 1973 and 1974. Detailed mapping of selected outcrops was accomplished by tape and compass. Where possible, a base line was constructed across the outcrops so that contacts and outcrop boundaries could be more accurately established. Where prohibited by terrain, pacing substituted for direct measurement.

Initially, a base map was constructed representing a plan view of outcrop distribution. Structural and lithologic features were then added to complete the map. Map scales vary in accordance with the size of the bodies and the amount of detail desired. Both mineralogical and textural criteria were employed to distinguish rock units and/or domains.

within each outcrop. The significance of textural distinctions is based upon the assumption that external morphology is a reflection of the mineralogy within a particular domain. Features include nodules, pits, foliation, and lineation. Magnetic susceptibility, determined with a pencil magnet, was a useful distinction due to the association of magnetite with partially serpentinized olivine. Planar and linear elements were measured with a Brunton Compass at recorded stations on the outcrops.

### Laboratory Methods

Microscopy. The petrography of selected representative samples was done both with transmitted and reflected light microscopes.

Mineral assemblages, some optical properties, textural relations, and relative abundances of phases were determined in thin sections under transmitted light. Modes of some of the freshest samples were determined by standard point counting methods (Chayes, 1956) based on 2000 counts per specimen. In some cases, sections were cut slightly thick (40-50 microns) to enhance distinction between pink orthopyroxene and colorless olivine.

The oblique illumination method, using oil immersion mounts of selected fractions of crushed and sieved samples from two localities, was employed to determine indices of refraction of pargasite, orthoamphibole, plagioclase, and garnet. Fayalite content of olivines from four localities was determined using the dispersion method (Morse and Berg, 1971). Complete statistical data are not yet available which provide irrefutable precision and accuracy to estimates of these measurements. The statistics that are available indicate accuracy of at least  $\pm 2$  mole percent over the entire range of compositions with increasing accuracy toward the forsterite end member (S.A. Morse and J.H. Berg, pers. comm.).

A study of the opaque mineralogy was conducted by reflected light investigation of polished thin-sections and polished rock-chips using both air and oil-immersion objectives. Polished thin-sections are preferred because they may be studied in both reflected and transmitted light.

X-ray diffraction. X-ray powder patterns of magnetite and graphite were made using a 57.3 millimeter powder camera with  $\text{FeK}_{\alpha 1}$  radiation and a manganese filter. Exposure times varied from 6 to 7 hours at 45 kilovolts and 10 milliamps.

Mineral separations. Partial separation of minerals was necessary in order to concentrate phases chosen for x-ray analysis, dispersion work, and refractive index determination. For oil immersion and dispersion techniques, samples were crushed and sieved to the size fraction between 100 and 200 mesh. These fractions were purified with a hand magnet and then passed through the Frantz Isodynamic Separator. Various tilts angles and current intensities were used and produced sufficient concentrations of pargasite, orthoamphibole, plagioclase, olivine, and garnet for optical investigation. In two cases, the hand magnet alone was sufficient to separate olivine due to the presence of small amounts of magnetite within this mineral. Actual separation of magnetite for x-ray study was accomplished by pulverizing a hand-magnet separate of olivine in order to free the magnetite. Minute grains of magnetite were then hand picked. Graphite grains were physically plucked from a polished rock-chip with a sharpened pick.

Electron microprobe analyses. Specimens for microprobe analyses were selected on the basis of outcrop location, freshness, and mineral



assemblage. Analyses were done on an ARL electron probe microanalyzer at the State University of New York at Stony Brook by A.E. Bence and on a MAC model 400 electron probe microanalyzer at the Massachusetts Institute of Technology, Cambridge, by Robert J. Tracy. Corrections of Bence and Albee (1968) were applied to all analyses. Many of the grains probed were photographed to provide quick identification and a permanent record of phases analyzed.

### Acknowledgments

The following persons and organizations contributed to assist in the completion of this thesis: Prof. Peter Robinson suggested the topic and, as thesis committee chairman, provided superior guidance and stimulation for the duration of the study. Prof. Howard W. Jaffe did optical work and performed mineral separations for wet-chemical analyses of selected phases. Robert J. Tracy performed most of the microprobe analyses and contributed much in the way of advice and consultation. Prof. Stephen E. Haggerty assisted in the identification and interpretation of the opaque mineralogy. Prof. Stearns A. Morse provided data and advice necessary for the determination of olivine compositions by the dispersion method. Jonathan H. Berg answered a multitude of questions and provided a great deal of insight into many of the problems associated with this work. Prof. A.E. Bence from S.U.N.Y. at Stony Brook performed and made available initial electron microprobe analyses. Mike Rhodes, of the University of Massachusetts, performed chemical analyses. Linda Newman, of Martin Marietta Corporation, typed the text and tables and assisted in the preparation of diagrams and captions. My wife, Gail, endured throughout and contributed immeasurably to my mental and physical well-being. Charles E. Kane ("Charlie the Janitor")

went out of his way on numerous occasions to drive the author home after the last bus had passed. Field, laboratory, and publication expenses were defrayed by NSF Grants GA-33857 and GA-33857A1 (to Peter Robinson), by U.S. Geological Survey Grant G-400 (to Robinson), and by a Grant-in Aid of Research from Sigma Xi to R.A. Wolff. Preparation of purified separates of pargasite and orthopyroxene by Howard W. Jaffe and the wet chemical analyses were supported by NSF Grant GA-467 (to Jaffe and Robinson). Microprobe analyses were partially supported by NSF Grant GA-467 (to Jaffe and Robinson). Microprobe analyses were partially supported by NSF Grant GA-31989 (to Jaffe and Robinson).

## DESCRIPTIVE GEOLOGY OF ULTRAMAFIC LENSES AND SURROUNDING ROCKS

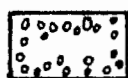
### Structural Setting and Regional History

The geology of the area shown in Figure 1 is characterized by a sequence of metamorphosed Ordovician, Silurian, and Devonian sedimentary and volcanic rocks overlying a series of gneisses of disputed origin and age which form the cores of domes and anticlines of the Bronson Hill Anticlinorium. The mantling Paleozoic sedimentary and volcanic units are correlated on the basis of tracing from fossil localities to the north (Robinson, 1967a). The gneisses and related rocks are more problematical. Rocks within the Pelham dome are believed to be early Cambrian or late Precambrian on the basis of a  $^{207}\text{Pb}/^{206}\text{Pb}$  date on zircon of  $575 \pm 30$  million years (Naylor et al., 1973). Preliminary isotopic studies by Naylor (1968) of similar rocks in New Hampshire suggest that the Monson Gneiss is Ordovician, possibly representing the lower part of the Ammonoosuc Volcanics (Thompson et al., 1968). Field relations in Massachusetts including a probable basal conglomerate in the Ammonoosuc Volcanics have led Robinson (1963; 1967; unpublished data) to suggest that Monson Gneiss is unconformably beneath and distinctly older than the Ammonoosuc Volcanics. None of the ultramafic rocks in this area lie within Silurian or younger rocks (Robinson, 1967a). The ultramafic rocks of this study, which lie within the Middle Ordovician Partridge Formation are thus, most probably, also Ordovician.

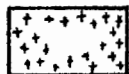
The deformational history of the area is characterized by the formation of regional nappe structures, local recumbent folding, and various stages of dome formation. The Paleozoic sedimentary and volcanic units were involved in the formation of three levels of regional nappes having east towards west overfolding and amplitudes up to 24 kilometers (Thompson et al., 1968). Subsequent recumbent folding involving all of the above units plus the dome gneisses resulted in a variety of features. An early phase of gneiss dome formation is seen in the main and Tully bodies of Monson Gneiss. The north end of the main body occurs as a south plunging syncline overlying an inverted sequence of younger units. This configuration appears to have been achieved by extreme northward and eastward overturning of the main and Tully bodies (Robinson, 1967a). This overturning folded the Clough and Littleton Formations on the upper limb of the nappe into an isoclinal syncline. The axial surface of this syncline has been refolded during the later, main phase of dome formation with which the predominant mineral lineation in this area is associated (Robinson, 1967a). Linear features in the western part of the area (Pelham dome) plunge gently northward while those in the east (main and Tully bodies of Monson Gneiss) plunge southward (Robinson, 1967a & b).

The most extensive metamorphism in this area is believed to have occurred in the Devonian Acadian orogeny, and was probably synchronous both with recumbent folding and dome formation. Metamorphic grade increases eastward from kyanite through sillimanite-orthoclase grade. The sillimanite zone has been subdivided into five zones, and the ultramafic rocks under consideration occur in four of them (Fig. 2). Based on phase relations in pelitic schists (Robinson, 1963; Tracy, 1975; Robinson, Tracy, and Ashwal, 1975), the temperature difference between zone II and zone V is believed to

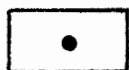
## ROCK TYPE



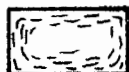
Mesozoic sedimentary and volcanic rocks



Paleozoic intrusive rocks



Ordovician through Devonian metamorphosed volcanic and sedimentary rocks. Showing ultramafic lenses.

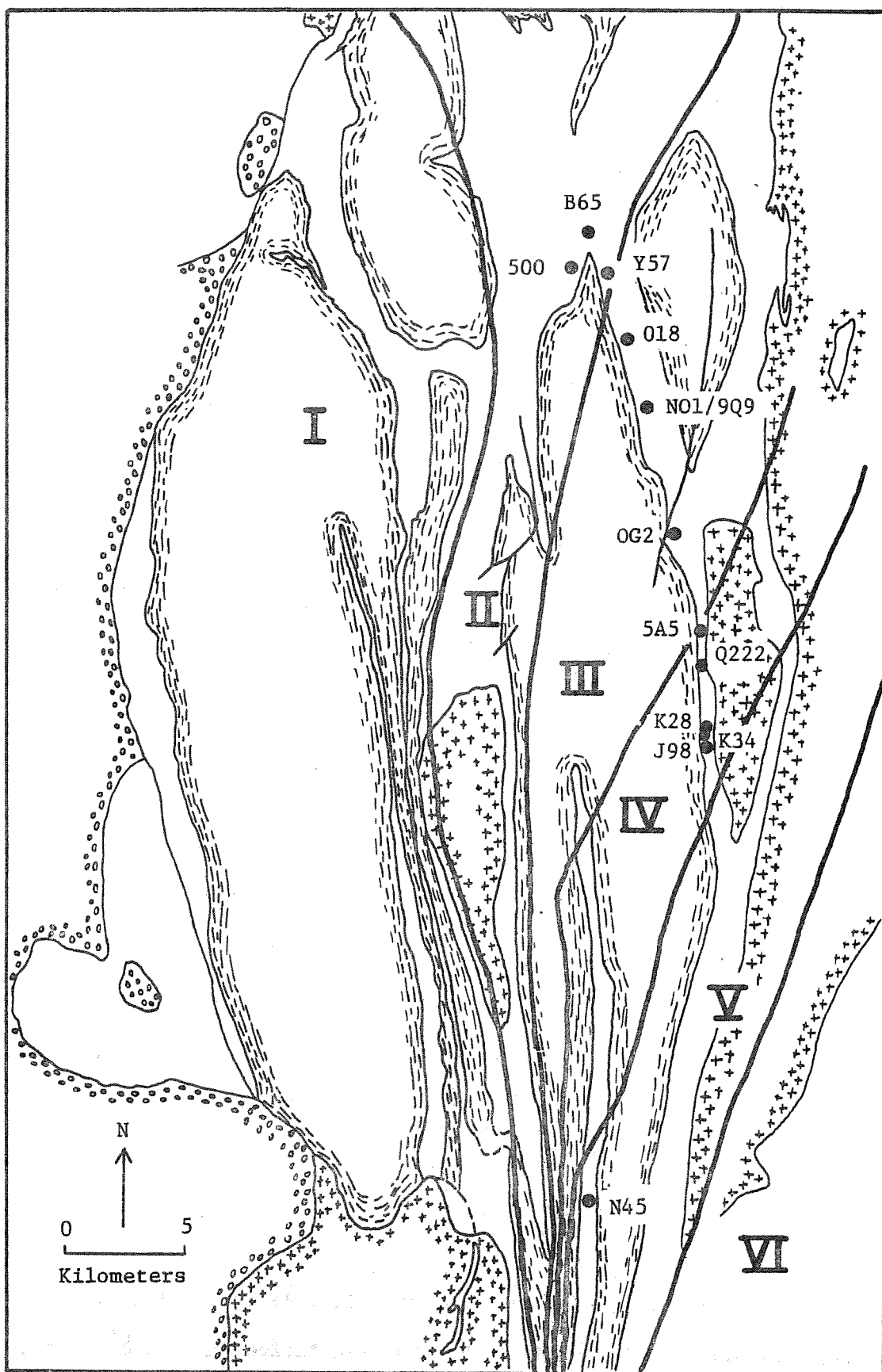


Gneisses and related rocks in cores of domes and anticlines. Late Precambrian and uncertain ages.

## METAMORPHIC ZONES

- I    Kyanite-muscovite-staurolite-garnet-biotite
- II   Sillimanite-muscovite-staurolite-garnet-biotite
- III   Sillimanite-muscovite-garnet-biotite
- IV   Sillimanite-muscovite-orthoclase-garnet-biotite
- V    Sillimanite-orthoclase-garnet-biotite
- VI   Sillimanite-orthoclase-cordierite-garnet-biotite

Figure 2. Generalized geologic map of north-central Massachusetts showing zones of metamorphic mineral assemblages in pelitic schists and location of ultramafic lenses. Location of boundaries from Peter Robinson and Robert J. Tracy, University of Massachusetts (pers. comm.); and Tracy (1975).





have been approximately 50°C at a pressure of 6 kilobars (Tracy, Robinson, and A.B. Thompson, 1976).

Localized, late-stage retrograde metamorphism, either in the waning stages of the Acadian orogeny or later in the Paleozoic, is associated with deformation of earlier-formed planar and linear features. Mesozoic brittle faulting and hydrothermal alteration are related to the Connecticut Valley Border Fault of Triassic-Jurassic age which lies near the west limb of the Bronson Hill Anticlinorium.

#### Geology of Ultramafic Lenses

Following are descriptions of the ultramafic lenses considered in this study. Maps accompany descriptions of those bodies with the best exposed contact relations and/or the most significant, mappable internal variations. The discussion will proceed from those bodies located in zone II to the north to those in zone V to the south (Fig. 2).

Y57. Y57 is located within the Mt. Grace, Massachusetts 7½-minute quadrangle. It lies on the west side of Temple Hill on the 1020' contour approximately 1.25 kilometers north-northwest of the intersection of North Orange and Poor Farm roads 150 meters west of the 1090' knob. The body consists primarily of three large outcrops which are spread over an area approximately 60 meters long and 25 meters wide (Plate 1). Although the edges of the lens are not exposed, the general shape of the outcrop is suggestive of two giant boudins. Contact relations at this locality are enigmatic. The overall color of the weathered outcrop surfaces is dark green.

Three major rock types occur at this locality: primary, hybridized, and retrograded ultramafic rock. Representative samples of each type

have been collected and are described in Table 1. Sample localities are shown on Plate 1. The primary metamorphic assemblage of the ultramafic rock at Y57 is pargasite-orthopyroxene-olivine-Mg-chlorite-spinel-ilmenite. Sulfides are common and graphite has been observed. Much of the northern outcrops is made up of primary ultramafic rock. The southern outcrop is characterized by retrograded rocks which contain secondary chlorite, talc, and carbonate. Small amounts of cummingtonite coexist with pargasite in five samples. Hybridized rocks, characterized by the presence of anorthophyllite, occur on the westernmost edge of the western of the two northern outcrops, and in a small rock about 80 meters to the north, which may be out of place. The most striking texture consists of coarse nodules (up to 3cm) which are pitted in the center. Thin sections show that these nodules are composed primarily of orthopyroxene. The pits probably formed as a result of the weathering out of olivine. Orthopyroxene and olivine, however, are not restricted to this particular textural type. Primary mineral associations range from rocks composed of a very high percentage of pargasite through various assemblages involving some or all of the primary metamorphic minerals (Table 1).

Structurally, the outcrop is characterized by a weak to moderate foliation and mineral lineation. The foliation strikes approximately north-south, dips steeply to the east or west, and is best developed in the southern, more altered outcrop. The mineral lineation is most commonly defined by pargasite plunging gently to the north (Fig. 3). These attitudes contrast with the local regional orientations of planar and linear structural features, as determined by Robinson (1963). The implication is that the ultramafic block or blocks at Y57 have undergone north-northwestward rotation by about 30 degrees during relatively late-stage boudinage.

Table 1. Modal analyses of samples from locality Y57.

Sample	E PC	F	G	H PC	I PC	J	K	L	M	N	O	P	Q	R
Pargasite	67.9	65	86	60.0	63.7	57	65	56	60	60	84	71	97	81
Cummingtonite				tr			tr	2	1				tr	
Anthophyllite						1				tr	7			
Orthopyroxene	23.8	27	2		10.0	36	tr		tr	30		5		8
Olivine	.6	1	2	10.4	7.5		tr		1	2		20		2
Spinel	6.8	6	7		3.9	2			tr	tr		2	tr	6
Chlorite (P)	.5	1	3	15.0	13.5	3	2	3	3	5	1	1		2
(S)		tr		7.8		tr	30	15	28	2	6		2	
Ilmenite	.4	tr	tr	1.2	.5	1	1	1	2	tr	tr	tr	1	1
Sulfides		tr	tr	.4	.9	tr	1	1	2	1	tr	1		tr
Magnetite										tr		tr		
Graphite					tr									
Phlogopite						tr					2			
Talc				5.2				22	3					
Carbonate				tr		tr	1							
Serpentine	tr									tr		tr		

Samples designated PC are point counted (2000 points). All others are estimated. Chlorite is broken down into primary (P), and secondary (S). Pyrrhotite is the most abundant sulfide. Pyrite and chalcopyrite occur in all samples in lower concentrations.

Descriptions of samples in Table 1. Locations of all samples are shown on Plate 1.

- Y57E: Dark-green, fine-grained, nonfoliated, weakly lineated orthopyroxene-olivine hornblendite. The lineation is defined by pargasite.
- Y57F: Dark-green, heteroblastic fine- to medium-grained, nonfoliated, well lineated orthopyroxene-olivine hornblendite. Orthopyroxene occurs as megacrysts ranging in size up to 8mm. The lineation is defined by pargasite.
- Y57G: Dark-gray, heteroblastic fine- to medium-grained, nonfoliated, weakly lineated orthopyroxene-olivine hornblendite. Fine pargasite defines the lineation; coarse pargasite occurs as megacrysts.
- Y57H: Gray, heteroblastic fine- to medium-grained, massive olivine-bearing hornblendite containing both primary and secondary chlorite. Secondary chlorite is distinguished by green color and replacement texture.
- Y57I: Medium-grained, massive orthopyroxene-olivine hornblendite. A trace of magnetite has been produced by serpentinization within expansion cracks in olivine.
- Y57J: Dark-green, medium-grained, massive orthopyroxene-bearing hornblendite. The rock is characterized by the presence of anthophyllite.
- Y57K: Gray, medium-grained, nonfoliated, weakly lineated chlorite-bearing hornblendite. Chlorite is in pale green pseudomorphs of orthopyroxene.
- Y57L: Light-gray, fine-grained, massive pargasite-rich rock containing large patches (1-2cm) of secondary talc and chlorite. Patches probably represent previous nodular orthopyroxene. Replacement of coarse, platy primary chlorite is also in evidence.
- Y57M: Dark-green, fine- to medium-grained, weakly foliated, well lineated orthopyroxene-olivine hornblendite characterized by numerous small patches of pale-green secondary chlorite; most with opaque centers. Replacement of primary by secondary chlorite is observed.
- Y57N: Dark-green, heteroblastic medium- to coarse-grained, massive orthopyroxene-olivine hornblendite characterized by nodules up to 2cm which are composed of orthopyroxene.
- Y57O: Dark-gray, fine- to medium-grained, massive anthophyllite-bearing hornblendite.
- Y57P: Dark-green, fine- to medium-grained, nonfoliated, well lineated orthopyroxene-olivine hornblendite.
- Y57Q: Dark-green, fine-grained, nonfoliated, well lineated hornblendite. A weak lineation is defined by trace amounts of brown cummingtonite.
- Y57R: Dark-green, heteroblastic fine- to medium-grained, massive orthopyroxene-olivine hornblendite.

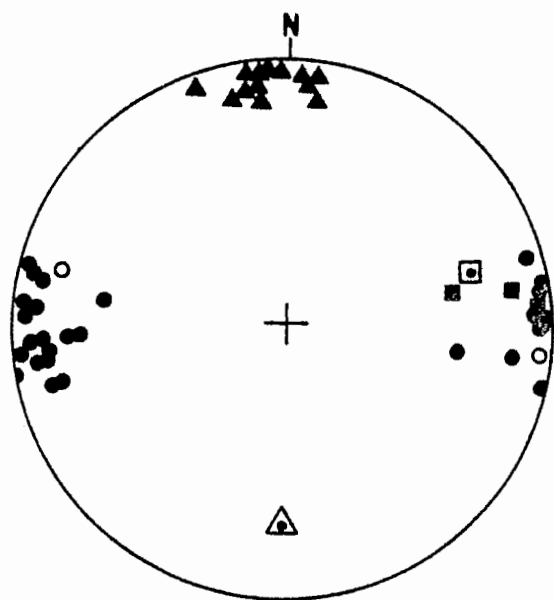


Figure 3. Lower hemisphere equal area projection of planar and linear elements at locality Y57. 27 poles to foliation of ultramafic rock (closed circles), 2 poles to foliation of amphibolite (open circles), 3 poles to foliation of sulfidic schist (squares), and 13 pargasite lineations within the ultramafic rock (triangles). Also shown are the approximate mean orientation of 110 foliation and 9 bedding measurements (open square with dot) and the approximate mean orientation of 49 mineral lineation and 19 minor fold axis measurements (open triangle with dot) taken from regional data (Sector 65) of Robinson (1963) in an area 7000 by 9000 feet surrounding the ultramafic body. In all cases, the mineral lineation and fold axes are those of the mainstage of gneiss dome formation in the region.

B65. B65 is located approximately 3.5 kilometers northwest of the village of North Orange, Massachusetts within the Mt. Grace 7½-minute quadrangle. It lies within the augen gneiss member of the Partridge Formation on the 930' contour 70 meters east of Johnsonian Pond, just north of the Worcester County line in an abandoned lumber mill (1973). The ultramafic rock is a brownish-green, homogeneous, massive pargasite-anthophyllite-orthopyroxene-spinel rock with accessory phlogopite, talc, ilmenite, and sulfides (Table 2). The body is approximately 5 meters in longest dimension and is bounded on the northeast by the augen gneiss (Fig. 4). The augen gneiss member consists of plagioclase, quartz, red-brown garnet, biotite, and muscovite. The ultramafic rock contains no measurable planar or linear features. The orientation of the foliation in the surrounding gneiss is conformable with regional foliation in this area.

Table 2. Estimated modes of ultramafic rock at locality B65.

Pargasite	93	Phlogopite	tr
Anthophyllite	2	Talc	tr
Orthopyroxene	3	Ilmenite	tr
Spinel	2	Sulfides	tr

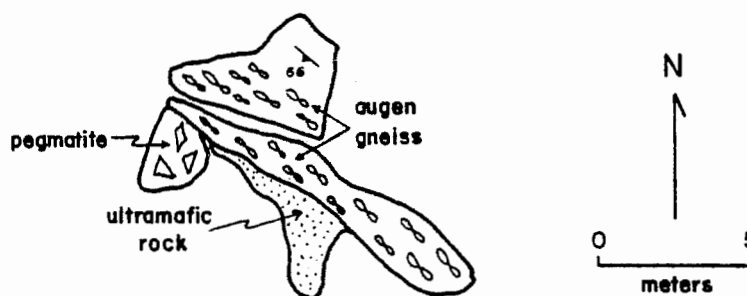
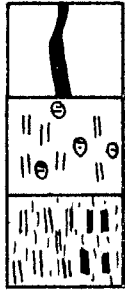


Figure 4. Sketch map of locality B65.

500. 500 is located on the 830' contour along the east side of North Orange Road, 1.1 kilometers northwest of the intersection of North Orange Road and North Main Street, northwest of the village of North Orange in the Mt. Grace 7½-minute quadrangle. The lens is approximately 15 meters in longest dimension. The outcrop weathers drab green and is visible from North Orange Road (Fig. 5). The ultramafic rock has been extensively hybridized and retrograded, and is dominated by coarse needles of chlorite after anthophyllite. On the easternmost margin of the outcrop, garnetiferous, rusty-weathering sulfidic schist is in direct contact with a knobby rock



## HYBRIDIZED MAFIC ROCKS:

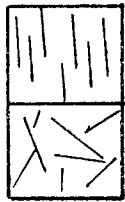


Biotite-cummingtonite-hornblende-plagioclase schist.

Knobby, cummingtonite-hornblende-phlogopite-quartz-plagioclase-garnet schist.

Hornblende-plagioclase-biotite schist grading to hornblende-biotite schist (left to right).

RETROGRADED HYBRIDIZED ULTRAMAFIC ROCKS: Characterized by chlorite pseudomorphs after anthophyllite.



Hornblende-anthophyllite-phlogopite schist. Anthophyllite lies in the plane of foliation.

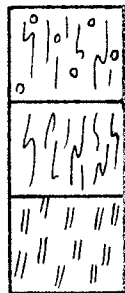
Hornblende-anthophyllite-phlogopite rock.

## HYBRIDIZED ULTRAMAFIC ROCKS:



Chlorite-hornblende-anthophyllite rock.

PARTRIDGE FORMATION: Sulfidic schist member.



Garnetiferous, rusty-weathering sulfidic schist.

Rusty-weathering phlogopite-quartz-plagioclase schist.

Hornblende-plagioclase amphibolite.



Observed contact.



Inferred contact.



Strike and dip of foliation.

500B-● Specimen locality.

Figure 5. Locality 500. See Table 3 for detailed rock descriptions.

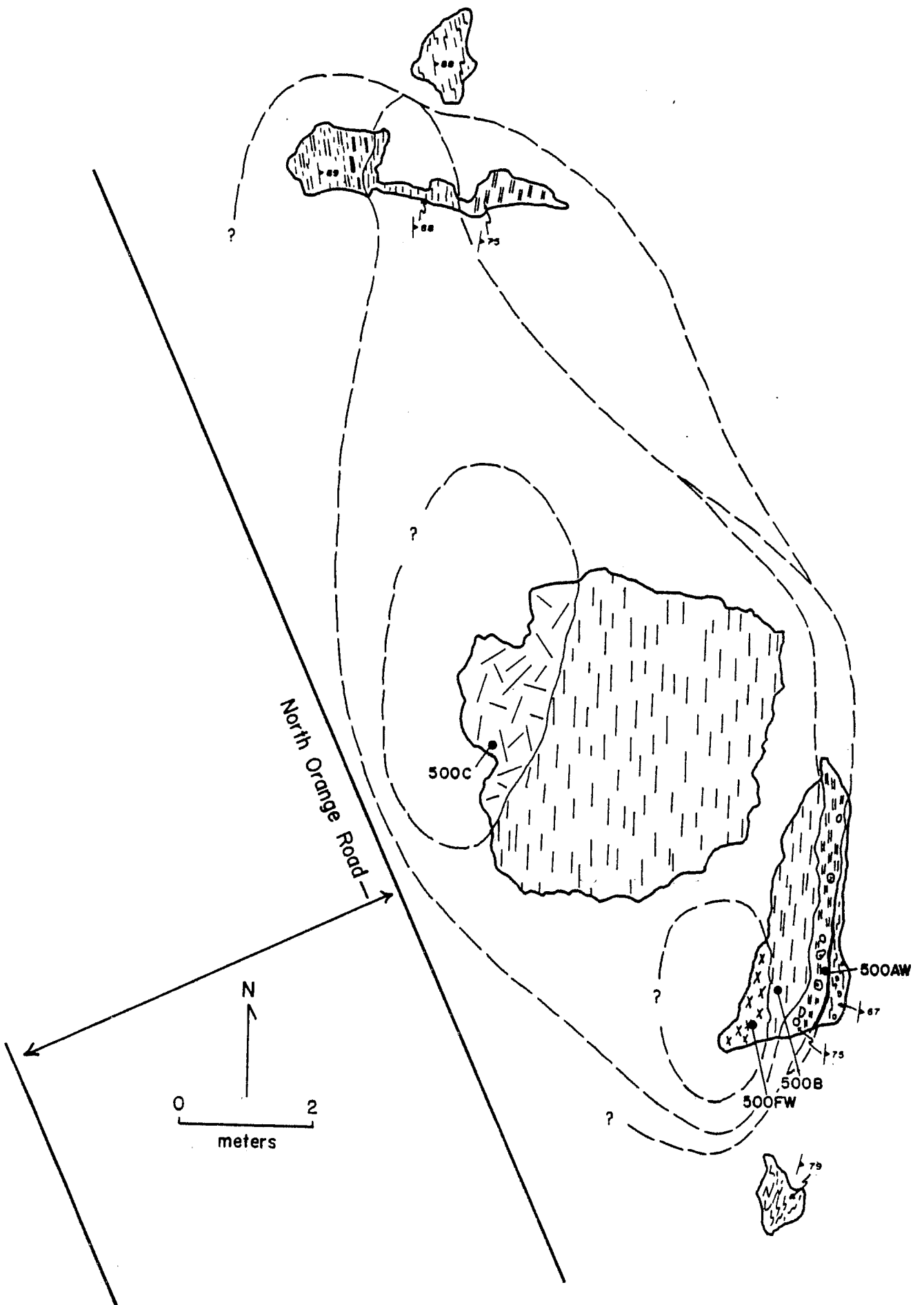


Table 3. Estimated modes of samples from locality 500.

Sample	AW	B	C	FW
Hornblende	28	86	54	40
Cummingtonite	30			
Anthophyllite				4
Garnet	tr			
Plagioclase	4	tr	2	tr
Quartz	3	tr	tr	tr
Chlorite	4	8	40	56
Biotite	24	6	4	tr
Ilmenite	1		tr	
Pyrrhotite <sup>1</sup>	1			
Zircon		tr	tr	tr
Tourmaline		tr	tr	tr
Sericite	5			

1. This includes traces of pyrite and chalcopyrite.

# Sample Descriptions

500AW: Blue-gray, fine- to medium-grained, well foliated, moderately layered, hornblende-cummingtonite-biotite-plagioclase-quartz-chlorite schist with bluish nodules composed of fine-grained quartz, plagioclase, hornblende, and a trace of garnet. The nodules contain a weak lineation which is rotated approximately 90° with respect to the general trend of foliation. Layering is defined by the presence or absence of biotite. A small number of coarse quartz augen occur within the biotite-deficient layers.

500B: Drab-green, fine- to medium-grained, moderately foliated, hornblende-chlorite-biotite rock. Chlorite occurs as pseudomorphs after anthophyllite.

500C: Drab-green, medium-grained, weakly foliated, hornblende-chlorite rock containing accessory biotite. Coarse chlorite needles occur as pseudomorphs after anthophyllite.

500FW: Gray-green, medium-grained, well foliated, chlorite-hornblende-anthophyllite schist containing a trace of biotite.

In samples 500B, C, and FW, trace amounts of quartz are associated with chlorite.

consisting predominantly of blue-green hornblende and brown cummingtonite. This rock also contains moderate amounts of biotite, plagioclase, chlorite, and quartz, with pink garnet occurring in some of the knobby areas. A stringer of biotite-cummingtonite-hornblende-plagioclase schist extends part way up the outcrop from the south, between the sulfidic schist and knobby hornblende-cummingtonite rock. The biotite-rich stringer and the knobby hornblende-cummingtonite rock are believed to be hybridization products of silica contamination.

Estimated modes and specimen descriptions are provided in Table 3. Sample locations are shown in Figure 5. In general, the body itself becomes enriched in hornblende as the amount of biotite decreases and quartz and cummingtonite disappear. Complete replacement of anthophyllite by chlorite distinguishes retrograded-hybridized from hybridized ultramafic rocks. Partial replacement of anthophyllite does occur in the latter. In the small northern outcrop, a hornblende-biotite-plagioclase schist becomes gradationally depleted in plagioclase toward the retrograded ultramafic rocks.

Overall, the body is elongated NNW-SSE. The foliation of the ultramafic rock, amphibolite, and schist strikes approximately north-south and dips steeply east or is vertical (Fig. 6). Anthophyllite needles which lie in the plane of foliation plunge randomly.

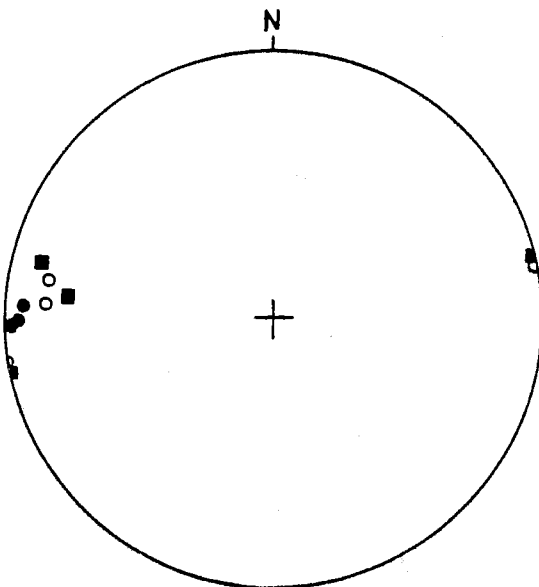


Figure 6. Lower hemisphere equal area projection of planar elements at locality 500. 3 poles to foliation of ultramafic rock (closed circles), 3 poles to foliation of amphibolite (open circles), and 3 poles to foliation of sulfidic schist (squares).

018. 018 is the largest of the bodies studied, the main part of which is located approximately 4.5 kilometers northeast of the village of Orange, Massachusetts. It lies in a cleared area at about 870-880' elevation, 550 meters due east of the junction along Athol Road marked 868 just south of the Athol-Lower Road junction in the Orange 7½-minute quadrangle. The body lies within the Partridge Formation, bounded on the east by schist and amphibolite of the sulfidic schist member, and on the west by the augen gneiss member, which is composed of quartz, plagioclase, sillimanite, biotite, and muscovite (Plate 2). It occurs as four major outcrops spread over an area 200 meters long and 90 meters wide. Contacts with country rock are unexposed and attempts to infer contacts result in considerable ambiguity. The general elongation of the outcrop parallel to regional foliation, and the folding of foliation within the ultramafic rock around the ends of the lens, however, indicate that this body behaved as a competent boudin with respect to enclosing schist and gneiss.

A wide range of primary, secondary, and hybrid ultramafic rocks occur at this locality. The primary metamorphic assemblage is pargasite-orthopyroxene-olivine-spinel-chlorite-ilmenite. Accessory sulfides are ubiquitous. The orthopyroxene nodules at this locality are coarser, higher, and rounder than those at Y57. Alteration and replacement by secondary minerals such as chlorite, talc, and carbonate is extensive. One area of slightly different character is composed of large (up to 4cm), subhedral orthopyroxene megacrysts associated with coarse olivine grains in a fine, fibrous matrix presumed to be composed of hornblende and chlorite (specimen 018AW). Hybridized rocks occur at the southern end of the small easternmost outcrop (Plate 2). This area is characterized by layers of amphibolite, biotite-chlorite-plagioclase schists, and massive to well foliated ultramafic rock (Fig. 7). Estimated modes and descriptions of two specimens are given in Table 4.

Table 4. Estimated modes and sample descriptions from locality 018.

Sample	AW	BW	<p>018AW: Dark-green, heteroblastic, well-foliated, well-lineated, orthopyroxene-olivine hornblendite. Characterized by subhedral orthopyroxene megacrysts up to 2.5cm across and slightly smaller olivine megacrysts in a matrix of very fine-grained pargasite and chlorite.</p> <p>018BW: Dark green, heteroblastic, weakly foliated, weakly lineated, orthopyroxene-olivine hornblendite.</p>
Pargasite	78	70	
Cummingtonite		tr	
Orthopyroxene	8	13	
Olivine	6	2	
Spinel	2	5	
Chlorite	5	9	
Ilmenite	1	1	
Pyrrhotite	tr	tr	
Magnetite	tr	tr	
Serpentine	tr	tr	
Carbonate		tr	

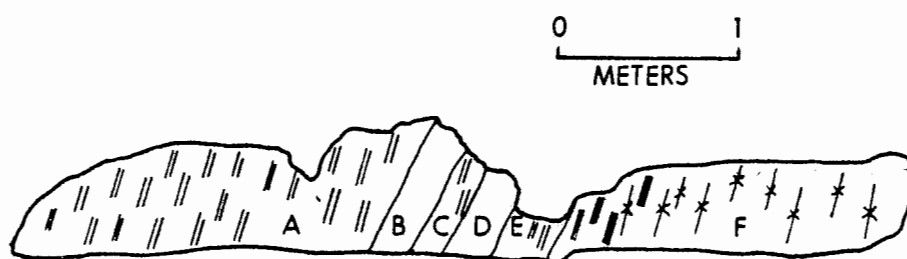


Figure 7. Locality 018. View looking northward at small exposure on southern end of easternmost outcrop of ultramafic body (Plate 2). Hb=hornblende, Cm=cummingtonite, Plag=plagioclase, Biot=biotite, Chl=chlorite, Opx=orthopyroxene. Minerals listed in order of decreasing abundance.

- |                                   |   |
|-----------------------------------|---|
| A. Hb-Plag amphibolite.           | D. Biot-Plag-Hb schist.   |
| B. Gritty Plag-Biot-Hb-Cm schist. | E. Hb-Plag-Chl schist.  |
| C. Hb-Cm-Plag amphibolite         | F. Hb-Opx-Chl rock grading westward (left) to massive hornblendite. |

Most of the foliation in the ultramafic rocks strikes north to northwest and dips steeply southwest or northeast (Fig. 8). Mineral lineations in the ultramafic rocks plunge gently to the northwest or southeast in contrast to the country rocks of the surrounding area in which lineation tends to plunge south.

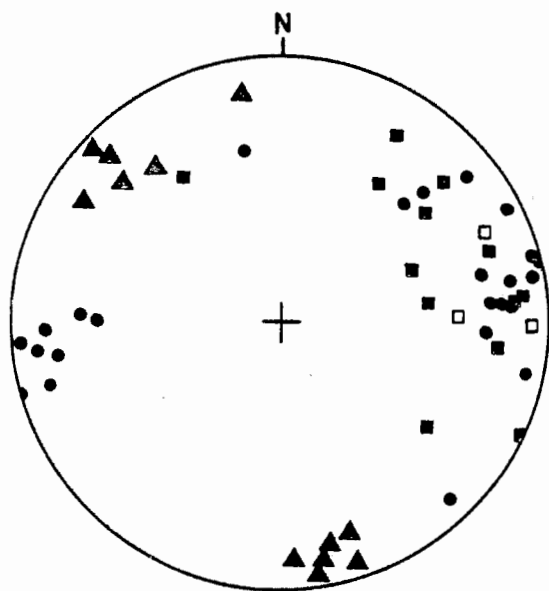


Figure 8. Lower hemisphere equal area projection of planar and linear elements at locality 018. 23 poles to foliation of ultramafic rock (closed circles), 13 poles to foliation of sulfidic schist (closed squares), 3 poles to foliation of augen gneiss (open squares), and 12 amphibole lineations within the ultramafic rock (triangles).

N01/9Q9. These two localities have been combined because of their proximity to each other. They may be part of the same body. 9Q9 is located on the 800' contour 1050 meters due north of the junction of routes 2A and 202 west of Athol, Massachusetts in the Orange 7½-minute quadrangle. N01 is located approximately 60 meters north of 9Q9 on the 830' contour. The entire lens, including both N01 and 9Q9, is spread over an area 130 meters long and 20 meters wide. Contact relations at this locality are less obscure than those previously discussed. The lens is elongated parallel to regional foliation and is enclosed in amphibolite of the sulfidic schist member of the Partridge Formation (Plate 3).

At N01, the ultramafic lens is approximately 6 meters across and is in contact with amphibolite or hornblende-plagioclase gneiss on both sides. Retrograde minerals dominate the ultramafic rock which is characterized by coarse pits on the weathered surface. These pits decrease in size outward and appear reddish-tan on fresh surfaces. The reddish-tan patches are dominated by platy Mg-chlorite, tan carbonate, talc, and fine-grained chlorite, with smaller amounts of apatite, and a trace of hematite. The remainder of the rock is composed predominantly of pargasite and chlorite with minor quantities of cummingtonite, talc, and apatite in most samples. Trace amounts of plagioclase and anthophyllite are also present. The body is bounded on the east by a hornblendite grading to amphibolite away from the contact, and on the west by a plagioclase-hornblende gneiss (Plate 3). The outcrop was sampled across the contact. Estimated modes and sample descriptions are given in Table 5. The body itself possesses a well developed foliation striking approximately north-south and dipping steeply westward (Fig. 9A). A mineral lineation, conformable with regional lineation in this area, plunges moderately southward in the plane of the foliation. Foliation of the adjacent amphibolite is conformable with that of the ultramafic rock. The schistose outcrop located six meters south-southeast of the ultramafic rock has a northeasterly striking foliation with a moderate northwest dip. This may be the result of the less competent schist bowing around the ultramafic rock.

Primary, secondary, and hybridized ultramafic rocks occur in abundance at 9Q9. The primary metamorphic assemblage at this locality is pargasite-olivine-orthopyroxene-chlorite-spinel-ilmenite. Coarse (5cm), blue-gray, magnetic patches dominate the primary rocks and are due to the presence of magnetite in serpentinized olivine. The abundance of secondary minerals increases away from the center of the outcrop. The patches become increasingly



Table 5. Estimated modes of samples from locality N01. Sample locations are shown of Plate 3.

Sample	N01A PR	N01B PR	N01C PR	N01D PR	N01E	N01F	N01G	N01H	N01I	N01J	N01K
Hornblende	75#	91	52	40	54	84	99	64	36	46	64
Cummingtonite*	2#							1	2	3	1
Anthophyllite										tr	
Plagioclase			45 An70	58 An55	45 An72**	15##	tr			tr	
Chlorite	20	9			x		x	24	58	50	34
Talc	3						x	6			
Biotite				1							
Ilmenite	tr	x	1	1	1	1	x	1	2	1	1
Rutile			tr								
Hematite								tr	tr		
Carbonate								4	2		
Epidote						tr					
Apatite	x	x	x	x	tr			x	x		

PR - data from Robinson (1963).

\* - cummingtonite in samples H-K lacks diagnostic polysynthetic twinning. It is distinguished from hornblende by high birefringence, pale color, slightly high relief, and optic sign (+,  $2V=80^\circ$ ).

# - modified from Robinson (1963) who showed 77% hornblende, possibly including 2-3% cummingtonite. This was later confirmed by microprobe analysis (Robinson and Jaffe, 1969).

x - less than 1%.

tr - trace.

\*\* - determined by Michel-Levy method.

## - heavily sericitized.

Descriptions of samples from Table 5. Samples N01A-N01D are directly from Robinson (1963).

- N01A: Dark-green, fine-grained, weakly layered, well foliated hornblende-chlorite-talc schist with light brown, circular talc-rich patches.
- N01B: Dark-green, medium-grained, non-layered, moderately foliated hornblende-chlorite schist.
- N01C: Coarse-grained, spotted hornblende-plagioclase gneiss.
- N01D: Medium-grained, hornblende-biotite amphibolite.
- N01E: Dark-gray and white, medium-grained, moderately foliated, weakly layered, well lineated hornblende-plagioclase amphibolite. Cross cutting veinlets contain traces of chlorite.
- N01F: Dark-gray, medium-grained, moderately foliated, well lineated, hornblende-plagioclase amphibolite. Plagioclase has been extensively sericitized.
- N01G: Dark-gray, medium-grained, well lineated hornblendite.
- N01H: Gray-green, medium-grained, moderately foliated, well lineated, hornblende-chlorite-talc schist with 2.5cm tan patches containing carbonate, chlorite, talc, and apatite.
- N01I: Gray-green, medium-grained, moderately foliated, well lineated, hornblende-chlorite schist with 2.5cm patches containing carbonate, platy chlorite, and apatite. Cummingtonite is observed, in thin section, to rim hornblende.
- N01J: Gray-green, medium-grained, weakly foliated, well lineated, hornblende-chlorite schist containing a small amount of cummingtonite.
- N01K: Dark-green, medium-grained, well foliated, well lineated, hornblende-chlorite schist containing a small amount of cummingtonite. Amphibole lineation wraps around 2mm patches of fine-grained chlorite.

Table 6. Modal analyses of samples from locality 9Q9.

Sample	9Q9A PC	9Q9B	9Q9C	9Q9D	9Q9E	9Q9F	9Q9G
Hornblende	42	53	85	99	80	96	91
Cummingtonite	tr	12			1	x	x
Orthopyroxene	10						
Olivine	27						
Spinel	4						
Chlorite	14	33	tr		18	3	8
Biotite		x	15				
Talc		2					
Serpentine	2						
Ilmenite	1	x	tr	x	1	1	1
Magnetite	tr						
Rutile				tr			
Pyrite	tr				tr	tr	
Chalcopyrite					tr	tr	
Apatite		tr					
Sphene				tr			

Sample designated PC is point counted (2000 points). All others are estimated.

x - less than 1%.

tr - trace.

Descriptions of samples in Table 6. Locations of all samples are shown on Plate 3.

- 9Q9A: Dark-green to blue-gray, heteroblastic medium- to coarse-grained, well foliated, well lineated orthopyroxene-olivine hornblendite. 3cm blue-gray magnetic patches are composed of serpentized olivine and magnetite. Fine hornblende lineation bends around these patches.
- 9Q9B: Brown-green, fine- to medium-grained, moderately foliated, well lineated hornblende-chlorite-cummingtonite schist containing light tan patches of talc and chlorite.
- 9Q9C: Dark-gray, medium-grained, well foliated, well lineated hornblende-biotite schist with a trace of chlorite.
- 9Q9D: Dark-gray, fine-grained, weakly foliated, well lineated hornblendite.
- 9Q9E: Light gray-green, medium-grained, well foliated, nonlineated hornblende-biotite-chlorite schist.
- 9Q9F: Dark gray-green, medium-grained, moderately foliated, well lineated hornblende-chlorite hornblendite.
- 9Q9G: Green-gray, medium-grained, moderately foliated, nonlineated hornblende-chlorite schist.

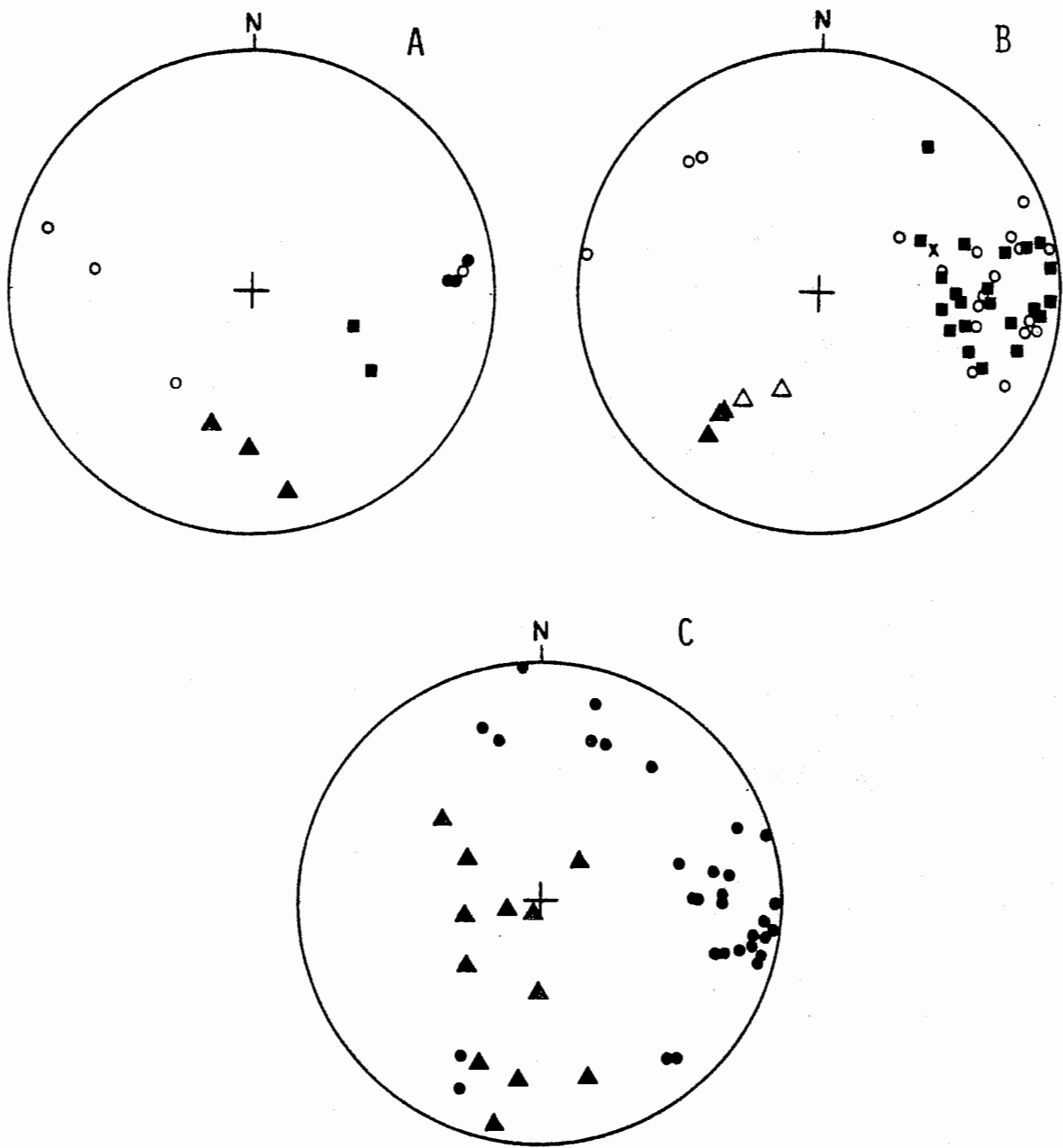


Figure 9. Lower hemisphere equal area projections of planar and linear elements at locality 9Q9/N01. Closed circles = poles to foliation of ultramafic rock; open circles = poles to foliation of amphibolite; squares = poles to foliation in sulfidic schist; x = pole to layering in plagioclase-hornblende gneiss; closed triangles = amphibole lineations; open triangles = minor fold axes.

- A. N01: 3 poles to foliation in ultramafic rock; 2 poles to foliation in schist; 4 poles to foliation in amphibolite; 3 amphibole lineations.
- B. 9Q9 country rock: 19 poles to foliation in amphibolite; 22 poles to foliation in schist; 1 pole to layering in plagioclase-hornblende gneiss; 3 amphibole lineations; 2 minor fold axes.
- C. 9Q9 ultramafic rock: 31 poles to foliation; 12 amphibole lineations.

tan in color and less magnetic, and eventually disappear as the rock grades to a pargasite-chlorite rock with traces of cummingtonite. Locally high concentrations of cummingtonite are present in hybrid rocks near the contacts. Hornblendites and biotite-chlorite schists are also considered hybrid rocks associated with the contacts. An envelope of hornblende-plagioclase amphibolite lies outside the hybrid rocks. Modal analyses and descriptions of representative samples are given in Table 6.

The planar and linear features of the country rock at 9Q9 (Fig. 9B) are oriented parallel to local regional trends. Amphibolites and schists strike approximately north-south and dip moderately-to-steeply westward. Mineral lineations plunge to the southwest. Planar and linear elements in the ultramafic rock are more varied (Fig. 9C). There is folded foliation at the southern end of the outcrop and a spread in lineation orientations. An earlier-formed lineation may have been preserved in the ultramafic rock and folded by a later episode associated with the southwestward-plunging minor fold axes observed in the country rock.

OG2. This body is located at the 680' contour on the northwest slope of a 700' knob, 450 meters due south of the intersection of South Athol and Conant roads near the western edge of the Athol 7½-minute quadrangle. It is a small, rounded, homogeneous body measuring about two meters across. It may be out of place. It was the first locality discovered in this area with the assemblage pargasite-orthopyroxene-spinel-olivine-chlorite-ilmenite. The rock is dark green, heteroblastic, and weakly foliated, containing accessory phlogopite, ilmenite, and sulfides and is characterized by 2cm subhedral magacrysts of orthopyroxene. A point counted mode of sample OG2B is provided in Table 7.

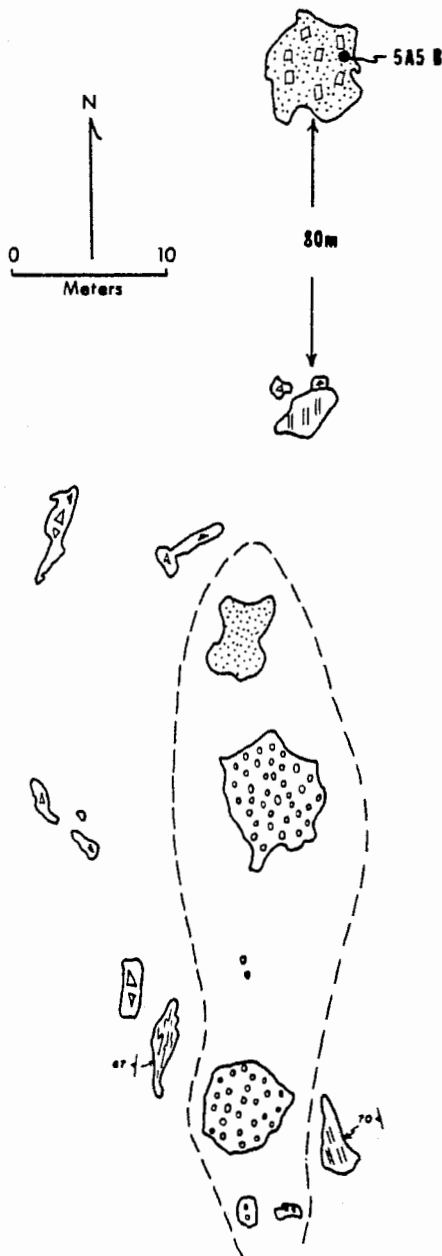
Table 7. Point-counted mode (2000 points) of sample OG2B.

Pargasite	62.9	Chlorite	2.2
Orthopyroxene	26.2	Phlogopite	tr
Olivine	2.2	Ilmenite	1.4
Spinel	5.1	Sulfides	tr
		Apatite	tr

5A5. 5A5 is located on the top of the 960' hill 600 meters south of the intersection of Turnpike and Flat Rock roads in the southwest corner of the Athol 7½-minute quadrangle. The body is divided into two subareas: a 30 meter row of small, low outcrops exposed on the crest of the hill; and a small, 2 meter high outcrop approximately 80 meters to the north (Fig. 10). The northern outcrop is made up of a dark green, heteroblastic, massive orthopyroxene-olivine hornblendite containing 2.5cm subhedral megacrysts of orthopyroxene. The rock has weakly magnetic areas due to the presence of magnetite in serpentinized olivine. A modal analysis of a sample from this outcrop is given in Table 8. This outcrop is similar in appearance to the rock at locality OG2. The outcrops to the south are finer grained, poorly foliated, and slightly richer in phlogopite. Exposure is generally poor and no contacts are exposed. Foliation in this area strikes approximately north-south and dips steeply west.

Table 8. Estimated mode of sample 5A5B.

Pargasite	55	Phlogopite	tr
Orthopyroxene	28	Serpentine	tr
Olivine	8	Ilmenite	1
Spinel	3	Magnetite	tr
Chlorite	5		

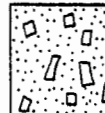


## INTRUSIVE ROCK

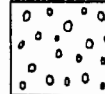


Pegmatite

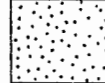
ULTRAMAFIC ROCKS: Contain the assemblage: par-gasite-orthopyroxene-olivine-spinel-chlorite-ilmenite.



Orthopyroxene-olivine hornblende characterized by the presence of 2.5cm megacrysts of orthopyroxene.



Nodular orthopyroxene-olivine hornblende containing a small amount of phlogopite.



Massive, fine grained orthopyroxene-olivine hornblende containing a small amount of phlogopite.

PARTRIDGE FORMATION: Sulfidic schist member.



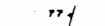
Hornblende-plagioclase amphibolite.



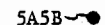
Rusty weathering, sillimanite-bearing sulfidic schist.



Inferred contact.



Strike and dip of foliation



Sample location.

Figure 10. Locality 5A5.



Q222. Q222 is located on the 950' contour on the southwest side of Bald Hill 500 meters northwest of the intersection of West Street and Camels Hump Road in the northwest corner of the Petersham, Massachusetts 7½-minute quadrangle. The rock is strongly foliated with a primary metamorphic assemblage of pargasite-olivine-orthopyroxene-spinel-chlorite-ilmenite (See Fig. 21). An estimated mode is given in Table 9. The rock is most similar in appearance to specimen 9Q9A; containing large olivine poikiloblasts that have been serpentized along cracks. The outcrop possesses patchy, weak magnetism. Small pale amphibole needles are visible in hand specimen as inclusions in olivine. Most of the rock at this locality occurs as loose material, however, two small pieces are believed to be in place (Fig. 11) and their foliation strikes east of north and dips steeply west.

Table 9. Estimated mode of sample Q222.

Pargasite	33	Chlorite	tr
Cumingtonite	tr	Serpentine	tr
Orthopyroxene	22	Ilmenite	1
Olivine	40	Magnetite	tr
Spinel	4		

K28. K28 is divided into two bodies designated K28N and K28S. K28N is located on the 950' contour southwest of Camels Hump Hill, 200 meters northwest of intersection 820 along Camels Hump Road, roughly 4 kilometers southwest of the village of Petersham, Massachusetts in the Petersham 7½-minute quadrangle. K28S is located approximately 60 meters

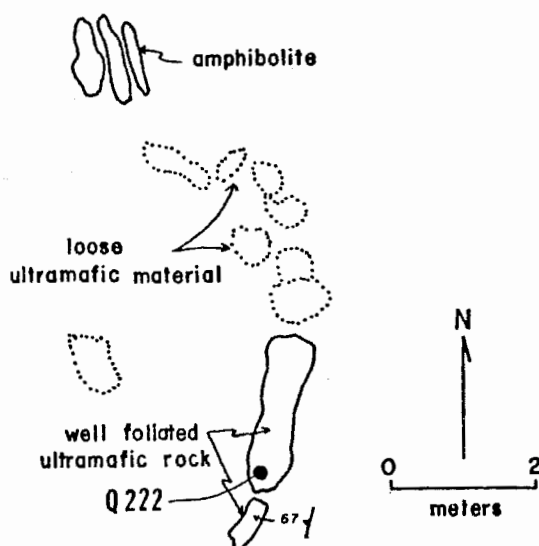


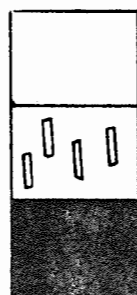
Figure 11. Sketch map of locality Q222 showing foliation and sample location.

south along strike and slightly downhill from K28N. Both bodies are characterized by the presence of primary and hybrid ultramafic rocks. The primary metamorphic assemblage is pargasite-orthopyroxene-olivine-spinel-chlorite-ilmenite.

At K28N (Fig. 12), the primary ultramafic rock is bounded on the west by a hornblende-plagioclase amphibolite which pinches out northward yielding to a hybrid rock composed of hornblende, anthophyllite, and plagioclase. West of the anthophyllite-bearing rock is a garnetiferous hornblende-plagioclase amphibolite which itself is in contact with rusty weathering hornblende schist on the west. A plagioclase-cummingtonite-hornblende gneiss occurs at the southeast corner of the lens and a garnet-bearing hornblendite lies further east and north. Descriptions of representative specimens are given in Table 10.

At K28S, contacts of the primary ultramafic rock are exposed on both the east and west sides (Fig. 13). To the west, the ultramafic rock is in contact with a hornblende-cummingtonite-plagioclase amphibolite. A thin

## HYBRIDIZED ROCKS

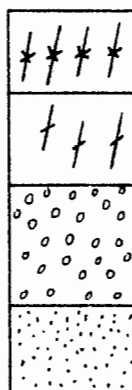


Weakly layered plagioclase-cummingtonite-hornblende-biotite gneiss.

Moderately foliated, well layered hornblende-anthophyllite-plagioclase rock.

Weakly layered hornblende-cummingtonite-plagioclase rock grading eastward to hornblende-plagioclase amphibolite.

ULTRAMAFIC ROCK: Primary metamorphic assemblage is pargasite-orthopyroxene-olivine-spinel-chlorite-ilmenite.



Well foliated orthopyroxene-olivine hornblendite.

Weakly foliated orthopyroxene-olivine hornblendite.

Massive orthopyroxene-olivine hornblendite characterized by small orthopyroxene megacrysts (0.5-1cm).

Massive, medium grained orthopyroxene-olivine hornblendite.

PARTRIDGE FORMATION: Sulfidic schist member.



Hornblende-plagioclase amphibolite.

Garnetiferous hornblende-plagioclase amphibolite.

Garnetiferous hornblende-plagioclase amphibolite grading to garnet-bearing hornblendite (east to west).

Rusty-weathering biotite-hornblende-quartz schist.



Observed contact.



Inferred contact.



Strike and dip of foliation.

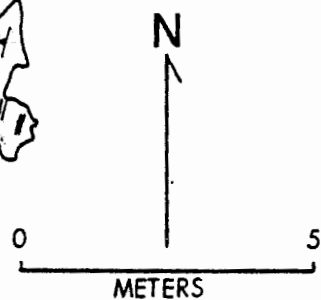
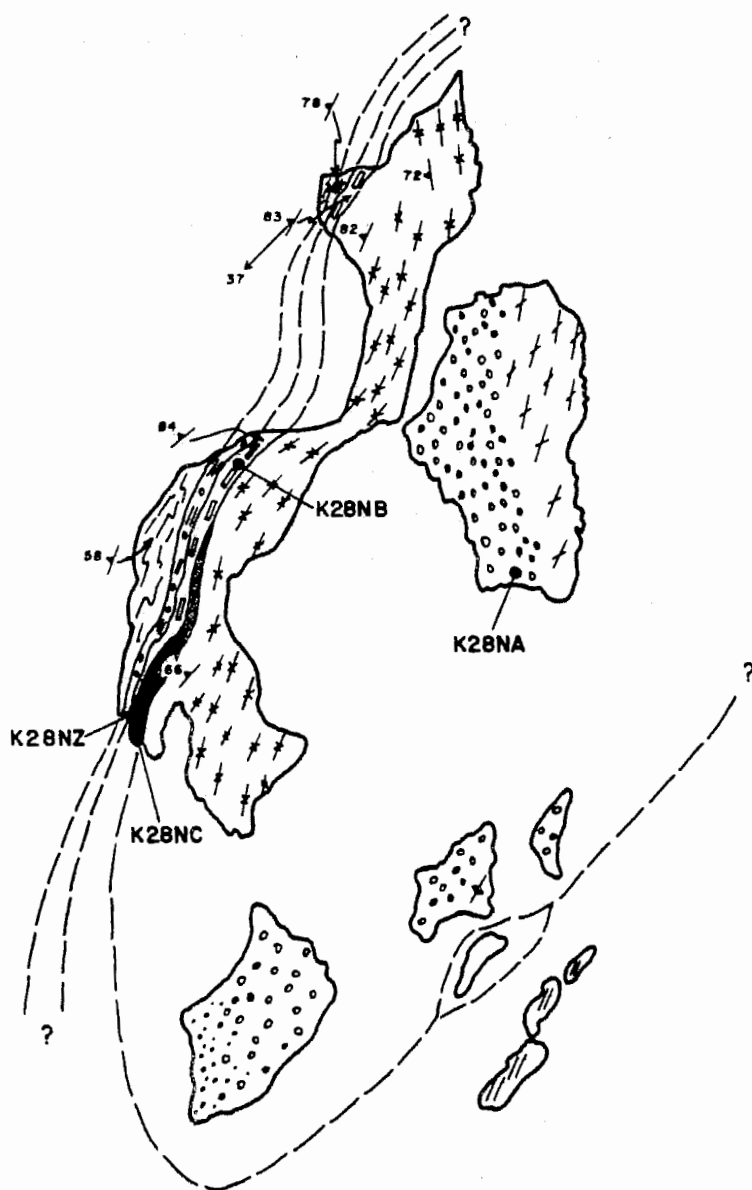


Mineral lineation.

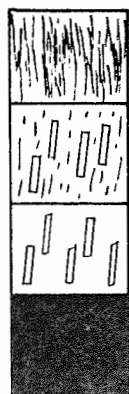


Specimen locality.

Figure 12. Locality K28N. Minerals listed in order of decreasing abundance.



## HYBRIDIZED ROCKS



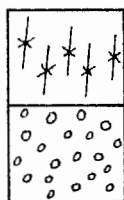
Well foliated biotite-chlorite-plagioclase-(hornblende) schist.

Fine- to medium-grained, weakly foliated hornblende-plagioclase-cummingtonite-biotite gneiss.

Medium-grained hornblende-cummingtonite-plagioclase amphibolite.

Medium-grained hornblendite grading eastward to hornblende-plagioclase amphibolite.

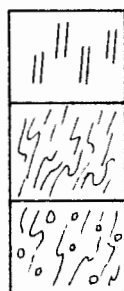
ULTRAMAFIC ROCKS: Primary metamorphic assemblage is pargasite-orthopyroxene-olivine-spinel-chlorite-ilmenite.



Weakly to moderately foliated, well lineated orthopyroxene-olivine hornblendite.

Massive orthopyroxene-olivine hornblendite containing small orthopyroxene megacrysts.

PARTRIDGE FORMATION: Sulfidic schist member.



Hornblende-plagioclase amphibolite.

Rusty-weathering biotite-plagioclase-quartz schist.

Garnetiferous rusty-weathering biotite schist.



Observed contact.



Inferred contact.



Strike and dip of foliation.



Trend and plunge of mineral lineation.

K28SA ● Specimen locality.

Figure 13. Locality K28S. Minerals listed in order of decreasing abundance.

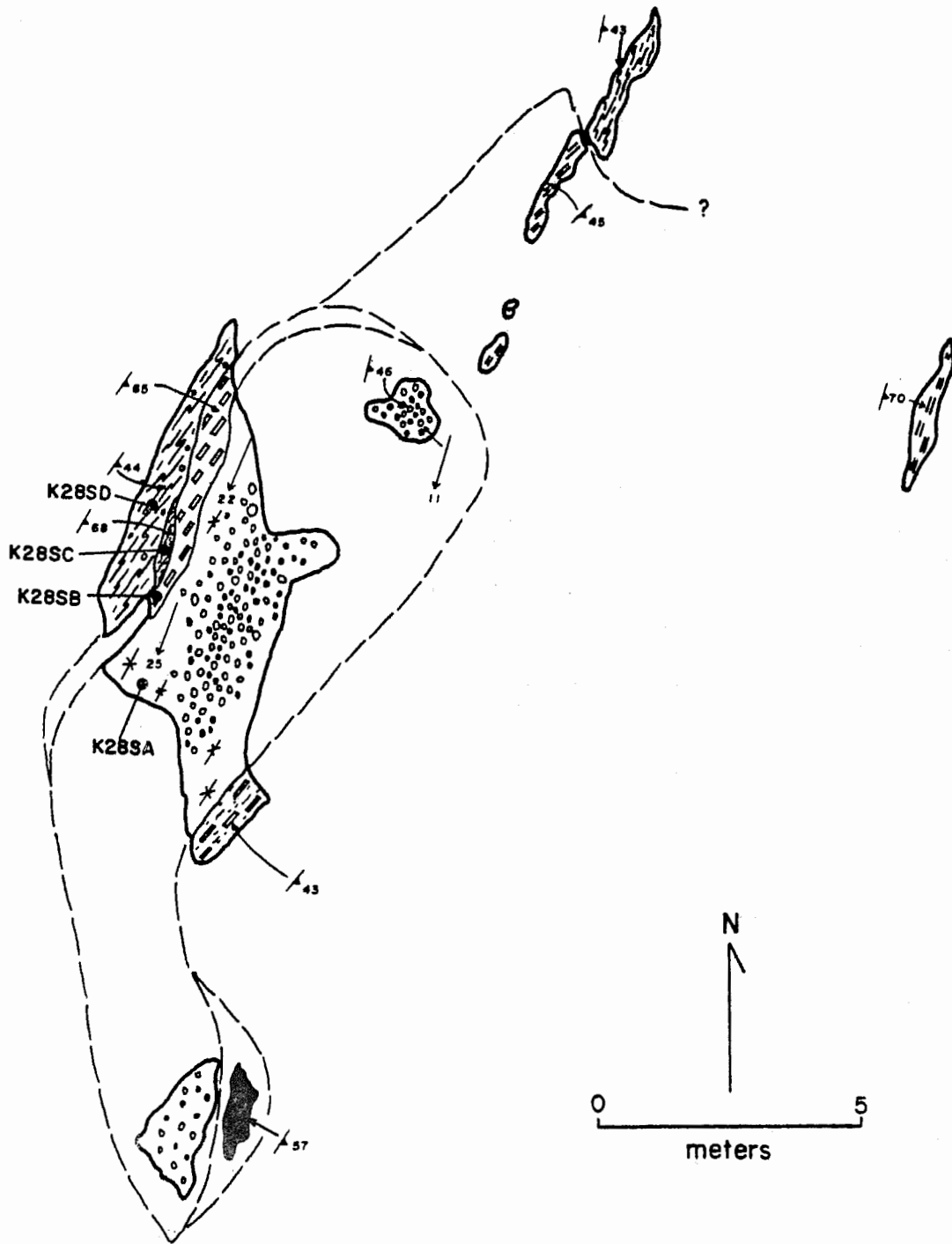


Table 10. Estimated modes of samples from K28N and K28S

Sample	K28NA	K28NB	K28NC	K28NZ	K28S
Hornblende	43	84	65	52	81
Cummingtonite				8	2
Anthophyllite		10			
Plagioclase		6	35	40	
Orthopyroxene	29				7
Olivine	22				9
Spinel	3				tr
Chlorite	1				tr
Phlogopite	tr				
Talc	tr				
Serpentine	tr				tr
Ilmenite	1		tr	tr	tr
Magnetite	1				tr
Rutile		tr			
Pyrrhotite	tr				tr
Pyrite	tr				tr
Carbonate	tr				1
Apatite			tr	tr	

\* - Hand specimen descriptions only. No thin section available.

tr - trace

# Sample Descriptions

K28NA: Dark-green, medium-grained, nonfoliated, moderately lineated orthopyroxene-olivine hornblendite.

K28NB: Dark-gray to pink, medium-grained, moderately foliated, strongly lineated, well layered, hornblende-anthophyllite-plagioclase rock. Light colored layers are concentrations of anthophyllite and plagioclase.

K28NC: Medium-gray, fine- to medium-grained, nonfoliated, moderately lineated, hornblende-plagioclase rock.

K28NZ: Gray to brown, fine-grained, moderately foliated, weakly layered hornblende-cummingtonite-plagioclase rock.

K28SA: Dark-green, medium-grained, well lineated, weakly foliated orthopyroxene-olivine hornblendite with accessory cummingtonite. Magnetite occurs within serpentinized olivine.

\*K28SB: Medium-gray, medium-grained, weakly foliated, weakly lineated, hornblende-cummingtonite-plagioclase rock.

\*K28SC: Dark-gray, medium-grained, well foliated, weakly layered, biotite-chlorite-plagioclase-(hornblende) schist.

\*K28SD: Red-brown, medium-grained, moderately foliated, well layered, biotite-plagioclase-quartz-garnet rock containing 2cm layers of red-weathering schist.

lens of biotite-chlorite schist lies west of the cummingtonite-bearing rock and passes westward into garnetiferous rusty-weathering biotite-plagioclase-quartz schist. On the east, the ultramafic rock is in contact with a hornblende-plagioclase-cummingtonite-biotite gneiss. A hornblendite grading eastward into hornblende-plagioclase amphibolite is located at the southeast corner of the lens. Representative specimen descriptions and a single estimated mode are given in Table 10.

Foliation in and around both outcrops strikes approximately north-northeast, however, at K28N it dips northwest; at K28S it dips southeast (Fig. 14A & B). This could result from the presence of a minor fold in the area with a hinge passing between the two outcrops. Mineral lineations in both outcrops plunge southwestward, parallel to the regional trend.

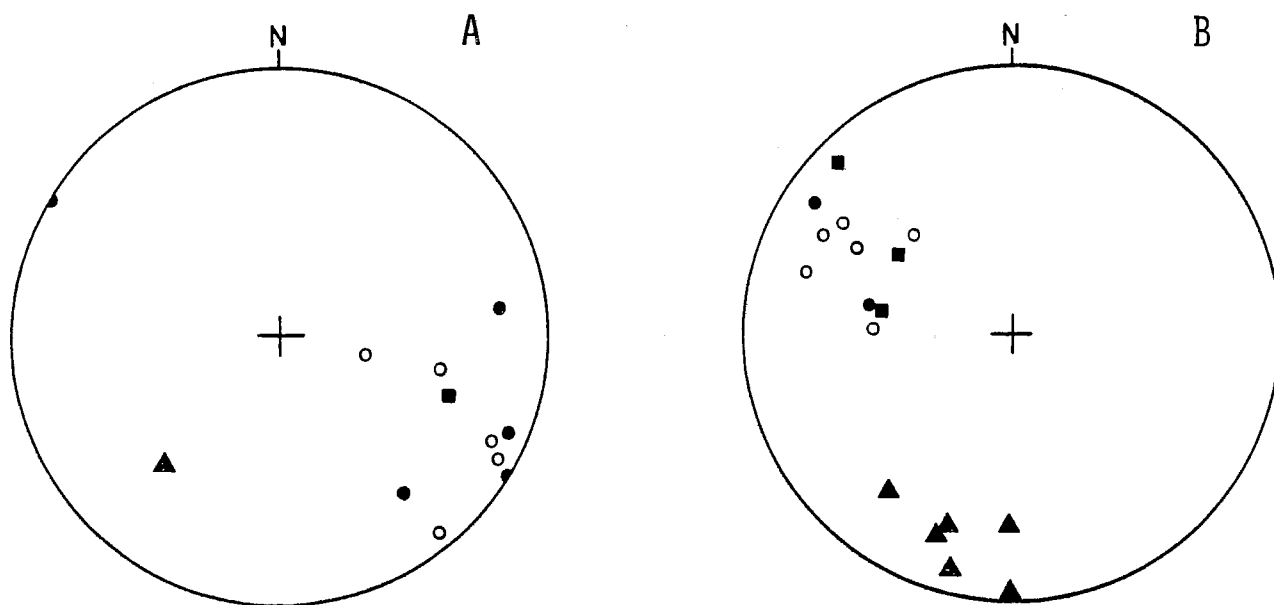


Figure 14. Lower hemisphere equal area projection of planar and linear features at localities K28N and K28S. Closed circles = poles to foliation in ultramafic rock; open circles = poles to foliation in amphibolite; squares = poles to foliation in rusty, biotite-plagioclase quartz rock; triangles = amphibole lineations in ultramafic rock.

- A. K28N: 4 foliations in ultramafic rock; 5 foliations in amphibolite; 1 foliation in rusty, biotite rock; 1 amphibole lineation in ultramafic rock.
- B. K28S: 2 foliations in ultramafic rock; 6 foliations in amphibolite; 3 foliations in rusty, biotite rock; 6 amphibole lineations in ultramafic rock.



K34. K34 is located on the 840' contour along the east side of Camels Hump Road, 150 meters south-southwest of intersection 820 in the Petersham 7½-minute quadrangle, approximately 4 kilometers southwest of the village of Petersham. The body is approximately 19 meters across, weathers gray to gray-green, and has poorly exposed contact relations (Fig. 15).

The body is composed entirely of hybridized rocks. The eastern side of the outcrop is made up of a massive, gray, medium-grained hornblende-anthophyllite-plagioclase rock which grades westward into a dark gray, hornblende-anthophyllite rock. A garnetiferous hornblende-anthophyllite rock with accessory orthopyroxene and sericitized plagioclase occurs in the center of the outcrop. A point counted mode of a sample of this rock (Specimen K34A) is given in Table 11. Very pale pink garnets (up to 5mm) are abundant in this area. The size and abundance of garnets decreases north and east away from the center. The anthophyllite displays a blue iridescence. Most of the country rock surrounding this body is hornblende-plagioclase or hornblende-plagioclase-garnet amphibolite. A rusty-weathering, plagioclase-biotite-quartz rock and a garnetiferous amphibolite occur on the western edge of the outcrop.

Table 11. Point-counted (2000 points) mode of specimen D34A.

Pargasite	71.0	Garnet	5.1
Anthophyllite	21.2	Orthopyroxene	tr
Plagioclase (An96*)	2.4	Ilmenite	0.3

\* Composition determined by microprobe analysis. Plagioclase is approximately 80% sericitized.

In general, planar features in both the ultramafic and country rock strike northward with moderate to shallow eastward dips (Fig. 16). Some open folding of foliation occurs along the western side of the body.

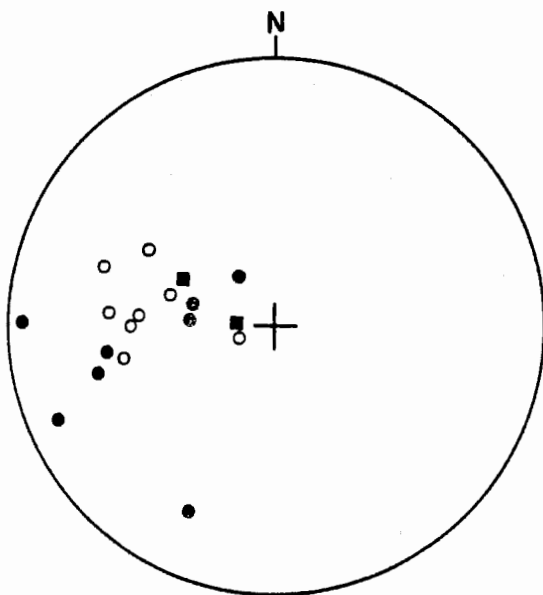
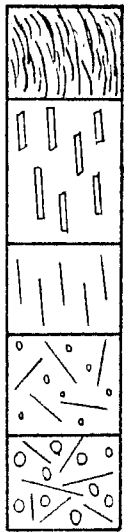


Figure 16. Lower hemisphere equal area projection of planar features at locality K34. 8 poles to foliation of ultramafic rock (closed circles); 8 poles to foliation of amphibolite (open circles); 2 poles to foliation of plagioclase-biotite-quartz rock (squares).

J98. J98 is located within the powerline on the 870' contour, 225 meters northwest of intersection 845 of Dugway and Camels Hump Roads in the northwest portion of the Petersham 7½-minute quadrangle, approximately 4 kilometers southwest of the village of Petersham. The body consists of two outcrops approximately 40 meters apart (Fig. 17). The northern outcrop is approximately 1 meter across and the outcrop to the south is 15 meters long and 5 meters wide. It lies within the sulfidic schist member of the Partridge Formation, however, no outcrop of country rock occurs in the immediate vicinity of this lens.

The lens is composed of primary and hybridized ultramafic rock. The primary rock is made up of pargasite, orthopyroxene, olivine, spinel, chlorite, and ilmenite and is divided into two rock types. The first is non-foliated but has a weak lineation defined by broken-up olivine grains.

## HYBRIDIZED ROCKS



Well foliated phlogopite-hornblende-(plagioclase) schist.

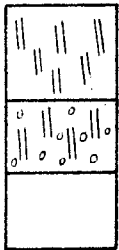
Moderately foliated hornblende-anthophyllite-plagioclase amphibolite in gradational contact with garnet-bearing hornblende-anthophyllite-(plagioclase) rocks.

Moderately foliated hornblende-anthophyllite-(plagioclase) rock.

Massive hornblende-anthophyllite-garnet-(plagioclase)-(orthopyroxene) rock. < 1% garnet.

Massive hornblende-anthophyllite-garnet-(plagioclase)-(orthopyroxene) rock. > 1% garnet.

## PARTRIDGE FORMATION: Sulfidic schist member.



Medium-grained hornblende-plagioclase amphibolite.

Medium-grained garnetiferous hornblende-plagioclase amphibolite.

Rusty-weathering plagioclase-biotite-quartz rock.



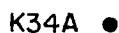
Observed contact.



Inferred contact.

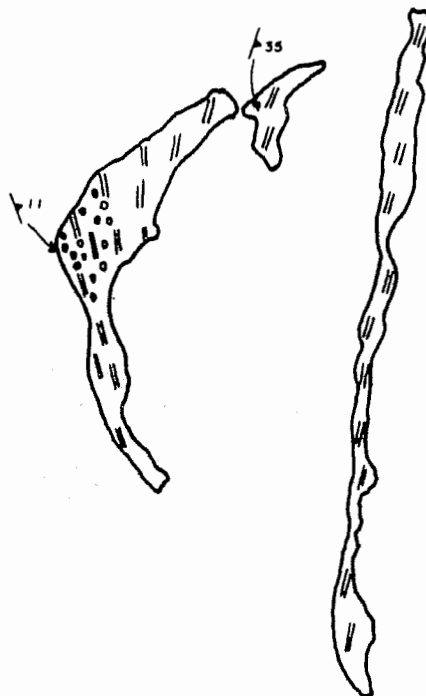
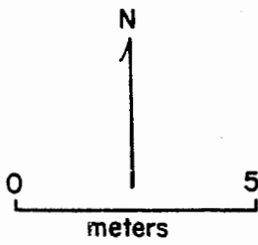
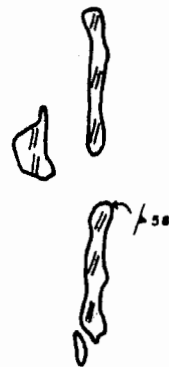
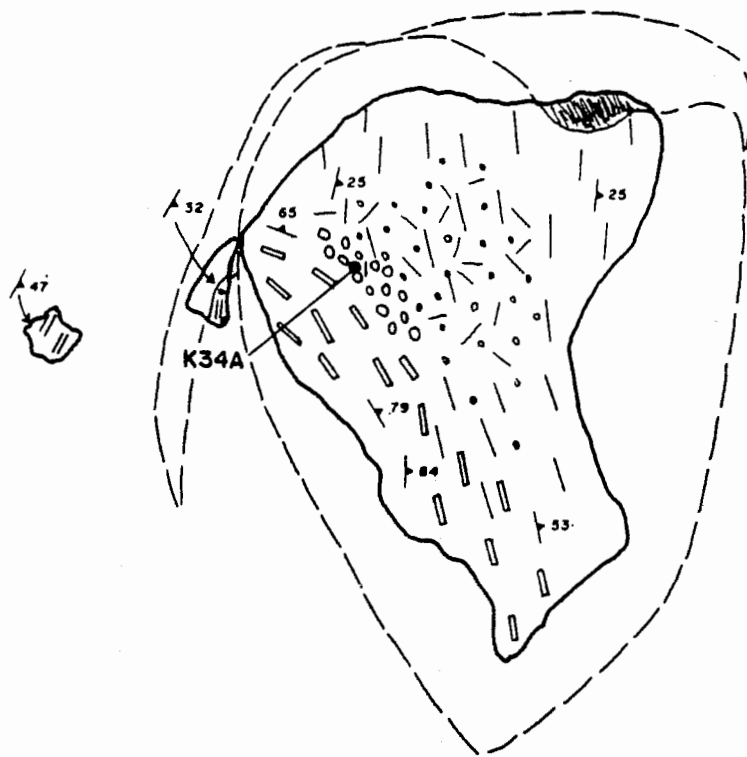


Strike and dip of foliation.



Specimen locality.

Figure 15. Locality K34. Minerals listed in order of decreasing abundance. Phases in parentheses are present in trace amounts.





Fine-grained, weakly lineated, orthopyroxene-olivine hornblendite.

459

\_\_\_\_\_

\_\_\_\_\_

747

11 \_\_\_\_\_

J98B —

Figure 17. Locality J98. Minerals listed in order of decreasing abundance.

The second possesses a weak foliation and amphibole lineation. Sample descriptions and modal analyses are provided in Table 12. The medium-grained, foliated type makes up most of the outcrop. The fine-grained, non-foliated type lies structurally beneath, but protrudes above the foliated rock. It is greener than the foliated rock due to a higher percentage of olivine. The hybrid rock occurs at the southwest corner of the outcrop. It is a layered rock composed of pargasite, anthophyllite, sericitized plagioclase, and orthopyroxene. The anthophyllite displays blue schiller.

Foliation in the main outcrop strikes north and dips moderately to steeply west (Fig. 18). Mineral lineation plunges gently south. The foliation in the small outcrop to the north strikes northeast and dips moderately northwest with a mineral lineation plunging southwestward. This may reflect a true change in orientation or indicate that the rock at this locality is really out of place.

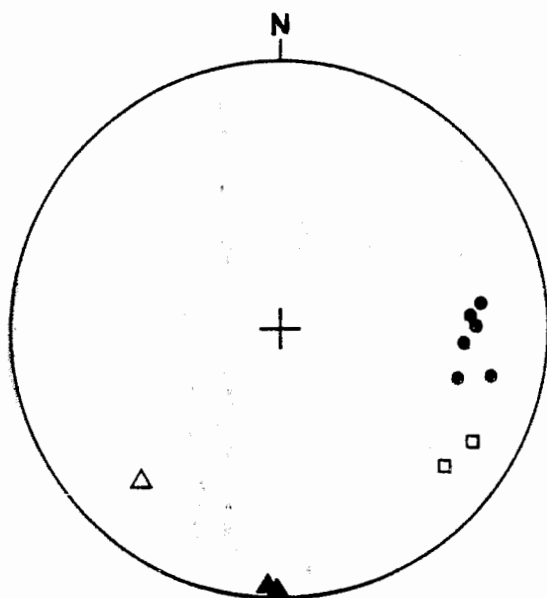


Figure 18. Lower hemisphere equal area projection of planar and linear features at locality J98. 6 poles to foliation of main outcrop (closed circles); 2 poles to foliation at northern pod (open squares); 2 amphibole lineations at main outcrop (closed triangles); 1 amphibole lineation at northern outcrop (open triangle).

Table 12. Estimated modes of samples from J98.

Sample	J98AW	J98BW	J98B
Hornblende	67	60	74
Anthophyllite			15
Plagioclase			9* (An 90-95)
Orthopyroxene	5	20	2
Olivine	25	15	
Spinel	2	5	
Chlorite	tr	tr	
Phlogopite			
Serpentine	tr	tr	tr
Ilmenite	tr	tr	
Magnetite	1	tr	
Pyrrhotite		tr	

\* Plagioclase composition determined by optical techniques.

Sample descriptions.

J98AW: Dark-green, fine-grained, weakly lineated orthopyroxene-olivine hornblendite. Lineation is defined by olivine. The rock contains randomly disseminated, weakly magnetic patches.

J98BW: Dark gray, medium-grained, weakly foliated orthopyroxene-olivine hornblendite.

J98B: Dark-gray to pale brown, medium-grained, weakly layered, well lineated hornblende-plagioclase-anthophyllite rock containing a small amount of orthopyroxene. Plagioclase has been extensively sericitized. Anthophyllite displays blue schiller.

N45. N45 is located on the 820' contour northeast of the summit of Brimstone Hill, just east of Fisherdkick Road approximately 1.5 kilometers east of Peppers Mill Pond in the Winsor Dam 7½-minute quadrangle. The body appears as a brown-weathering outcrop approximately 3 meters long and 1 meter wide. Nearby country rocks include sillimanite-biotite schist and amphibolite of the sulfidic schist member of the Partridge Formation. The rock is a heteroblastic fine- to medium-grained, moderately foliated, moderately lineated pargasite-orthopyroxene-olivine-chlorite-spinel rock with accessory phlogopite, ilmenite, sulfides, and carbonate (Table 13). No structural features could be measured at this locality.

Table 13. Point-counted (2000 points) modes of specimen N45A.

Pargasite	50.1	Phlogopite	tr
Orthopyroxene	37.3	Ilmenite	0.6
Olivine	4.7	Sulfides	0.5
Spinel	4.1	Carbonate	tr
Chlorite	2.7		

---



## DESCRIPTIVE PETROGRAPHY

As evident from the maps presented above, three general rock types are encountered within these lenses: primary prograde metamorphosed ultramafic rocks, hybridized rocks due to reactions between ultramafic and country rocks, and retrograded rocks. The compositions of 23 primary prograde rocks are plotted in terms of hornblende, orthopyroxene, and olivine in Figure 19. A majority of the specimens fall within or near the orthopyroxene-hornblendite division and a few in the olivine-hornblendite division. On the basis of this scheme, therefore, these prograde rocks are referred to as orthopyroxene-olivine hornblendites, with the understanding that spinel, chlorite, and ilmenite comprise the remainder of the assemblage. Hybrid rocks are taken to include both ultramafic and immediately-adjacent country rocks which have been chemically altered by metasomatic processes in the contact zones, in most cases well before the peak of regional metamorphism. Some portions of both primary prograde and hybridized rocks have been affected by retrograde metamorphism. The ensuing discussion will consider the important petrographic features of all of the above rock types.

Orthopyroxene-Olivine Hornblendite

The texture of the hornblendites varies with locality from massive, fine-grained, equigranular rocks to well foliated, megacrystic rocks. Some possess an amphibole lineation. Surface textures vary as shown on maps presented above. Small patches of high magnetic susceptibility are found in some fresh hornblendites and are due to the presence of magnetite in serpentinized olivine. At locality 9Q9, the patches are magnetic and appear metallic blue-gray (Specimen 9Q9A). Orthopyroxene, olivine, and/or amphibole occur as megacrysts in some of the specimens.

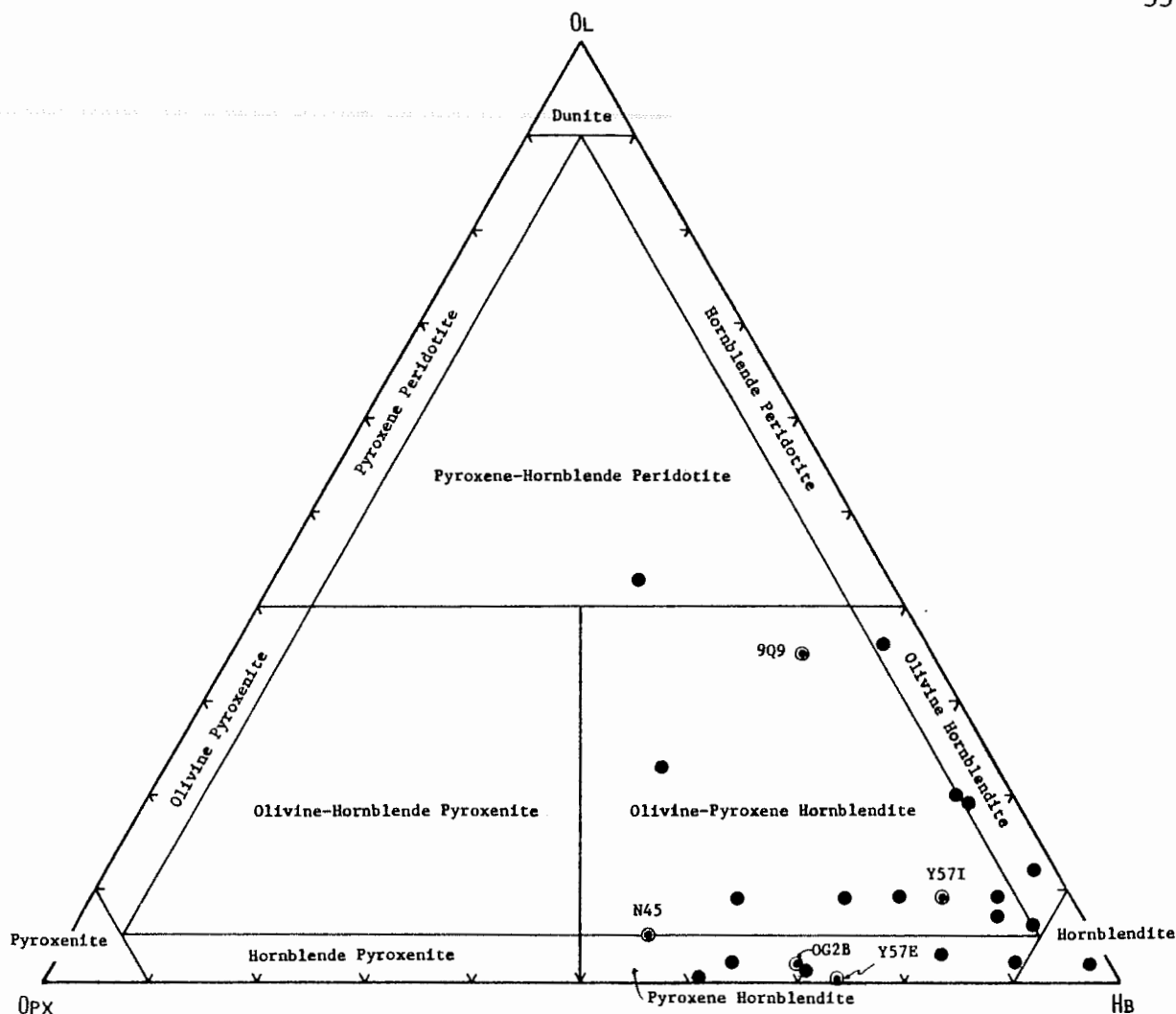


Figure 19. Five point-counted (bullseye) and 18 visually estimated (closed circles) modes of primary ultramafic rocks plotted in terms of olivine (Ol), orthopyroxene (Opx), and hornblende (Hb). Classification scheme is modified from Streckeisen (1973) in that all pyroxene is Opx.

Pale, blue-green amphibole is the most common constituent of these hornblendites. Optic sign varies from just negative to just positive, commonly within a single grain. All such amphibole is referred to as pargasite. Darker green or greenish-brown varieties are all optically negative and are referred to as hornblende. The pargasite generally has a bimodal grain-size distribution. The smaller grains occur as interlocking subhedral crystals which may or may not define a foliation. The larger grains usually have less well defined grain boundaries and contain inclusions

of all other phases including small pargasite grains (Fig. 20). In some sections, lenticular pargasite grains are oriented subparallel to each other within the plane of foliation. Where foliation is most strongly developed, olivine, orthopyroxene, spinel, and Mg-chlorite are elongated in the foliation plane suggesting syntectonic metamorphic equilibration (Fig. 21). A number of specimens contain optically continuous clusters of pargasite grains intergrown with orthopyroxene (Fig. 22).

Orthopyroxene is pale pink and is seen as randomly oriented, subhedral megacrysts evenly disseminated throughout the specimen (Fig. 23). It also occurs as a major constituent of the nodules in the primary rocks which have not been too heavily affected by retrograde alteration. A cut across a nodule in specimen Y57N reveals an orthopyroxene grain which has been slightly broken up and rotated (Fig. 24). A smaller amount of olivine is associated with orthopyroxene within these nodules, lying in a matrix of randomly oriented, fine- to medium-grained, pargasite, spinel, chlorite, and ilmenite.

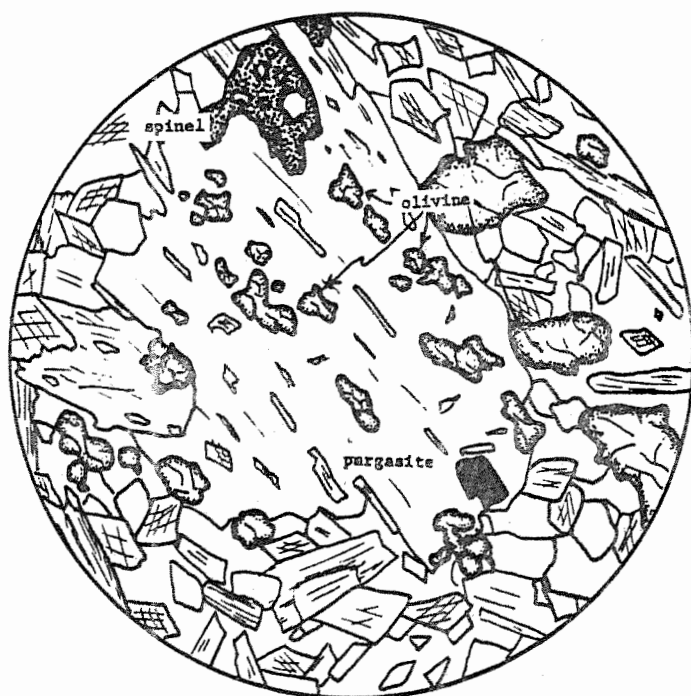


Figure 20. Sketch of orthopyroxene-olivine hornblendite illustrating coarse and fine pargasite grains and the relationship between pargasite and olivine. Included within the large pargasite grain are olivine, chlorite, spinel, and smaller, euhedral pargasite grains. Chlorite laths are parallel to cleavage in the pargasite. All olivine, both inside and outside of the pargasite grain, is optically continuous. Matrix is composed of fine-grained pargasite and chlorite. Diameter of circle is 3mm. Specimen Y57I.



Figure 21. Sketch of foliated orthopyroxene-olivine hornblendite illustrating textural relations. Opaque areas represent ilmenite and sulfides. Most inclusions in megacrysts are pargasite. Note elongation of orthopyroxene, olivine, spinel, and chlorite in plane of foliation. Long dimension is 3.4mm. Specimen Q222.

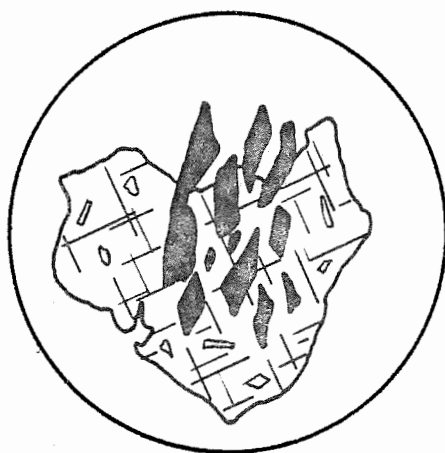


Figure 22. Sketch of orthopyroxene megacryst within orthopyroxene-olivine hornblendite showing the relationship between pargasite and orthopyroxene. Pargasite, shown in black, is optically continuous. Small inclusions within the orthopyroxene are pargasite and chlorite. Diameter of circle is 2mm. Specimen Y57I.

In most specimens, olivine appears as a colorless mineral of high relief which occurs as megacrysts. A slight degree of serpentinization is evident in some of the grains in which expansion cracks are filled with

serpentine and magnetite. In no case, however, has serpentinization been extensive enough to replace all, or even a major portion, of any olivine grain. Where not megacrysts, olivine occurs as separate, small grains. Some of these small grains occur in optically continuous clusters to the extent that olivine inclusions within an amphibole grain are optically continuous with grains outside of the amphibole as shown in Figure

Dark green, anhedral spinel grains are ubiquitous in most specimens, although in a few cases, a weak layering is defined by spinel enrichment. In some of the specimens, most notably 9Q9A, the spinel is optically zoned from brownish-green to green outward. The larger spinel grains always appear poikiloblastic, most inclusions being small, euhedral pargasite grains.

Primary chlorite is an optically positive, colorless, magnesian variety which occurs as coarse plates or lath-shaped grains. It is easily recognizable by low relief, "birds eye maple" texture, and polysynthetic twinning on (001). Modal abundance ranges from trace amounts up to 15%.

Opaque minerals constitute one to two percent of the samples and appear evenly disseminated throughout. Reflected light microscopy reveals the opaques to be composed primarily of ilmenite and sulfides. The ilmenite grains are subhedral and homogeneous. The sulfides include pyrrhotite, pyrite, chalcopyrite, and pentlandite. Pyrrhotite is the most abundant sulfide. It displays flame lamellae and contains euhedral to subhedral inclusions of pyrite. Chalcopyrite and pentlandite are also found within pyrrhotite. A very small amount of graphite was detected within specimen Y57I. An additional opaque phase with a very limited occurrence is chromian spinel, rimmed by magnetite. This phase occurs in the center of small, rounded blebs of fine-grained chlorite found only within the nodules of specimen Y57N (Fig. 24).

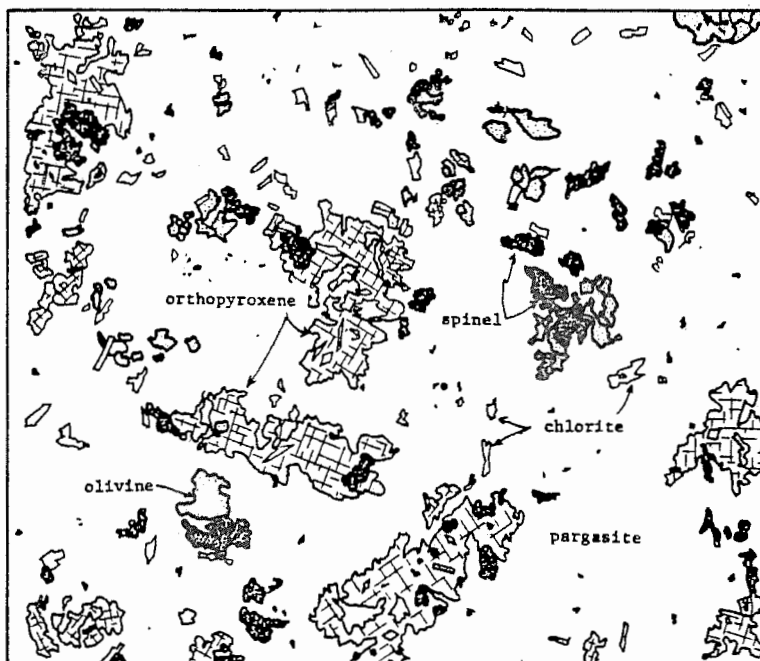


Figure 23. Sketch of specimen Y57I showing subhedral, randomly oriented orthopyroxene megacrysts. Blank areas represent fine- to medium-grained pargasite. Opaques are ilmenite and sulfides. Section is 1cm across.



Figure 24. Sketch of cut across pitted nodule in orthopyroxene-olivine hornblendite. Cr-rich spinel, rimmed by magnetite, is surrounded by fine grained chlorite. Randomly oriented pargasite, chlorite, spinel, and ilmenite make up the matrix. Long dimension is 2cm. Specimen Y57N.

### Hybridized Ultramafic Rocks

Phases characterizing hybridized rocks include anthophyllite, cummingtonite, plagioclase, quartz, garnet, phlogopite, and biotite. Depending on the predominant mineral(s), these rocks are divided into four categories, although some of the rocks overlap into more than one.

Two-amphibole rocks. Edges of some of the larger lenses and some entire small lenses are dominated by rocks which contain more than one amphibole. The amphiboles identified thus far are pargasite, hornblende, anthophyllite, and cummingtonite. Pargasite or hornblende is invariably present and may coexist with either of the other amphiboles. The presence of a pale amphibole can usually be detected in the field but distinction between anthophyllite and cummingtonite is difficult. At localities J98 and K34, the anthophyllite can be distinguished by a blue- to blue-green iridescence, characteristic of aluminous anthophyllite (Robinson, Ross, and Jaffe, 1971) that has exsolved to anthophyllite plus gedrite on a submicroscopic scale. Very commonly, these minerals exist in the plagioclase-bearing rocks. Pargasite in these rocks usually contains exsolution lamellae of cummingtonite. It may be optically zoned and, in most respects, appears similar to pargasite in the non-hybridized rocks.

The anthophyllite is pale pink and, in at least two specimens (Y570 and 500F), contains microscopic (010) exsolution lamellae. In many specimens, anthophyllite is seen as relatively coarse, poorly terminated, prismatic grains which may or may not be intergrown with pargasite. If in a foliated rock, anthophyllite lies within the plane of foliation and may define a weak layering.

Cummingtonite has various modes of occurrence: as an accessory phase;

as a major phase coexisting with pargasite; and as a major phase with hornblende overgrowths. It is distinguishable from pargasite by its lack of color, slightly higher birefringence, and, in some specimens, polysynthetic twinning. In some samples it is intergrown with pargasite. In specimen 500AW, a plagioclase-quartz bearing rock, pale pink (in thick section) cummingtonite has overgrowths of blue-green hornblende, with which it is optically continuous. The cummingtonite contains exsolution lamellae of hornblende. In no specimen are pargasite, anthophyllite, and cummingtonite all seen in mutual contact, although they may all be present in the same rock.

Plagioclase-bearing rocks. The only lens with discernible plagioclase within the body of ultramafic rock is at locality K34. At localities O18, K28N, K28S, and J98, plagioclase is present in contact-zone rocks which are considered to be part of the ultramafic bodies.

Specimen K34A contains 2.4% plagioclase, which is fine grained, evenly disseminated, and partially sericitized. Its composition as determined by microprobe analysis is An 96.

In contact-zone rocks, this mineral may be evenly disseminated or define a weak layering. It has a milky appearance in hand specimen if sericitization has been extensive. It occurs in hornblende-anthophyllite or hornblende-cummingtonite rocks. In specimen J98B, the composition as determined by optical methods is An 90-95.

Garnetiferous rocks. K34 is the only locality where garnet is observed to occur within the body of a lens. It is a stable part of an assemblage which includes pargasite, anthophyllite, and plagioclase. In hand specimen, the garnet is very pale pink and evenly distributed, with grains up to 4mm across. Where more abundant, the grains are coarser. This garnet is colorless in thin section and occurs as anhedral- to subhedral poikiloblasts



commonly intergrown with pargasite (Fig 25). It contains inclusions of both pargasite and plagioclase. Orthopyroxene is present in this rock but in very minor abundances. Ilmenite is the only oxide detected.

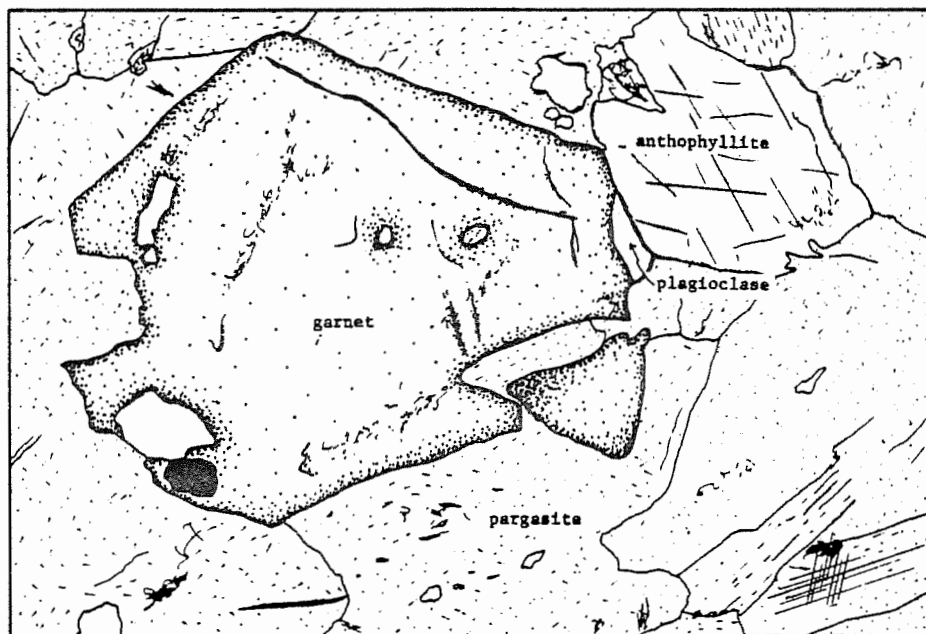


Figure 25. Sketch of Specimen K34A illustrating textural relationships between garnet, anthophyllite, pargasite, and plagioclase. Note "100" and "101" exsolution lamellae in pargasite at lower right. Long dimension = 1.36mm.

Biotite rocks. Abundant biotite is most notable at localities 500, 018, and 9Q9/N01, where it occurs in association with chlorite and/or hornblende, making up between 10 and 80% of given specimens. It forms very gritty rock and is usually restricted to zones of contact between the ultramafic lenses and country rock. In specimen 500AW, biotite forms a strong foliation and defines layering, bowing around pinch-and-swell layers of plagioclase and quartz. In the other samples from this locality, biotite is a more evenly distributed phase.

### Retrograded Rocks

Talc-carbonate assemblages are among the more common associations considered to be products of retrograde metamorphism of the ultramafic rocks. Such rocks were selectively avoided when collecting specimens for analyses. Rocks less severely affected by retrograde metamorphism contain pale green, fine grained magnesian chlorite. The occurrence of this phase in the orthopyroxene-olivine hornblendites usually corresponds to a decrease in the abundance of olivine, spinel, and/or orthopyroxene. The pargasite-chlorite rocks which result dominate major portions of outcrops at Y57, 9Q9/N01, and 500.

At localities Y57 and 9Q9, pargasite-chlorite rocks formed directly from non-hybridized orthopyroxene-olivine hornblendites. Fine-grained, secondary chlorite occurs in clusters believed to be pseudomorphs after orthopyroxene (Fig. 26). Optical zonation of pargasite is more prevalent in

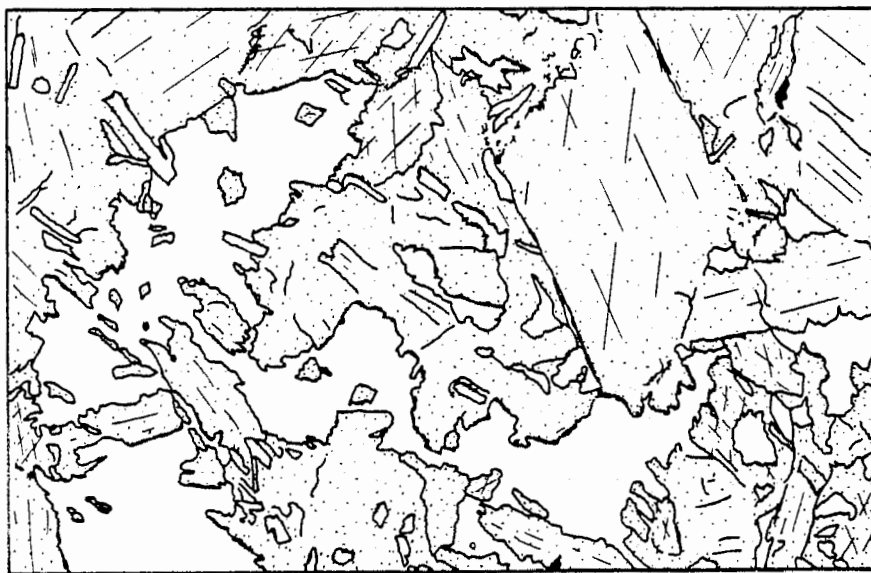


Figure 26. Sketch of retrograded orthopyroxene-olivine hornblendite showing relationships between secondary chlorite and pargasite. Stipple = pargasite; blank areas = secondary, pale-green chlorite. Chlorite is thought to be pseudomorphing orthopyroxene (compare with Figure 23). Long dimension = 1.36mm. Specimen Y57H.

the retrograded orthopyroxene-olivine hornblendites. Remaining olivine and orthopyroxene may occur either as scattered, discrete, small grains, or maintain their megacrystic nature. Traces of phlogopite are noted in many of these rocks. Small amounts of serpentine and magnetite appear in the expansion cracks of olivine that has been affected by late-stage hydration and oxidation. Similarly, magnetite-rich rims on chromian spinels within the nodules of specimen Y57N are believed to be oxidation products (Golding and Bayliss, 1968). Traces of carbonate are present near fine fractures.

At locality N01, pargasite-chlorite rocks contain up to 3% cummingtonite (Specimen N01J) and at 500, chlorite occurs as pseudomorphs after anthophyllite. These characteristics indicate that hybridization preceded retrograde metamorphism. The red-brown patches which characterize the outcrop at N01 are surface expressions of rounded patches within the rock which are composed of platy or fine-grained chlorite, carbonate, and/or talc, and are, apparently, replacing orthopyroxene or olivine. Carbonate, where present in specimens not characterized by these patches, occurs only adjacent to fine cracks.

#### Adjacent Country Rock

In most cases where a contact with the country rock is exposed, the country rock is an amphibolite or amphibolite grading to hornblendite. The most thoroughly investigated contact is at locality N01 (Plate 3) where a dark gray hornblende-plagioclase amphibolite grades to a hornblendite, approaching the contact with the retrograded and hybridized ultramafic rock (Specimens N01E, F, and G, resp.). Thin sections of these samples show the hornblende to be brown-green, equigranular, and euhedral. Plagioclase in one specimen (N01F) is completely sericitized, however, in another (N01E) it makes up about 45% of the sample. It has well developed twinning and contains fine intergrowths caused by unmixing.

## MINERALOGY

Hornblende

A pargasitic variety of hornblende dominates most of the specimens studied. It is optically homogeneous to weakly zoned in most prograde samples, with the exception of specimen 9Q9A, in which amphibole is distinctly zoned from colorless to pale-green, outward. Grain-size distribution is generally bimodal, with no significant compositional differences between coarse and fine fractions. Table 14 gives optical properties of selected homogeneous pargasites from prograde and hybridized rocks and of the zoned amphibole in specimen 9Q9A.

The homogeneous or weakly zoned pargasites contain exsolution lamellae which are indexed " $\bar{1}01$ " and "100", assuming a space group  $C2/m$  (Robinson, et al., 1971). In most of the pargasite observed, the "100" lamellae are more

Table 14. Optical properties of pargasites and zoned hornblende.

	<u>Orthopyroxene-Olivine Hornblendites</u>			<u>Hybridized Rocks</u>	
	Y57I	OG2B <sup>*</sup>	9Q9A (zoned)	K34A	J98B
Color:	pale green	pale green	colorless-pale green, outward	pale green	pale green
Indices: $\alpha$	1.630	1.634	1.625	1.635	1.639
$\beta$	1.641	1.645	1.639	1.645	1.648
$\gamma$	1.654	1.657	1.651	1.663	1.663
Estimated $2V_Z$ :	88°	88°	92-95°	88°	88°
$Z_{Ac}$ :	20°		18°	15°	
Twinning:				(100) lamellar	

\* Data provided by H.W. Jaffe, University of Massachusetts.

numerous yet finer than " $\bar{1}01$ ". One exception to this is specimen K34A, in which pargasite, coexisting with anthophyllite, garnet, and plagioclase, contains very well developed " $\bar{1}01$ " and " $100$ " lamellae. In all cases, the lamellae are too fine for optical determination of composition. However, because of the association in many of the specimens of pargasite and cummingtonite or anthophyllite, these lamellae are presumed to be  $\underline{P2}_1/\underline{m}$  cummingtonite (Robinson and Jaffe, 1969; Ross, Papike, and Shaw, 1969).

One wet chemical and numerous electron microprobe analyses are presented in Table 15. Structural formulae, first calculated on the basis of cations per 23 oxygens, have been adjusted for ferric iron by one of two methods: by assuming a ratio of A-site occupancy to tetrahedral aluminum of 0.300 (Robinson *et al.*, 1971) or, on the assumption that the formula contains 15 cations exclusive of Na and K, thus excluding Ca from the A-site and Na from the (M4) site.

All hornblende compositions, both before and after ferric iron correction, are plotted in terms of A-site occupancy and tetrahedral Al in Figure 27. For formulae in which the A-site occupancy to tetrahedral aluminum ratio is greater than .300, ferric iron was added until sufficient to achieve this ratio. This method is based upon a plot of numerous hornblende wet analyses that show compositional ranges along a line representing a constant ratio of A-site occupancy to tetrahedral aluminum of .300 (Robinson *et al.*, 1971; Robinson, pers. comm.; Ashwal, 1974). Note that the wet chemical formula from sample OG2B plots very close to this line indicating that correction of electron microprobe analyses on this basis should give good approximation of ferric iron content of the structural formula. This correction also has the effect of reducing calculated Ca content of the A-site. If Ca is still present in the A-site after application of the above adjustment or, if the initial A-site occupancy to tetrahedral aluminum ratio is less than .300, ferric iron is calculated on the basis of

Table 15. Thirty five analyses of pargasitic and actinolitic hornblende. All by electron microprobe, except where noted.

Locality	Y57I					9Q9A						
Analysis No.	2	3	4	10	22	42	43	53	54	9b	10b	11b
						Core	Rim	Core	Rim	Core	Rim	Rim
SiO <sub>2</sub>	46.95	46.88	47.78	50.37	49.14	56.95	54.00	54.02	49.53	54.80	50.67	50.80
TiO <sub>2</sub>	.52	.49	.51	.47	.47	.03	.23	.24	.53	.15	.40	.37
Al <sub>2</sub> O <sub>3</sub>	11.11	11.30	10.69	8.62	10.91	1.87	5.36	5.51	9.66	3.96	8.06	7.41
Cr <sub>2</sub> O <sub>3</sub>	.13	.10	.09	.21	.13	.03	.27	.18	.30	.23	.31	.33
FeO	6.98	6.69	7.00	8.44	7.01	4.62	6.29	5.61	5.90	5.26	6.02	5.32
MnO	.14	.07	.16	.22	.10	.08	.14	.12	.04	.09	.11	.09
MgO	18.18	18.52	17.68	20.05	17.34	22.49	20.40	20.17	18.25	21.46	19.73	19.01
NiO					.00	.00	.03	.02	.00			
CaO	11.96	12.05	11.99	9.37	11.52	11.92	10.68	11.70	12.03	11.80	11.15	11.98
Na <sub>2</sub> O	1.52	1.79	1.68	1.05	1.43	.16	.69	.54	1.02	.35	.87	.68
K <sub>2</sub> O	.21	.27	.25	.13	.24	.00	.08	.11	.14	.02	.11	.11
Total	97.70	98.16	97.83	98.93	98.29	98.15	98.12	98.22	97.40	98.12	97.43	96.10

# Structural formulae

Locality	Y57I					9Q9A						
Analysis No.	2	3	4	10	22	42	43	53	54	9b	10b	11b
						Core	Rim	Core	Rim	Core	Rim	Rim
Formula Basis*	.300	.300	.300	.300	.300	15	23	23	15	15	15	15
Si	6.604	6.542	6.708	6.982	6.873	7.807	7.477	7.469	6.968	7.550	7.090	7.204
P												
Al	<u>1.396</u>	<u>1.458</u>	<u>1.292</u>	<u>1.018</u>	<u>1.127</u>	<u>.193</u>	<u>.523</u>	<u>.531</u>	<u>1.032</u>	<u>.450</u>	<u>.910</u>	<u>.796</u>
$\Sigma$ (T site)	8.000	8.000	8.000	8.000	8.000	8.000	8.000	8.000	8.000	8.000	8.000	8.000
Al	.446	.401	.478	.391	.671	.110	.352	.367	.571	.193	.420	.443
Fe <sup>3+</sup>	.440	.601	.423	.201	.097	.026	.000	.000	.008	.100	.116	.030
Ti	.055	.051	.054	.049	.049	.003	.024	.025	.056	.016	.042	.039
Cr	.014	.011	.010	.023	.014	.003	.030	.020	.033	.025	.034	.037
Mg	3.811	3.851	3.699	4.141	3.615	4.595	4.210	4.156	3.827	4.407	4.115	4.017
Ni	.000	.000	.000	.000	.000	.000	.003	.002	.000	.000	.000	.000
Fe <sup>2+</sup>	<u>.234</u>	<u>.085</u>	<u>.336</u>	<u>.195</u>	<u>.554</u>	<u>.263</u>	<u>.381</u>	<u>.430</u>	<u>.505</u>	<u>.259</u>	<u>.273</u>	<u>.434</u>
$\Sigma$ M(1,2,3)	5.000	5.000	5.000	5.000	5.000	5.000	5.000	5.000	5.000	5.000	5.000	5.000
Fe <sup>2+</sup>	.148	.094	.063	.583	.168	.240	.347	.218	.182	.247	.315	.167
Mn	.017	.008	.019	.026	.012	.009	.016	.014	.005	.011	.013	.011
Ca	1.803	1.802	1.804	1.391	1.726	1.751	1.584	1.733	1.813	1.742	1.672	1.821
Na	<u>.032</u>	<u>.096</u>	<u>.114</u>	<u>.000</u>	<u>.093</u>	<u>.000</u>	<u>.053</u>	<u>.035</u>	<u>.000</u>	<u>.000</u>	<u>.000</u>	<u>.001</u>
$\Sigma$ M(4)	2.000	2.000	2.000	2.000	2.000	2.000	2.000	2.000	2.000	2.000	2.000	2.000
Na	.382	.389	.343	.282	.293	.043	.133	.110	.278	.094	.236	.186
K	<u>.038</u>	<u>.048</u>	<u>.045</u>	<u>.023</u>	<u>.043</u>	<u>.000</u>	<u>.014</u>	<u>.019</u>	<u>.025</u>	<u>.004</u>	<u>.020</u>	<u>.020</u>
$\Sigma$ (A site)	.420	.437	.388	.305	.336	.043	.147	.129	.303	.098	.256	.206

	Y57I					9Q9A						
	2	3	4	10	22	42	43	53	54	9b	10b	11b
x	.420	.437	.388	.305	.337	.043	.147	.129	.303	.098	.256	.206
y	1.010	1.115	1.019	.713	.880	.150	.430	.437	.729	.352	.654	.590
z	1.396	1.458	1.292	1.018	1.127	.193	.523	.531	1.032	.450	.910	.796
x+y	1.430	1.552	1.406	1.018	1.217	.193	.577	.566	1.032	.450	.910	.796
w	.034	.094	.114	.000	.090	.000	.054	.065	.000	.000	.000	.000
w/x+y	.024	.061	.081	.000	.074	.000	.094	.062	.000	.000	.000	.000
x/z	.300	.300	.300	.300	.300	.223	.281	.243	.294	.218	.281	.259
x/x+y	.294	.282	.276	.300	.277	.229	.255	.228	.295	.219	.281	.259
fe	.095	.046	.101	.163	.169	.100	.150	.137	.153	.105	.127	.132
Ca/Ca+Na	.813	.788	.798	.831	.817	.976	.895	.923	.867	.949	.876	.907
Fe <sup>3+</sup> /Fe <sup>3+</sup> +Fe <sup>2+</sup>	.536	.770	.515	.205	.118	.049	.000	.000	.012	.165	.165	.048

\* Fe<sup>3+</sup> corrections for microprobe analyses are made either on the basis of 15 cations, exclusive of Na and K (15), or by adjusting the A-site occupancy/tetrahedral Al ratio to .300 by addition of Fe<sup>3+</sup> (.300). 23 = 23 oxygens.

$$fe = Fe^{2+} + Mn / Fe^{2+} + Mn + Mg$$

x = Total of Na + K in the A site (A occupancy).

y = Total of Al + Fe<sup>3+</sup> + Cr<sup>3+</sup> + 2Ti in the M(2) site.

z = Total of Al + P in the T (tetrahedral) site.

w = x+y-z = Na in M(4) site.



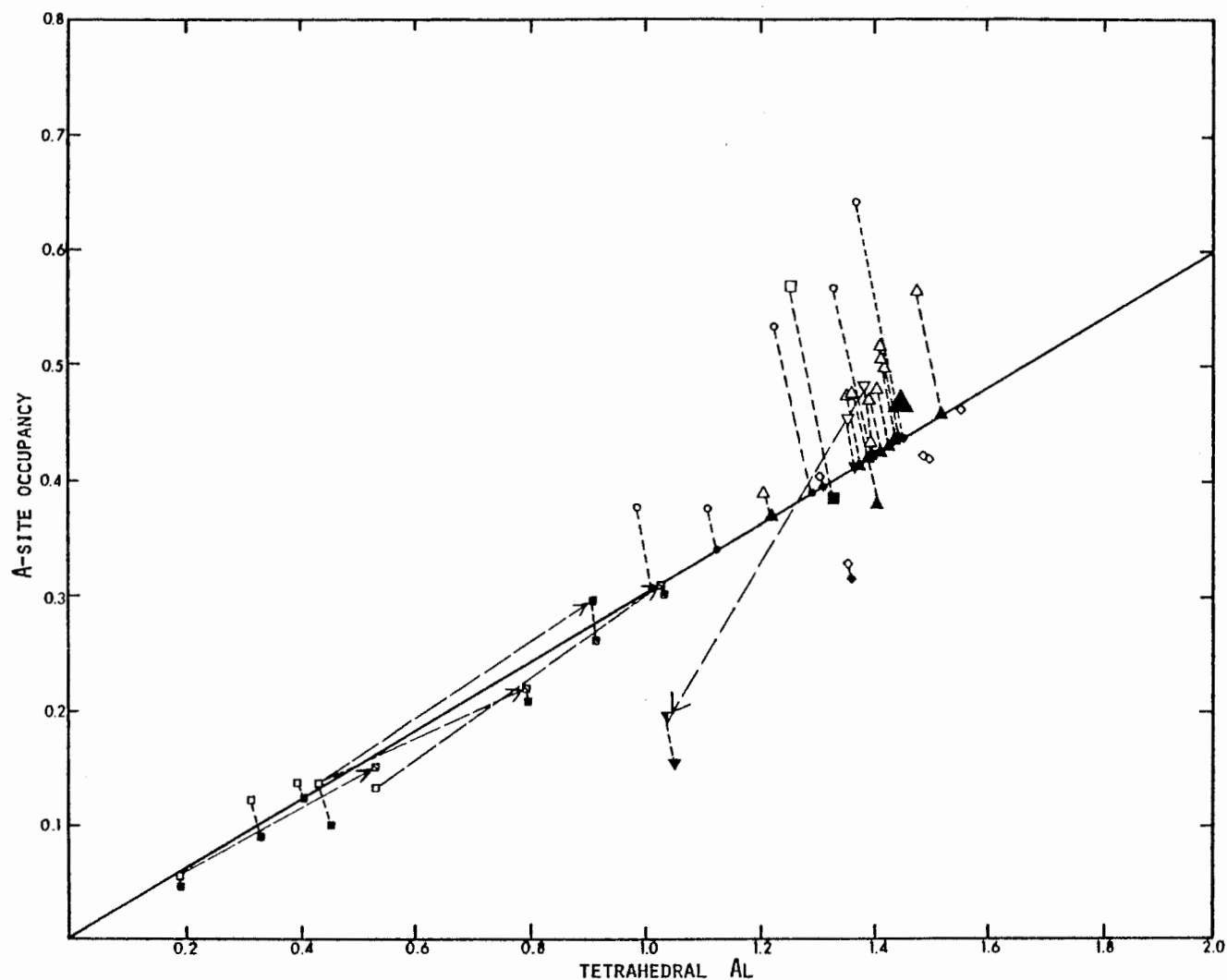


Figure 27. Plot of A-site occupancy versus tetrahedral Al for pargasitic and actinolitic amphiboles. Open symbols reflect uncorrected formulae and filled symbols formulae corrected for  $\text{Fe}^{3+}$  (see text). Solid diagonal line is a constant ratio of A-site occupancy to tetrahedral Al of .300. Corrected analyses are constrained to this line unless they are corrected to 15 cations or where no  $\text{Fe}^{3+}$  can be assigned. Circles = Y57I, small squares = 9Q9A (open = cores; with diagonals = rims), large squares = N01, small triangles = OG2B (large filled triangle = wet analysis), inverted triangles = N45A (open = cores; half filled = rims), diamonds = K34A. Arrows point from compositions of cores to compositions of rims.

Table 15. (Continued).

Locality Analysis No.	OG2B										
	wet <sup>1</sup>	3B <sup>2</sup>	7B	8B	15B	17B	18B	23B	28B	30B	34B
SiO <sub>2</sub>	46.28	46.80	46.20	47.00	46.00	46.80	46.20	46.50	46.10	46.00	46.60
TiO <sub>2</sub>	.64	.74	.68	.57	.74	.11	.03	.22	.06	.01	.04
Al <sub>2</sub> O <sub>3</sub>	12.65	13.00	12.90	12.30	12.80	13.30	13.60	14.30	13.90	13.70	12.00
Fe <sub>2</sub> O <sub>3</sub>	1.63										
Cr <sub>2</sub> O <sub>3</sub>	.14										
FeO	6.32	8.04	7.74	8.39	7.75	7.99	7.96	8.17	7.98	7.98	7.86
MnO	.13	.11	.11	.15	.13						
MgO	16.77	16.50	16.50	16.90	16.90	17.00	16.80	16.60	16.50	16.30	16.80
NiO	.04										
CaO	11.74	11.90	11.50	12.30	12.30	10.40	10.80	9.25	10.60	10.70	9.71
Na <sub>2</sub> O	1.58	1.77	1.62	1.39	1.67	1.72	1.75	1.86	1.80	1.66	1.48
K <sub>2</sub> O	.19										
H <sub>2</sub> O <sup>+</sup>	1.93										
H <sub>2</sub> O <sup>-</sup>	.23										
P <sub>2</sub> O <sub>5</sub>	.03										
F	.00										
Total	100.30	98.86	97.25	99.00	98.29	97.32	97.14	96.90	96.94	96.35	94.49

1 Mahito Kumanomido, analyst; Japan Analytical Research Institute. Grain-count of purified separate by H. W. Jaffe yielded 0.2% impurities of unknown composition.

2 A. E. Bence, analyst.

## Structural formulae

Locality		OG2B									
Analysis No.	wet	3B	7B	8B	15B	17B	18B	23B	28B	30B	34B
Formula Basis*		.300	.300	15	.300	.300	.300	.300	.300	.300	.300
Si	6.547	6.551	6.568	6.588	6.474	6.615	6.548	6.601	6.549	6.582	6.777
P	.003										
Al	<u>1.450</u>	<u>1.449</u>	<u>1.432</u>	<u>1.412</u>	<u>1.526</u>	<u>1.385</u>	<u>1.452</u>	<u>1.399</u>	<u>1.451</u>	<u>1.418</u>	<u>1.223</u>
$\Sigma$ (T site)	8.000	8.000	8.000	8.000	8.000	8.000	8.000	8.000	8.000	8.000	8.000
Al	.656	.696	.730	.621	.597	.832	.820	.995	.878	.893	.835
Fe <sup>3+</sup>	.178	.208	.144	.292	.312	.170	.235	.029	.185	.133	.063
Ti	.070	.078	.073	.060	.078	.012	.003	.023	.006	.001	.004
Cr	.017										
Mg	3.537	3.442	3.495	3.530	3.544	3.581	3.549	3.513	3.494	3.475	3.641
Ni	.009										
Fe <sup>2+</sup>	<u>.533</u>	<u>.576</u>	<u>.558</u>	<u>.497</u>	<u>.469</u>	<u>.405</u>	<u>.393</u>	<u>.440</u>	<u>.437</u>	<u>.498</u>	<u>.457</u>
$\Sigma$ M(1,2,3)	5.000	5.000	5.000	5.000	5.000	5.000	5.000	5.000	5.000	5.000	5.000
Fe <sup>2+</sup>	.211	.157	.218	.194	.131	.369	.315	.501	.326	.325	.436
Mn	.017	.013	.013	.018	.015	.000	.000	.000	.000	.000	.000
Ca	1.771	1.785	1.752	1.788	1.854	1.575	1.640	1.407	1.614	1.640	1.514
Na	<u>.002</u>	<u>.045</u>	<u>.017</u>	<u>.000</u>	<u>.001</u>	<u>.056</u>	<u>.045</u>	<u>.092</u>	<u>.060</u>	<u>.035</u>	<u>.050</u>
$\Sigma$ M(4)	2.000	2.000	2.000	2.000	2.000	2.000	2.000	2.000	2.000	2.000	2.000
Na	.428	.435	.430	.378	.456	.416	.436	.420	.436	.426	.367
K	<u>.035</u>										
$\Sigma$ (A site)	.463	.435	.430	.378	.456	.416	.436	.420	.436	.426	.367
OH	1.939										
F	.000										

## OG2B

	wet	3B	7B	8B	15B	17B	18B	23B	28B	30B	34B
x	.463	.435	.430	.378	.456	.416	.436	.420	.436	.426	.367
y	.992	1.060	1.020	1.033	1.071	1.026	1.061	1.070	1.075	1.028	.906
z	1.453	1.449	1.432	1.411	1.526	1.385	1.452	1.399	1.451	1.418	1.223
x+y	1.455	1.495	1.450	1.411	1.527	1.442	1.497	1.490	1.511	1.454	1.273
w	.002	.046	.018	.000	.001	.057	.045	.091	.060	.036	.050
w/x+y	.001	.031	.012	.000	.001	.040	.030	.061	.040	.025	.039
x/z	.319	.300	.300	.268	.300	.300	.300	.300	.300	.300	.300
x/x+y	.319	.291	.297	.268	.299	.288	.291	.282	.289	.293	.288
fe	.177	.178	.184	.167	.148	.178	.166	.211	.179	.191	.197
Ca/Ca+Na	.805	.788	.797	.825	.803	.770	.773	.733	.765	.781	.784
Fe <sup>3+</sup> /Fe <sup>3+</sup> +Fe <sup>2+</sup>	.193	.221	.157	.297	.342	.180	.250	.030	.196	.139	.066

\* Fe<sup>3+</sup> corrections for microprobe analyses are made either on the basis of 15 cations, exclusive of Na and K (15), or by adjusting the A-site occupancy/tetrahedral Al ratio to .300 by addition of Fe<sup>3+</sup> (.300).

$$fe = Fe^{2+} + Mn / Fe^{2+} + Mn + Mg$$

x = Total of Na + K in the A site (A occupancy).

y = Total of Al + Fe<sup>3+</sup> + Cr<sup>3+</sup> + 2Ti in the M(2) site.

z = Total of Al + P in the T (tetrahedral) site.

w = x+y-z = Na in M(4) site.

15 cations exclusive of Na + K, which automatically excludes Ca from the A-site. Those analyses with initial A-site occupancy to tetrahedral aluminum ratios of less than .300 and with no Ca assigned to the A-site are assumed to contain no ferric iron.

Analysis N01A was originally presented by Robinson and Jaffe (1969; Table 4) with its structural formula calculated on the basis of 23 oxygens. This formula has been recalculated on the basis of 15 cations, exclusive of Na and K in order to remove Ca from the A site. The resulting formula has a large amount of  $\text{Fe}^{3+}$ , causing a significant reduction in the  $\text{Fe}^{2+}/(\text{Fe}^{2+}+\text{Mg})$  ratio.

The corrected hornblende compositions, along with those of cummingtonite and anthophyllite from these lenses (Tables 15 and 17, respectively) are plotted in a modified ACF diagram in Figure 28. The loosely-clustered aluminous hornblendes are considered to be pargasite. Of this group, some of those from specimen K34A, a hybridized rock, contain the most Al. These same formulae also contain the least amount of ferric iron (Table 15). Note that the compositions of pargasites from K34A trend towards cummingtonite. This is most likely due to overlap of the microprobe beam with the cummingtonite exsolution lamellae. Therefore, the most aluminous of these analyses should represent the composition of the host pargasite. Similar reasoning accounts for the anomalous Ca-deficient composition from specimen Y57I (Analysis #10).

The pargasite in specimen N45A is weakly zoned, becoming depleted in Al and Na outward. Fe/Mg ratio also decreases. This pargasite (filled inverted triangles) trends outward toward actinolite, but still projects within the composition range of pargasite. The zoning of this pargasite is much weaker than, and directly opposite to, that of the hornblende at 9Q9.

Neither cores nor rims of the zoned amphiboles in specimen 9Q9A fall within the cluster defined by the pargasite composition. The cores are

Table 15. (Continued).

Locality	9Q9A		N45A			K34A						N01A
Analysis No.	8a	9a	1	2	3	32	38	9a	10a	11a	12a	N01A <sup>1</sup>
	Core	Core	Core	Rim	Core							
SiO <sub>2</sub>	55.61	54.58	46.12	48.57	46.17	44.88	46.29	44.85	46.62	44.95	45.67	47.20
TiO <sub>2</sub>	.07	.16	.95	.74	.90	1.41	.86	.84	.70	.90	.76	
Al <sub>2</sub> O <sub>3</sub>	2.80	3.93	11.98	9.05	12.02	14.74	13.04	14.10	12.33	14.08	13.00	10.50
Cr <sub>2</sub> O <sub>3</sub>	.00	.02	.17	.09	.23	.09	.13	.01	.02	.04	.00	
FeO	5.61	4.86	6.57	6.05	6.71	10.01	10.33	9.24	10.83	9.51	10.35	7.80
MnO	.09	.08	.01	.08	.06	.05	.08	.00	.00	.00	.00	.30
MgO	22.34	20.91	16.30	18.12	16.96	13.88	15.47	14.75	16.11	14.73	15.61	18.00
NiO						.00	.11					
CaO	10.95	12.03	12.28	12.07	11.89	10.72	9.66	10.89	9.20	10.57	9.16	12.40
Na <sub>2</sub> O	.32	.55	1.45	1.00	1.42	1.66	1.55	1.43	1.38	1.52	1.04	1.40
K <sub>2</sub> O	.00	.02	.27	.20	.29	.17	.18	.14	.11	.11	.11	
Total	97.79	97.14	96.19	95.97	96.65	97.61	97.70	96.25	97.29	96.41	95.70	97.60

1 Analysis from Robinson and Jaffe (1969).

Structural formulae

Locality	9Q9A		N45A			K34A						N01A
Analysis No.	8a	9a	1	2	3	32	38	9a	10a	11a	12a	N01A
	Core	Core	Core	Rim	Core							
Formula Basis*	15	.300	.300	15	.300	23	.300	23	.300	23	15	15
Si	7.670	7.598	6.625	6.943	6.592	6.437	6.616	6.497	6.681	6.503	6.631	6.664
P												
Al	<u>.330</u>	<u>.402</u>	<u>1.375</u>	<u>1.057</u>	<u>1.408</u>	<u>1.563</u>	<u>1.384</u>	<u>1.503</u>	<u>1.319</u>	<u>1.497</u>	<u>1.369</u>	<u>1.336</u>
$\Sigma$ (T site)	8.000	8.000	8.000	8.000	8.000	8.000	8.000	8.000	8.000	8.000	8.000	8.000
Al	.126	.242	.655	.468	.618	.930	.814	.906	.764	.905	.857	.412
Fe <sup>3+</sup>	.104	.035	.120	.262	.167	.000	.002	.000	.014	.000	.033	.540
Ti	.007	.017	.104	.080	.097	.152	.092	.092	.075	.098	.083	.000
Cr	.000	.002	.019	.010	.025	.010	.015	.001	.002	.005	.000	.000
Mg	4.591	4.338	3.491	3.860	3.610	2.967	3.295	3.185	3.440	3.176	3.378	3.787
Ni	.000	.000				.000	.013	.000	.000	.000	.000	
Fe <sup>2+</sup>	<u>.172</u>	<u>.366</u>	<u>.612</u>	<u>.320</u>	<u>.482</u>	<u>.941</u>	<u>.464</u>	<u>.816</u>	<u>.705</u>	<u>.816</u>	<u>.649</u>	<u>.261</u>
$\Sigma$ M(1,2,3)	5.000	5.000	5.000	5.000	5.000	5.000	5.000	5.000	5.000	5.000	5.000	5.000
Fe <sup>2+</sup>	.371	.165	.057	.141	.152	.260	.464	.303	.579	.335	.574	.121
Mn	.011	.009	.012	.010	.007	.006	.010	.000	.000	.000	.000	.004
Ca	1.618	1.794	1.891	1.849	1.820	1.647	1.479	1.690	1.413	1.639	1.426	1.875
Na	<u>.000</u>	<u>.032</u>	<u>.040</u>		<u>.021</u>	<u>.087</u>	<u>.047</u>	<u>.008</u>	<u>.007</u>	<u>.030</u>	<u>.000</u>	<u>.000</u>
$\Sigma$ M(4)	2.000	2.000	2.000	2.000	2.000	2.000	2.000	2.000	2.000	2.000	2.000	2.000
Na	.086	.116	.364	.139	.371	.375	.382	.394	.379	.401	.293	.383
K	<u>.000</u>	<u>.004</u>	<u>.049</u>	<u>.018</u>	<u>.052</u>	<u>.031</u>	<u>.033</u>	<u>.026</u>	<u>.020</u>	<u>.020</u>	<u>.020</u>	<u>.000</u>
$\Sigma$ (A site)	.086	.120	.413	.157	.423	.406	.415	.420	.396	.421	.313	.383

	9Q9A		N45A			K34A					N01A	
	8a	9a	1	2	3	32	38	9a	10a	11a	12a	N01A
x	.086	.120	.413	.157	.423	.406	.415	.420	.396	.421	.313	.383
y	.244	.313	1.002	.900	1.004	1.244	1.015	1.091	.930	1.106	1.056	.953
z	.330	.402	1.375	1.057	1.408	1.563	1.384	1.503	1.319	1.497	1.369	1.336
x+y	.330	.433	1.415	1.057	1.427	1.650	1.431	1.511	1.326	1.527	1.369	1.336
w	.000	.031	.040	.000	.021	.087	.047	.008	.007	.030	.000	.000
w/x+y	.000	.072	.028	.000	.015	.053	.033	.005	.005	.020	.000	.000
x/z	.261	.300	.300	.149	.300	.260	.300	.279	.300	.281	.229	.287
x/x+y	.261	.277	.292	.104	.170	.246	.290	.278	.299	.276	.229	.287
fe	.108	.111	.163	.122	.151	.289	.274	.260	.272	.266	.266	.092
Ca/Ca+Na	.950	.924	.824	.930	.823	.781	.775	.808	.787	.794	.830	.830
Fe <sup>3+</sup> /Fe <sup>3+</sup> +Fe <sup>2+</sup>	.161	.061	.152	.362	.208	.000	.002	.000	.011	.000	.026	.586

\* Fe<sup>3+</sup> corrections for microprobe analyses are made either on the basis of 15 cations, exclusive of Na and K (15), or by adjusting the A-site occupancy/tetrahedral Al ratio to .300 by addition of Fe<sup>3+</sup> (.300). 23 = 23 oxygens.

$$fe = Fe^{2+} + Mn / Fe^{2+} + Mn + Mg$$

x = Total of Na + K in the A site (A occupancy).

y = Total of Al + Fe<sup>3+</sup> + Cr<sup>3+</sup> + 2Ti in the M(2) site.

z = Total of Al + P in the T (tetrahedral) site.

w = x+y-z = Na in M(4) site.



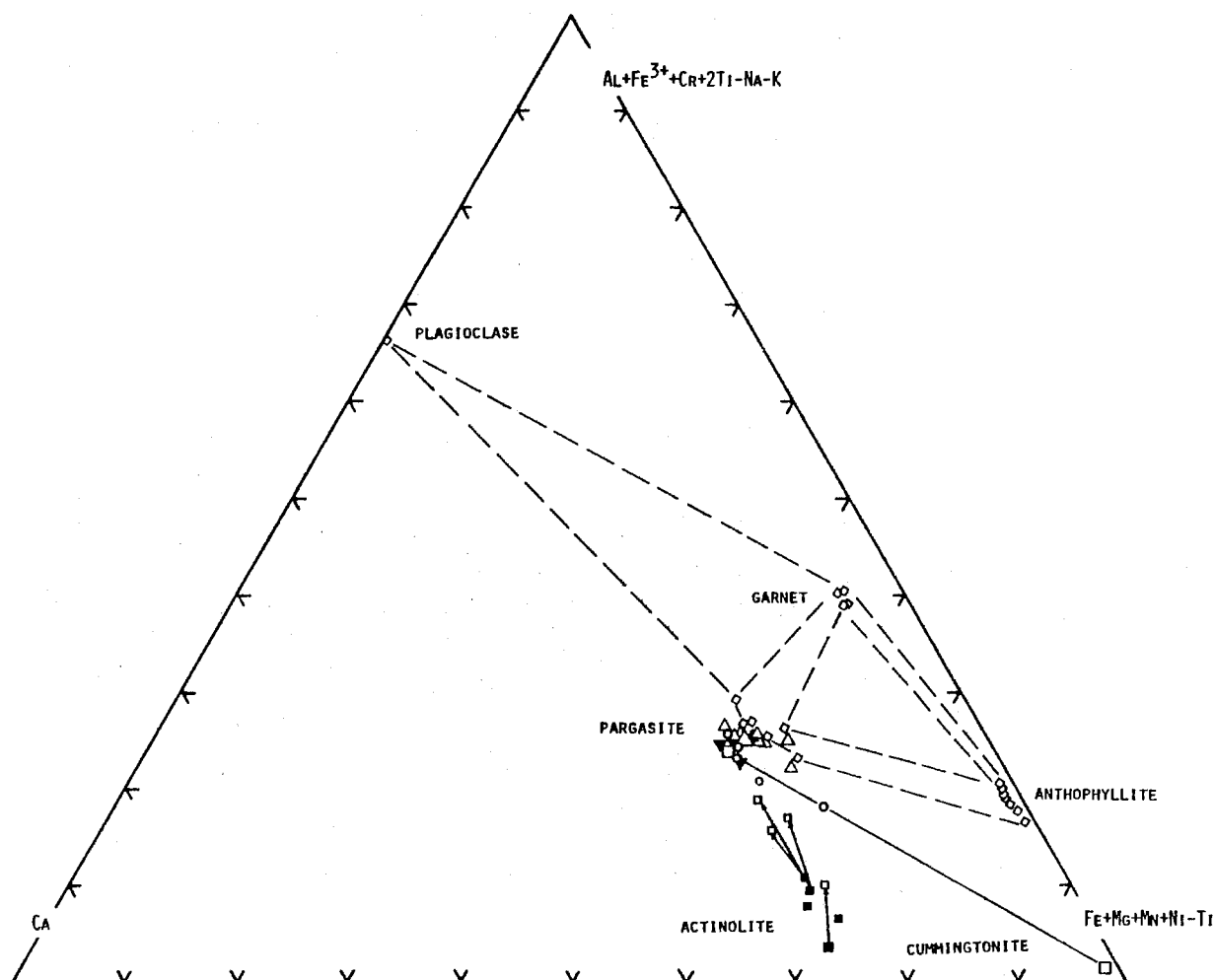


Figure 28. Modified ACF diagram showing compositions of amphiboles, garnet, and plagioclase. Open circles = Y57I, squares = 9Q9A (filled = amphibole cores; open = amphibole rims), large squares = N01, triangles = OG2B (large triangle = wet analysis), inverted filled triangles = N45A, diamonds = K34A.

depleted in Al and trend toward actinolite. The rims are iron enriched with respect to the cores (Table 15). The fact that exsolution lamellae do not extend into these rims indicates that the cummingtonite component decreases outward, with increasing  $\text{Fe}/(\text{Fe}+\text{Mg})$  ratio. This is contrary to the findings of Ross, Papike, and Shaw (1969) who report a decrease in cummingtonite phase in host actinolite with decreasing  $\text{Fe}/(\text{Fe}+\text{Mg})$  ratio. This difference suggests that some other property, such as increasing alumina content, may be over-shadowing the effect of changing  $\text{Fe}/(\text{Fe}+\text{Mg})$  ratio. The possibility also exists that the low-alumina hornblende was cleansed of cummingtonite component by the metamorphic reaction which formed the aluminous rims.

#### Cummingtonite

Cummingtonite most commonly occurs in trace amounts in many of the orthopyroxene-olivine hornblendites, where it is seen as poorly terminated prismatic grains which may or may not lie within the foliation plane. It is more common in the hybrid rocks, reaching 20 to 25 modal percent in specimen 9Q9B (Table 6). In this particular specimen, cummingtonite appears both as discrete grains within the foliation plane and as overgrowths on pale-green hornblende. In specimen 500AW, a plagioclase-quartz bearing rock, cummingtonite occurs with optically continuous blue-green hornblende overgrowths. Diagnostic optical properties are given in Table 16.

Table 16. Optical properties of cummingtonite.

Color: colorless  
 Birefringence: high with respect to pargasite (second order blue).  
 Twinning: lamellar (100) common but not always present.  
 $Z_{\text{Ac}}$ :  $19^\circ$   
 Estimated  $2V$ :  $80-85^\circ$   
 Optic sign: positive

Table 17. Electron probe analyses of cummingtonite and anthophyllite.

Locality	<u>Cummingtonite</u>			<u>Anthophyllite</u>					Ave <sup>2</sup> (3)
	N01A <sup>1</sup>			K34					
Analysis No.		28	40	41	1a	<u>6a</u>	<u>7a</u>	<u>8a</u>	
SiO <sub>2</sub>	56.20	49.18	49.89	48.64	49.35	48.45	48.48	49.16	48.70
TiO <sub>2</sub>		.50	.40	.40	.14	.29	.34	.31	.31
Al <sub>2</sub> O <sub>3</sub>	.60	9.93	9.24	10.55	9.35	9.78	10.21	9.81	9.93
Cr <sub>2</sub> O <sub>3</sub>		.14	.09	.02	.00	.00	.00	.00	.00
FeO	17.40	16.36	16.43	16.11	16.17	15.75	15.70	15.95	15.80
MnO	.70	.44	.24	.26	.13	.09	.18	.12	.13
MgO	21.20	19.58	20.09	20.09	20.37	20.43	20.08	20.38	20.30
NiO		.21	.00	.05					
CaO	.80	.87	.81	.82	.60	.87	.84	.85	.85
Na <sub>2</sub> O	.10	1.15	1.12	1.28	1.21	1.00	1.24	1.13	1.12
K <sub>2</sub> O		.02	.00	.00	.00	.00	.00	.00	.00
Total	97.00	98.38	98.31	98.22	97.33	96.66	97.07	97.71	97.14

1 Analysis provided by Robinson and Jaffe (1969).

2 Underlined analyses are averaged. 6a, 7a, and 8a are the same grain.

Formulae containing Fe<sup>3+</sup> calculated on the basis of 15 cations; others on the basis of 23 oxygens.

<u>Cumingtonite</u>		<u>Anthophyllite</u>							
Analysis No.	N01A	28	40	41	1a	6a	7a	8a	Ave
Si	8.021	6.969	7.054	6.886	7.039	6.941	6.934	6.976	6.949
Al		<u>1.031</u>	<u>.946</u>	<u>1.114</u>	<u>.961</u>	<u>1.059</u>	<u>1.066</u>	<u>1.024</u>	<u>1.051</u>
Total	8.021	8.000	8.000	8.000	8.000	8.000	8.000	8.000	8.000
Al	.090	.628	.594	.647	.608	.589	.654	.625	.620
Ti		.053	.043	.043	.012	.030	.034	.034	.033
Cr		.016	.010	.002					
Fe <sup>3+</sup>				.026		.132		.022	.056
Mg	4.520	4.135	4.233	4.239	4.327	4.249	4.281	4.310	4.291
Ni		.024		.006					
Fe <sup>2+</sup>	<u>.390</u>	<u>.144</u>	<u>.120</u>	<u>.037</u>	<u>.053</u>		<u>.031</u>	<u>.009</u>	
Total	5.000	5.000	5.000	5.000	5.000	5.000	5.000	5.000	5.000
Mg						.109			.026
Fe <sup>2+</sup>	1.690	1.795	1.823	1.845	1.871	1.752	1.845	1.860	1.828
Mn	.090	.053	.029	.031	.012	.009	.020	.012	.016
Ca	.120	.132	.123	.124	.087	.130	.126	.128	.130
Na	<u>.030</u>	<u>.020</u>	<u>.025</u>		<u>.030</u>		<u>.009</u>		
Total	1.930	2.000	2.000	2.000	2.000	2.000	2.000	2.000	2.000
Na		.296	.282	.352	.301	.278	.335	.308	.310
K		<u>.004</u>							
Total		.300	.282	.352	.301	.278	.335	.308	.310
<u>Fe+Mn</u>	.324	.325	.318	.311	.309	.288	.340	.304	.299
Fe+Mn+Mg									
Ca									
Ca+Na	.817	.295	.286	.261	.224	.319	.273	.294	.295
A-site									
Tet Al		.291	.298	.316	.313	.263	.314	.301	.295

No exsolution lamellae are resolved in the cummingtonite occurring within the orthopyroxene-olivine hornblendite; however, the cummingtonite in specimen 500AW, which has hornblende overgrowths, contains very fine ("101") and ("100") exsolution lamellae, assumed to be  $\underline{C2/m}$  hornblende (Robinson et al., 1968).

The only analysis of cummingtonite coexisting with pargasite from these lenses is provided by Robinson and Jaffe (1969) from locality N01 (Fig. 2; Plate 3). This analysis and calculated structural formula is presented in Table 17 and plotted along with coexisting hornblende in Figure 28. Cummingtonite is enriched in iron relative to coexisting hornblende, however, the Ca/Ca+Na ratios are similar in spite of the small amount of sodium and calcium present in the cummingtonite.

### Anthophyllite

Pale pink anthophyllite is found in hybridized rocks, generally associated with the margins of these bodies, where it appears as poorly terminated prismatic grains which may or may not lie within the plane of foliation. It coexists with pargasite and plagioclase in most cases, and is associated with orthopyroxene in specimens J98B and K34A. The latter two specimens are considered to represent slightly higher grade rocks than specimens from lenses to the north (Fig. 2).

A sufficient amount of anthophyllite was separated from specimens K34A and J98B for oil immersion study. These are plagioclase-bearing, hybridized rocks. Optical properties are given in Table 18.

Table 18. Optical properties of anthophyllite.

	K34A	J98B
Pleochroism:	Y = Z = pale pink X = colorless	Y = Z = pale pink X = colorless
Indices: $\alpha$	1.641	1.635
$\beta$	1.650	1.652
$\gamma$	1.662	1.665
Calculated 2V: *	80°(+)	86°(-)
Dispersion:	r < v, weak	r < v, weak
Extinction	parallel	parallel

\* calculated from Mertie chart (Mertie, 1942).

Electron microprobe analyses of anthophyllite from specimen K34A are given in Table 17. Ferric iron estimates are made on the basis of 15 cations, assuming no Ca in the A-site. Figure 29 shows the tetrahedral Al content of the K34A anthophyllite plotted against A-site occupancy. The heavy line represents a constant ratio of A-site occupancy to tetrahedral Al of .25, as suggested by a plot of published anthophyllite-gedrite wet chemical analyses calculated on the basis of 23 oxygens (Robinson *et al.*, 1971, Fig. 4). All of the analyses, even after the ferric iron correction on the basis of 15 cations, plot slightly above this line. Adjustment of these analyses to bring them onto this linear trend would result in the addition of a small amount of ferric iron and a slight reduction in A-site occupancy. However, in view of the fact that the coexisting hornblende is also very low in ferric iron (Table 15), this minor adjustment was not deemed worthwhile. Correction on the basis of 15 cations was considered necessary to insure expulsion of calcium from the A-site, as seems probable on crystal chemical grounds (Robinson *et al.*, 1971).

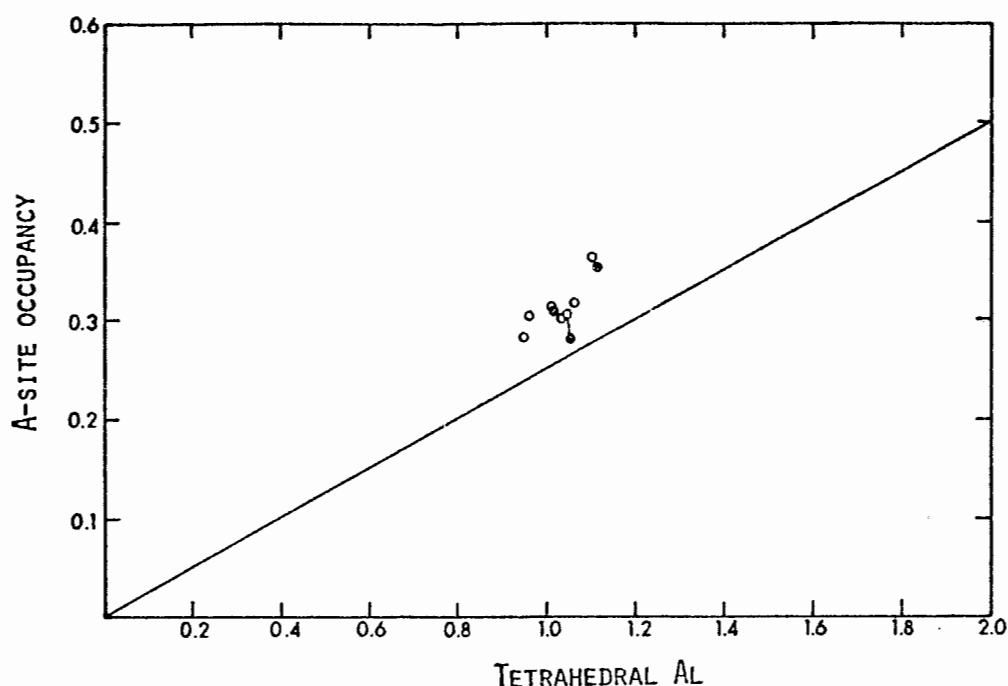


Figure 29. Electron microprobe analyses of anthophyllite from locality K34 plotted in terms of A-site occupancy versus tetrahedral Al. Diagonal line represents a constant ratio of A-site to tetrahedral Al of .25 based on numerous wet analyses of anthophyllites (Robinson *et al.*, 1971). Open circles are uncorrected formulae; closed circles are formulae corrected on the basis of 15 cations exclusive of Na and K.

These compositions are plotted along with coexisting pargasite and garnet in Figure 28, a modified ACF diagram. They lie approximately midway between end-member anthophyllite (the F apex) and ideal gedrite, ignoring iron to magnesium ratios. A plot in terms of Fe/Fe+Mg against tetrahedral Al, however, shows these analyses to lie midway between two idealized end members in a system involving ideal gedrite and anthophyllite in which 2 Fe<sup>2+</sup> ions have substituted for Mg<sub>2</sub> in the (M4) site (Fig. 30). The composition at the midpoint is Na<sub>.25</sub>(Fe<sub>2</sub>)(Mg<sub>4.25</sub>Al<sub>.75</sub>)Si<sub>7</sub>Al<sub>10</sub>O<sub>22</sub>(OH)<sub>2</sub>. The composition of analysis K34-28, which plots closest to this point, is Na<sub>.30</sub>(Na<sub>.02</sub>Ca<sub>.13</sub>Mn<sub>.05</sub>Fe<sub>1.8</sub><sup>2+</sup>)(Mg<sub>4.14</sub>Fe<sub>.14</sub><sup>2+</sup>Ni<sub>.02</sub>Al<sub>.63</sub>Cr<sub>.02</sub>Ti<sub>.05</sub>)Si<sub>6.97</sub>Al<sub>1.03</sub>O<sub>22</sub>(OH)<sub>2</sub>. This is similar to the compositions of an anthophyllite from

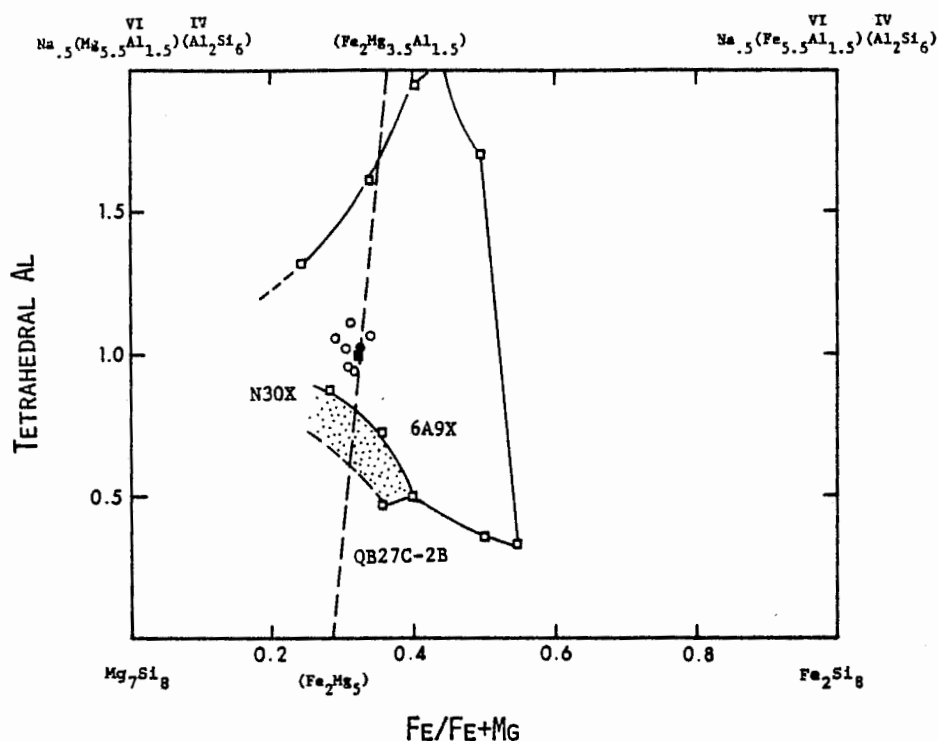


Figure 30. Electron microprobe analyses of anthophyllite from locality K34 plotted in terms of tetrahedral Al versus Fe/Fe+Mg. Dashed line represents the locus of compositions with  $2\text{Fe}^{2+}$  ions substituting for Mg. Open squares are compositions limiting the field of anthophyllite stability in sillimanite muscovite zone extended to include the stippled area in the sillimanite-orthoclase zone as taken from Robinson *et al.* (1971; Figure 10). Open circles K34A anthophyllites, closed circle = anthophyllite K34A-28. Closed square = midpoint of dashed line.

Greenland in which Bøggild (1905) first reported iridescence (Robinson *et al.*, 1971), and similar to specimen I34B, an iridescent anthophyllite from the "Amphibole Hill Area" within the sillimanite zone (Robinson and Jaffe, 1969).

Iridescence colors observed in the anthophyllite at localities K34 and J98 range from yellowish green to deep blue. No exsolution lamellae are discernible under the microscope, consistent with the findings of Robinson *et al.* (1971) that anthophyllite displaying iridescence contains



(010) lamellae below the resolving power of the light microscope. Their findings also indicate a lower Al content in iridescent anthophyllite than in anthophyllite with visible lamellae. The anthophyllite in specimen Y570 is observed to have very fine (010) exsolution lamellae which have branching and variable thickness characteristics similar to lamellae in sample I38DX (Robinson et al., 1971, Fig. 12). If, indeed, lamellae thickness is a function of Al content, then the anthophyllite at locality Y57 should be more aluminous than that at K34 and J98.

Figure 30 also shows the stability field of anthophyllite coexisting with plagioclase in sillimanite-zone rocks. Compositions N30X and 6A9X are in the sillimanite-muscovite zone and coexist with hornblende. Composition QB27C-2B coexists with hornblende and cummingtonite in the sillimanite-orthoclase zone, and is seen to extend the field of anthophyllite stability (Robinson et al., 1971). Note that the compositions from K34A, which is in the sillimanite-orthoclase-muscovite zone, are not consistent with the trend established by QB27C-2B, N30X, and 6A9X.

Figure 31 represents the actinolite-hornblende-anthophyllite-gedrite ternary reciprocal system. In Figure 31A, compositions of pargasite from specimen K34A are plotted along with coexisting anthophyllite. Four of the pargasite analyses, represented by open circles in this figure, are of a single grain and extend over a significant range of Ca and Al content. This is a random compositional change with respect to distance from grain edge and is not due to zoning. This grain, however, does contain coarse exsolution lamellae, which are probably cummingtonite, as shown by the trend of the pargasite compositions. Any analysis which includes part of a lamella will be correspondingly lower in Ca and Al. Therefore, the composition of the pargasite host is taken as the most calcic and aluminous analysis, and is labelled K34A-9A in Figure 31. This pargasite grain is

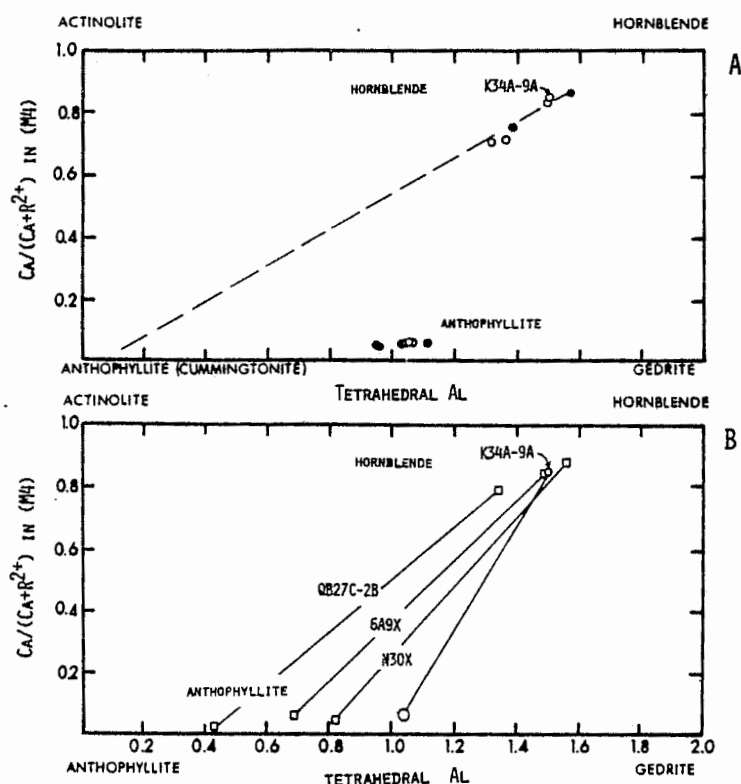


Figure 31. Actinolite-hornblende-anthophyllite-gedrite ternary reciprocal system.

A. Pargasite-anthophyllite pairs from locality K34. Closed circles are individual analyses of separate grains; open circles are analyses of a single pargasite and a single anthophyllite grain. Dashed line indicates the trend of analyses of exsolved pargasite toward cummingtonite composition of lamellae.

B. Sillimanite zone pargasite-anthophyllite pairs from localities K34 (this study), 6A9X, N30X, and QB27C-2B (Robinson *et al.*, 1971). Large open circle is an average of 3 analyses of a single anthophyllite grain. K34A-9A is the most aluminous of four analyses of a single pargasite. QB27C-2B is from sillimanite-orthoclase zone rocks.

in contact with an anthophyllite grain of which three analyses are available. These are shown as open circles at the bottom of Figure 31A and show no significant variation in composition. The closed circles in Figure 31A represent analyses of individual pargasite or anthophyllite grains. The composition of anthophyllite coexisting with pargasite K34A-9A is taken as the average (corrected for  $\text{Fe}^{3+}$ ) of the single anthophyllite grain and is plotted in Figure 31B. Composition 6A9X

and N30X are compositions from wet chemical analyses, first reported by Robinson and Jaffe (1969), which have been recalculated on the basis of 23 oxygens (Robinson *et al.*, 1971). The fractionation of tetrahedral Al between coexisting hornblende and anthophyllite in these two samples is greater than in specimen K34A. This is consistent with a lower temperature of formation for these rocks as compared to specimen K34A, which lies in the sillimanite-orthoclase-muscovite zone (Figure 2). Specimen QB27C-2B, however, which is from the sillimanite-orthoclase zone, has more strongly fractionated tetrahedral Al than specimen K34A. This is in direct conflict with the trends noted in the other specimens.

### Orthopyroxene

Pale pink orthopyroxene occurs in varying abundances in the orthopyroxene-olivine hornblendites, most commonly in the form of megacrysts ranging in size up to 2.5cm. Small amounts are also found in anthophyllite-bearing hybridized rocks (specimens K34A and J98B).

Sufficient orthopyroxene was separated from specimen Y57I for oil immersion study. This mineral was also separated from specimen OG2B by H.W. Jaffe (University of Massachusetts). Optical properties and estimated maximum Fs content of these separates are given in Table 19.

Table 19. Optical properties of orthopyroxene.

	Y57I	OG2B*
Pleochroism:	Y = Z = colorless X = pale pink	
Indices: $\alpha$	1.677	1.681
$\beta$	1.686	1.688
$\gamma$	1.691	1.693
Estimated $2V_X$ :	$85^\circ (-)$	$88^\circ (-)$
Dispersion:	$r > v$ , weak	$r > v$ , weak
Estimated Composition:	Fs 22	Fs 24

\* Optical data provided by H.W. Jaffe, University of Massachusetts.

Both wet chemical and electron microprobe analyses of orthopyroxene, with calculated structural formulae, are given in Table 20. In view of the small amount of ferric iron in the wet analysis, adjustment of the microprobe analyses for  $\text{Fe}^{3+}$  was not considered worthwhile. There is a wider variation in the individual analyses from specimen OG2B than from the other samples. For this reason, only the five most similar analyses are included in the average.

Figure 32 shows orthopyroxene compositions in terms of Si,  $(\text{Al}+\text{Cr}+\text{Fe}^{3+})$ , and  $(\text{Mg}+\text{Fe}+\text{Mn}+\text{Ca})$ . With the exception of N45A, the averaged compositions plot very close together and are slightly deficient in Si. N45A has a similar Al content, but is more enriched in Si. A single composition derived from a microprobe analysis (#19, OG2B; Table 20) plots close to that calculated from the wet chemical analysis. The latter has been recalculated so that all Fe is considered  $\text{Fe}^{2+}$  for better comparison with the microprobe formula. In these compositions, Al is significantly higher than in the others. The high Al of the wet analysis might be due to impurities (.1% pargasite, .1% spinel, .8% unknowns). S. A. Morse (pers. comm.) suggests that it is erroneous and due to incorrect analysis of some  $\text{MgO}$  as  $\text{R}_2\text{O}_3$ . Note the low cation sum of the wet analysis (Table 20). There is no evidence however, that the microprobe beam overlapped any aluminous phase and analysis 19 is more likely correct, suggesting specimen inhomogeneity resulting from local disequilibrium.

Aluminum is accommodated in orthopyroxene by the coupled substitution  $\text{Al}-\text{Al}$  for  $\text{Mg}-\text{Si}$ . It substitutes for Mg over Fe because of more similar ionic radii, and will, therefore, tend to increase the  $(\text{Fe}/\text{Fe}+\text{Mg})$  ratio. The Al content of orthopyroxene in equilibrium with olivine and spinel is considered to be an effective geothermometer (Anastasiou and Seifert, 1972; Obata, 1976; Fujii, 1976; Danckwerth and Newton, 1978). These orthopyroxenes, however, show no significant compositional variations correlative with the estimated metamorphic temperature gradient across this region (Tracy, 1975).

Table 20. Twenty three analyses of orthopyroxene. All by electron microprobe except as noted.

Locality	Y571						9Q9A					
Analysis No.	<u>1</u>	<u>11</u>	<u>2a</u>	<u>4a</u>	<u>10a</u>	Ave <sup>#</sup> (5)	<u>44</u>	<u>56</u>	<u>57</u>	5a	7a	Ave <sup>#</sup> (3)
SiO <sub>2</sub>	54.34	54.17	53.27	54.06	54.27	54.02	53.68	54.54	54.63	54.66	54.26	54.35
TiO <sub>2</sub>	.06	.05	.05	.03	.03	.04	.05	.04	.05	.04	.00	.04
Al <sub>2</sub> O <sub>3</sub>	2.27	2.19	2.36	2.16	2.35	2.27	2.22	2.19	2.11	2.27	2.17	2.19
Cr <sub>2</sub> O <sub>3</sub>	.02	.00	.00	.00	.00	.00	.10	.08	.06	.07	.00	.06
FeO	15.04	14.77	15.75	14.89	15.01	15.09	13.68	13.61	13.81	13.76	13.72	13.72
MnO	.33	.33	.29	.30	.20	.29	.27	.29	.27	.25	.30	.28
MgO	28.63	28.70	28.41	29.05	28.72	28.70	29.95	28.93	29.38	29.36	29.56	29.44
NiO							.00	.05	.00			.02
CaO	.17	.19	.19	.16	.20	.18	.16	.19	.19	.15	.16	.17
Na <sub>2</sub> O	.00	.00	.03	.08	.05	.03	.00	.01	.02	.08	.01	.02
K <sub>2</sub> O	.02	.00	.00	.00	.00	.00	.00	.00	.00	.00	.00	.00
Total	100.88	100.40	100.35	100.73	100.83	100.62	100.11	99.93	100.52	100.64	100.18	100.29

# Underlined analyses are averaged.

Formulae calculated on the basis of 6 oxygens.

Analysis No.	Y57I						9Q9A					
	<u>1</u>	<u>11</u>	<u>2a</u>	<u>4a</u>	<u>10a</u>	Ave (5)	<u>44</u>	<u>56</u>	<u>57</u>	5a	7a	Ave (3)
Si	1.935	1.935	1.916	1.929	1.931	1.929	1.916	1.946	1.939	1.937	1.933	1.935
Al	.065	.065	.084	.071	.069	.071	.084	.054	.061	.063	.067	.065
Total	<u>2.000</u>	<u>2.000</u>	<u>2.000</u>	<u>2.000</u>	<u>2.000</u>	<u>2.000</u>	<u>2.000</u>	<u>2.000</u>	<u>2.000</u>	<u>2.000</u>	<u>2.000</u>	<u>2.000</u>
Al	.030	.026	.015	.019	.029	.025	.008	.025	.027	.032	.024	.027
Ti	.001		.001			.001	.001	.001	.001			.001
Cr							.002	.002	.001	.001		.002
Mg	1.519	1.528	1.523	1.545	1.524	1.528	1.593	1.539	1.555	1.551	1.569	1.562
Ni								.001				
Fe <sup>2+</sup> *	.447	.441	.473	.444	.446	.451	.409	.405	.410	.408	.409	.409
Mn	.010	.010	.009	.008	.005	.009	.007	.008	.007	.007	.008	.008
Ca	.006	.006	.006	.005	.007	.007	.005	.006	.006	.005	.005	.006
Na			.002	.005	.003	.002			.001	.005		.001
Total	<u>2.013</u>	<u>2.011</u>	<u>2.029</u>	<u>2.026</u>	<u>2.014</u>	<u>2.023</u>	<u>2.025</u>	<u>1.987</u>	<u>2.012</u>	<u>1.999</u>	<u>2.005</u>	<u>2.016</u>
<u>Fe+Mn</u>												
Fe+Mn+Mg	.231	.228	.240	.226	.228	.231	.207	.212	.211	.211	.210	.211

\* All Fe in microprobe analyses is taken as Fe<sup>2+</sup>.

Table 20. (Continued).

Locality	OG2B										N45A
Analysis No. #	14	16	19	<u>25</u>	<u>29</u>	<u>31</u>	<u>35</u>	<u>37</u>	Ave. (5)	wet**	Ave. (5)
SiO <sub>2</sub>	54.20	53.80	53.80	53.80	53.60	53.50	53.10	53.30	53.46	53.46	53.77
TiO <sub>2</sub>	.00	.01	.00	.03	.03	.03	.05	.07	.04	.09	.05
Al <sub>2</sub> O <sub>3</sub>	1.37	1.62	3.45	2.36	2.15	1.95	2.25	2.15	2.17	3.11	2.25
Fe <sub>2</sub> O <sub>3</sub>										1.42	
Cr <sub>2</sub> O <sub>3</sub>										.04	.06
FeO	16.20	15.90	17.00	17.30	16.60	17.30	16.90	16.70	16.96	14.28	14.10
MnO	.24	.23								.30	.29
MgO	28.00	28.44	27.20	27.00	27.60	27.40	27.00	27.40	27.28	26.92	28.12
NiO										.03	
CaO	.18	.13	.06	.13	.12	.13	.15	.15	.14	.45	.22
Na <sub>2</sub> O										.10	.01
K <sub>2</sub> O										.02	
H <sub>2</sub> O <sup>+</sup>										.40	
H <sub>2</sub> O <sup>-</sup>										.21	
P <sub>2</sub> O <sub>5</sub>										.01	
Total	<u>100.19</u>	<u>100.13</u>	<u>100.51</u>	<u>100.62</u>	<u>100.10</u>	<u>100.31</u>	<u>99.45</u>	<u>99.77</u>	<u>100.05</u>	<u>100.84</u>	<u>98.87</u>

Formulae calculated on the basis of 6 oxygens.

Analysis No.	OG2B									N45A	
	14	16	19	<u>25</u>	<u>29</u>	<u>31</u>	<u>35</u>	<u>37</u>	Ave. (5)	wet	Ave. (5)
Si	1.953	1.939	1.916	1.937	1.935	1.934	1.933	1.933	1.934	1.904	1.942
Al	<u>.047</u>	<u>.061</u>	<u>.084</u>	<u>.063</u>	<u>.065</u>	<u>.066</u>	<u>.067</u>	<u>.067</u>	<u>.066</u>	<u>.096</u>	<u>.058</u>
Total	2.000	2.000	2.000	2.000	2.000	2.000	2.000	2.000	2.000	2.000	2.000
Al	.011	.008	.060	.037	.027	.018	.030	.025	.027	.035	.036
Ti				.001	.001	.001	.001	.002	.002	.002	.001
Cr										.001	.001
Fe <sup>3+</sup>										.038	
Mg	1.504	1.527	1.443	1.449	1.485	1.477	1.465	1.481	1.472	1.429	1.514
Ni										.001	
Fe <sup>2+*</sup>	.488	.479	.506	.521	.501	.523	.515	.506	.513	.425	.424
Mn	.007	.007								.009	.008
Ca	.007	.005	.002	.005	.005	.005	.006	.006	.004	.017	.006
Na										.007	
K										.001	
Total	2.017	2.026	2.011	2.013	2.019	2.024	2.017	2.020	2.018	1.965	1.990
<u>Fe+Mn</u>											
Fe+Mn+Mg	.248	.241	.260	.265	.252	.262	.260	.255	.258	.233	.222

\* All Fe in microprobe analyses is taken as Fe<sup>2+</sup>.

\*\* Mahito Komanomido, analyst; Japan Analytical Research Institute. Grain count of purified mineral separate by H.W. Jaffe yielded the following impurities: pargasite = .1%, spinel = .1%, unknowns = .8%.

# Underlined analyses are averaged. Total number involved shown in parentheses.



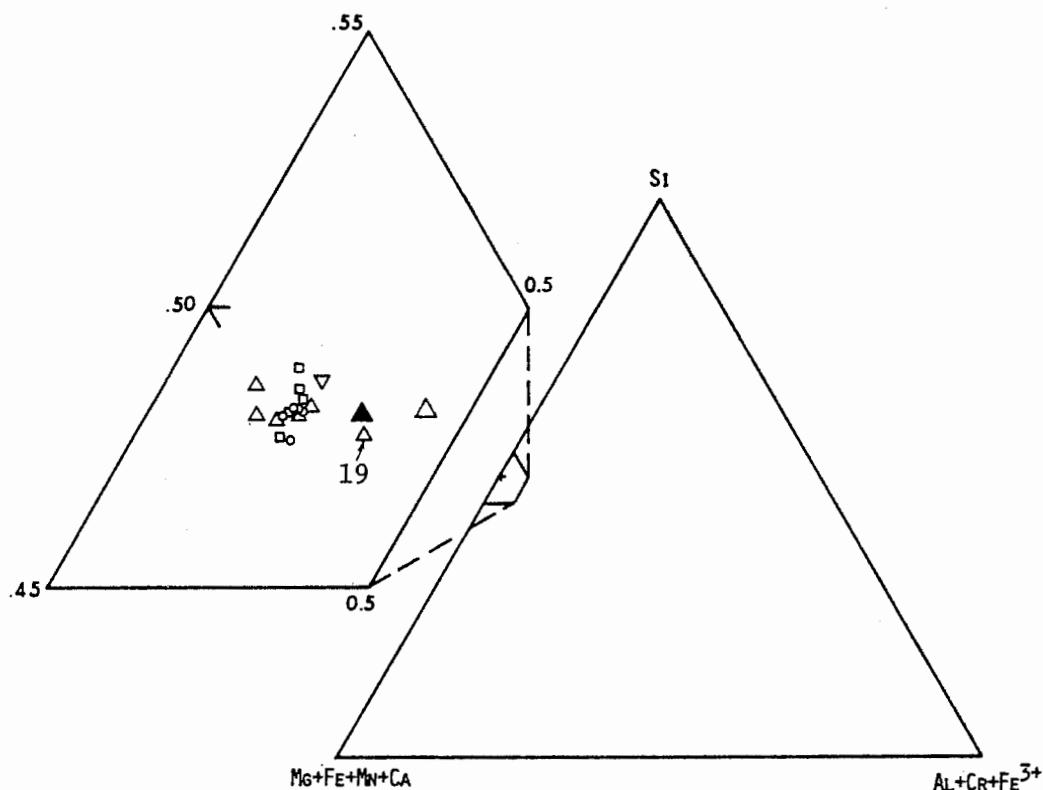


Figure 32. Orthopyroxene compositions plotted in terms of Si, (Al + Cr + Fe<sup>3+</sup>), and (Mg + Fe<sup>2+</sup> + Mn + Ca) showing variation in Al and Si content. Circles = Y57I, squares = 9Q9A, small triangles = OG2B probe analyses, large open triangle = OG2B wet analysis; closed triangle = wet analysis with all Fe recalculated as Fe<sup>2+</sup>. Small inverted triangle = average of 5 analyses from N45A.

### Olivine

Concentrated separates of olivine from six localities were obtained for the purpose of optical study. Refractive index determinations were employed to estimate the fayalite content of olivines from specimens OG2B and 9Q9A. Diagnostic properties are given in Table 21. The dispersion method was applied to olivines from four other localities, yielding the following compositions: O18 = Fa 33; J98 = Fa 31; Q222 = Fa 26 = K28S.

Electron microprobe analyses and calculated structural formulae of selected olivines from four localities are given in Table 22. The average

Table 21. Optical properties of olivine.

	OG2B <sup>*</sup>	9Q9A
Color:		colorless
Indices: $\alpha$	1.688	1.675
$\beta$	1.710	1.699
$\gamma$	1.731	1.720
Estimated $2V_X$ :	$88^\circ(-)$	$85 - 88^\circ(-)$
Dispersion:	$r > v$ , mod.	$r < v$ , weak
Composition:	Fa 27 - 28	Fa 21 - 23

\* Optical data provided by H.W. Jaffe, University of Massachusetts.

olivine and orthopyroxene compositions from each locality are plotted in Figure 33, a ternary reciprocal system which illustrates the Fe/Mg fractionation between these minerals. Optically determined compositions are also included and indicate about 2 At% less  $Fe^{2+}$  than analogous microprobe averages. The olivine-orthopyroxene pair from Y57 is the most strongly fractionated; however, no correlation exists between observed fractionation trends and metamorphic temperature gradient across the area. The Fe/Mg fractionation shown in Figure 33 suggests that orthopyroxene from localities J98 and O18 should be the most iron rich.

No attempt is made to determine temperature by means of distribution coefficients because of the effect of Al on the Fe/Mg ratio of orthopyroxene (See "Orthopyroxene"). A very small change in distribution coefficient would result in a very large change in temperature for olivine-orthopyroxene pairs with these approximate compositions (Saxena, 1969).

Table 22. Electron probe analyses of olivine.

Locality	Y57I						9Q9A				
Analysis No.	17	18	19	6a	7a	Ave	55	58	11a	12a	Ave
SiO <sub>2</sub>	37.55	37.59	37.05	37.17	37.19	37.31	37.99	38.18	37.48	37.56	37.80
TiO <sub>2</sub>	.00	.00	.00	.00	.00	.00	.02	.01	.00	.04	.02
Al <sub>2</sub> O <sub>3</sub>	.05	.00	.02	.05	.05	.03	.00	.00	.02	.03	.01
Cr <sub>2</sub> O <sub>3</sub>	.04	.06	.07	.00	.00	.03	.02	.03	.00	.00	.01
FeO *	25.75	26.14	26.32	26.18	26.32	26.14	22.42	22.14	22.25	22.81	22.41
MnO	.38	.32	.34	.32	.29	.33	.29	.23	.24	.25	.25
MgO	36.50	36.04	36.30	36.71	36.72	36.45	38.63	39.05	39.21	38.82	38.93
NiO	.07	.05	.03			.05	.11	.14			.13
CaO	.02	.02	.02	.01	.02	.02	.01	.02	.00	.00	.01
Na <sub>2</sub> O	.01	.00	.02	.07	.14	.05	.01	.00	.07	.06	.04
K <sub>2</sub> O	.00	.00	.00	.00	.00	.00	.00	.00	.00	.00	.00
Total	100.37	100.22	100.17	100.51	100.73	100.42	99.50	99.80	99.27	99.57	99.61

Formulae calculated on the basis of 4 oxygens.

Analysis No.	Y57I						9Q9A				
	17	18	19	6a	7a	Ave	55	58	11a	12a	Ave
Si	.990	.993	.983	.981	.981	.987	.996	.995	.984	.986	.990
Al	.002			.002	.001	.001				.001	
Ti											
Cr	<u>.001</u>	<u>.001</u>	<u>.002</u>			<u>.001</u>					
Total	.993	.994	.985	.983	.982	.989	.996	.995	.984	.987	.990
Mg	1.436	1.420	1.437	1.446	1.444	1.437	1.510	1.518	1.535	1.518	1.520
Ni	.001	.001					.002	.002			
Fe	.568	.578	.585	.578	.581	.578	.491	.482	.489	.500	.491
Mn	.008	.007	.007	.007	.006	.007	.006	.005	.005	.005	.006
Ca						.001					
Na			<u>.001</u>	<u>.003</u>	<u>.007</u>	<u>.002</u>			<u>.003</u>	<u>.002</u>	<u>.002</u>
Total	2.013	2.006	2.030	2.034	2.038	2.025	2.009	2.007	2.032	2.025	2.019
<u>Fe+Mn</u>											
Fe+Mn+Mg	.282	.292	.292	.288	.289	.289	.248	.243	.243	.250	.246

\* All Fe in these analyses is taken as Fe<sup>2+</sup>.

Table 22. (Continued).

Locality		OG2B			N45					
Analysis No.	1B	11T	12T	Ave	1	2	3	4	5	Ave
SiO <sub>2</sub>	36.74	36.05	35.74	36.18	37.89	37.87	37.87	38.03	38.07	37.95
TiO <sub>2</sub>	.02	.03	.00	.02	.00	.00	.00	.00	.01	.00
Al <sub>2</sub> O <sub>3</sub>	.41	.00	.03	.15	.00	.02	.00	.00	.00	.00
Cr <sub>2</sub> O <sub>3</sub>	.01	.06	.00	.02	.05	.16	.11	.12	.14	.12
FeO*	26.57	26.54	26.77	26.63	23.19	22.46	22.74	22.68	23.27	23.07
MnO		.41	.35	.38	.27	.20	.22	.28	.28	.25
MgO	35.97	37.65	37.26	36.96	39.08	38.46	38.82	38.04	38.46	38.67
NiO										
CaO	.03	.00	.00	.01	.02	.02	.01	.03	.00	.02
BaO		.09	.09	.09						
Na <sub>2</sub> O		.04	.04	.04	.00	.00	.00	.00	.00	.00
K <sub>2</sub> O		.00	.00	.00	.00	.00	.00	.00	.00	.00
Total	99.74	100.87	100.24	100.46	100.50	99.69	99.77	99.18	100.23	100.08

Formulae calculated on the basis of 4 oxygens.

Analysis No. #	OG2B				N45					
	1B	11T	12T	Ave	1	2	3	4	5	Ave
Si	.979	.955	.954	.962	.986	.990	.990	1.000	.993	.991
Al	.013			.005		.001				
Ti		.001								
Cr		.001			.001	.003	.002		.003	.002
Total	.992	.957	.954	.967	.987	.994	.992	1.000	.996	.993
Cr								.002		
Mg	1.428	1.487	1.483	1.465	1.515	1.518	1.513	1.491	1.495	1.505
Ni										
Fe	.594	.588	.598	.592	.505	.491	.497	.499	.508	.504
Mn		.009	.008	.009	.006	.004	.005	.006	.006	.006
Ca	.001		.001			.001		.001		.001
Ba		.001								
Na		.002		.001						
Total	2.023	2.087	2.090	2.067	2.026	2.014	2.015	1.999	2.009	2.016
<u>Fe+Mn</u>										
Fe+Mn+Mg	.294	.286	.290	.291	.252	.246	.249	.253	.256	.253

\* All Fe in these analyses is taken as Fe<sup>2+</sup>.

# Capital letters following analyses numbers indicate analyst. B = A.E. Bence; T = R.J. Tracy.

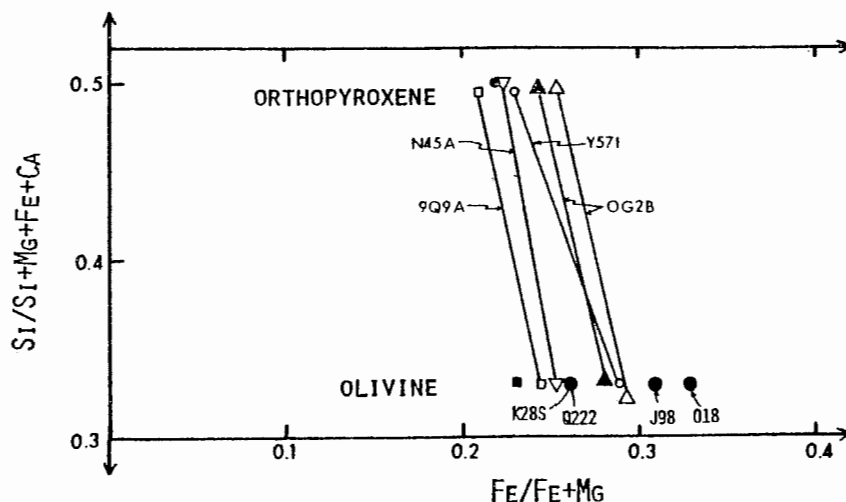


Figure 33. Forsterite-fayalite-enstatite-ferrosilite ternary reciprocal system showing the compositions of olivine and orthopyroxene. Open symbols are microprobe determinations, closed symbols are optical determinations. Small circles = Y57I, squares = 9Q9A; triangles = OG2B, inverted triangles = N45A, large circles are from localities Q222, K28S, J98, and 018, as indicated.

Brown and Prewitt (1973) have shown that distribution of Fe and Mg between M1 and M2 sites of selected olivines becomes more ordered as a function of differential octahedral distortion. With increasing temperature, Fe will preferentially go into M1. Site occupancy of olivine from OG2B determined by single crystal diffraction methods (Brown and Prewitt, 1973) indicates this olivine to be disordered. These authors suggest that temperature of metamorphism was too low for significant cation ordering.

### Spinels

Spinels within these lenses are of three major types: aluminous spinels, including dark green and optically zoned varieties; chromian spinels; and magnetite. The dark green spinel occurs as small, anhedral grains disseminated throughout many of the fresh orthopyroxene-olivine hornblendites and ranges in abundance from trace amounts to 6.8 modal percent (Y57E, Table 1). Optically zoned spinel with brownish green cores and pale green rims was observed at localities 9Q9 and J98. These

spinel is slightly chrome-enriched relative to the dark green variety. Chromian spinel occurs within the olivine-orthopyroxene nodules in specimen Y57N, invariably within a matrix of fine-grained chlorite. When observed in reflected light, these spinels appear as gray grains of low reflectivity in sharp contact with more highly reflective rims composed of ferritic chromite. A trace amount of magnetite appears as a cream colored, isotropic phase with moderate to high reflectivity within serpentinized cracks in olivine.

Electron microprobe analyses and calculated structural formulae of spinels of each type are given in Tables 23 and 24. Where applicable, analyses have been corrected for ferric iron on the basis of a three cation structural formula. In spite of consistently low sums, analyses of the chromian spinels are presented in Table 24 for the purpose of comparison with other spinels and to illustrate compositional variation from core to rim. The low sums may be due to the presence of an element not analyzed.

Figure 34 is a plot of all of the spinel analyses in terms of  $\text{Cr}^{3+}$ ,  $\text{Al}^{3+}$ , and  $(\text{Fe}^{2+}+2\text{Ti}^{4+})$ . All of the aluminous spinels plot above the 90% Al join. A blow-up of this apex shows a distinct zonation in the 909 spinels; the brown-green cores being enriched in  $\text{Cr}^{3+}$  with respect to the rims. Y57I spinels also display a range of compositions; however, there is no obvious chemical gradient from core to rim. The trend is mostly in the direction of  $\text{Fe}^{3+}$  and is more a function of oxidation. The compositions of magnetite from within serpentinized olivines plot as a single point, almost on the  $\text{Fe}^{3+}$  apex.

The cores and rims of the chromian spinels in specimen Y57N fall in two loose clusters. The rims are depleted in Al and enriched in  $\text{Fe}^{3+}$ . Although there is a wide range of Cr contents within each cluster, this element is not strongly fractionated between cores and rims. Cores and



Table 23. Electron probe analyses of aluminous spinel and magnetite.

<u>Aluminous Spinel</u>												
Locality	Y57I				9Q9A							
Analysis No.	8	9	20	21	2a	6a	1b	2b	3b	4b	5b	6b
	core	rim	core	rim			core	rim	core		core	rim
SiO <sub>2</sub>	.00	.04	.04	.14	.36	.22	.15	.22	.16	.28	.14	.29
TiO <sub>2</sub>	.06	.06	.00	.00	.00	.00	.03	.00	.03	.07	.00	.01
Al <sub>2</sub> O <sub>3</sub>	61.27	58.98	61.75	61.35	60.30	60.63	60.85	60.46	59.00	60.03	61.43	60.79
Fe <sub>2</sub> O <sub>3</sub> *	2.60	4.03	1.37	1.73								
Cr <sub>2</sub> O <sub>3</sub>	2.38	2.78	2.58	2.38	4.78	4.62	4.48	3.27	7.06	5.63	4.04	4.66
FeO	19.36	18.53	20.91	20.33	21.00	20.15	19.68	19.46	20.08	20.62	19.75	20.14
MnO	.29	.21	.19	.21	.23	.19	.21	.11	.26	.21	.19	.17
MgO	14.54	14.68	13.65	13.93	14.08	14.76	13.61	15.18	13.95	14.51	14.64	14.22
CaO	.02	.00	.02	.09	.04	.02	.02	.01	.03	.01	.04	.04
Na <sub>2</sub> O	.03	.01	.02	.00	.13	.06	.00	.00	.00	.00	.00	.00
K <sub>2</sub> O	.00	.00	.00	.00	.00	.00	.00	.00	.00	.00	.00	.00
Total	100.55	99.33	99.90	100.27	100.92	100.65	99.03	100.71	100.57	101.36	100.23	100.32

Analysis No.	Y57I				9Q9A							
	8	9	20	21	2a	6a	1b	2b	3b	4b	5b	6b
Si		.001	.001	.004	.009	.005	.004	.005	.004	.007	.003	.007
Ti	.001	.001								.001		
Al	1.897	1.856	1.917	1.909	1.869	1.875	1.911	1.914	1.844	1.853	1.902	1.887
Cr <sub>3+</sub>	.049	.059	.054	.050	.100	.096	.094	.067	.148	.116	.083	.097
Fe <sup>3+</sup>	<u>.051</u>	<u>.081</u>	<u>.027</u>	<u>.034</u>	<u>.021</u>	<u>.032</u>				<u>.014</u>	<u>.008</u>	
Total	1.998	1.998	1.999	1.997	1.999	2.008	2.009	1.986	1.996	1.991	1.996	1.991
Mg	.569	.584	.536	.548	.553	.577	.540	.588	.551	.567	.573	.558
Fe <sup>2+</sup>	.425	.414	.461	.449	.440	.410	.438	.423	.445	.437	.426	.443
Mn	.006	.005	.004	.005	.005	.004	.005	.002	.005	.005	.004	.003
Ca	<u>.001</u>		<u>.001</u>	<u>.003</u>	<u>.001</u>						<u>.001</u>	<u>.001</u>
Total	1.001	1.003	1.002	1.005	.999	.992	.983	1.013	1.001	1.009	1.004	1.005
Sp.	.949	.929	.959	.958	.939	.936	.953	.966	.926	.934	.954	.951
Chr.	.025	.030	.027	.025	.050	.048	.047	.034	.074	.058	.042	.049
Mag.	.026	.041	.014	.017	.011	.016	.000	.000	.000	.007	.004	.000
Usp.	.001	.001	.000	.000	.000	.000	.000	.000	.000	.001	.000	.000
<u>Fe+Mn</u>												
Fe+Mn+Mg	.431	.418	.465	.453	.446	.418	.451	.420	.450	.438	.429	.444

\* Ferric iron adjustments made on the basis of 3 cation structural formula. Formulae with no Fe<sup>3+</sup> were cation deficient when calculated on the basis of 4 oxygens.

Table 23. (Continued).

Locality Analysis No.	9Q9A		<u>Aluminous Spinel</u>					<u>Magnetite</u>	
	7b	8b	OG2B		N45			9Q9A	
	rim	core	5	11	1	2	3	60	61
SiO <sub>2</sub>	.17	.10	.00	.00	.06	.04	.11	.81	.66
TiO <sub>2</sub>	.03	.03	.01	.00	.00	.01	.00	.15	.34
Al <sub>2</sub> O <sub>3</sub>	61.96	58.76	62.80	62.60	62.25	62.12	62.50	.15	.14
Fe <sub>2</sub> O <sub>3</sub> *			1.27	1.71				65.32	65.46
Cr <sub>2</sub> O <sub>3</sub>	4.05	6.18	1.69	1.87	3.25	3.29	3.35	.11	.17
FeO	19.64	20.38	23.86	22.86	21.95	21.78	21.45	30.10	30.41
MnO	.13	.25	.00	.09	.10	.10	.13	.26	.22
MgO	14.80	13.49	12.20	12.80	12.73	11.93	12.91	.73	.59
NiO								.31	.38
CaO	.02	.02	.04	.01	.04	.03	.04	.07	.06
Na <sub>2</sub> O	.00	.00	.00	.00	.00	.00	.00	.00	.01
K <sub>2</sub> O	.00	.00	.00	.00	.00	.00	.00	.04	.03
Total	100.80	99.21	101.87	101.94	100.38	99.30	100.49	98.05	98.47

Analysis No.	9Q9A		Aluminous Spinel				Magnetite	
	7b	8b	OG2B		1	N45 2	3	9Q9A 60 61
			5	11				
Si	.004	.002			.001	.001	.003	.031 .025
Ti		.004						.004 .009
Al	1.904	1.859	1.940	1.928	1.938	1.953	1.938	.006 .006
Cr	.083	.131	.035	.039	.068	.069	.070	.004 .005
Fe <sup>3+</sup>		.001	.025	.034				<u>1.912</u> <u>1.912</u>
Total	1.991	1.997	2.000	2.001	2.007	2.023	2.011	1.957 1.957
Mg	.575	.541	.476	.498	.501	.474	.506	.043 .035
Ni								.009 .012
Fe <sup>2+</sup>	.428	.456	.523	.499	.485	.486	.472	.979 .987
Mn	.002	.006		.002	.002	.002	.003	.009 .007
Ca			.001		.001	.001	.001	<u>.002</u> <u>.002</u>
Total	1.005	1.003	1.000	.999	.989	.963	.982	1.042 1.043
Sp.	.958	.930	.970	.964	.966	.966	.965	.003 .003
Chr.	.042	.066	.018	.019	.034	.034	.035	.002 .003
Mag.	.000	.001	.013	.017	.000	.000	.000	.991 .985
Usp.	.000	.004	.000	.000	.000	.000	.000	.004 .009
<u>Fe+Mn</u>								
Fe+Mn+Mg	.428	.461	.524	.502	.493	.507	.484	.958 .966

\* Ferric iron adjustments made on the basis of 3 cation structural formula. Formulae with no Fe<sup>3+</sup> were cation deficient when calculated on the basis of 4 oxygens.

Table 24. Electron probe analyses of chromian spinel and chrome magnetite.

Locality		Y57N								
Analysis No.	1-2	1-3	1-4	1-5	1-6	2-1	2-4	3-2	5-1	5-2
	core	rim	core	rim	rim	core	core	rim	rim	rim
SiO <sub>2</sub>	.38	1.78	.45	.47	.45	.21	.35	.43	.38	.33
TiO <sub>2</sub>	.14	.71	.23	.88	.59	.15	.11	.68	1.88	2.05
Al <sub>2</sub> O <sub>3</sub>	41.93	5.73	32.39	4.21	3.48	33.12	38.55	.72	1.01	.62
Fe <sub>2</sub> O <sub>3</sub> *	1.18	30.83	7.77	40.54	44.66	28.81	2.69	53.22	41.95	36.14
Cr <sub>2</sub> O <sub>3</sub>	19.42	24.94	21.39	20.17	18.36	25.44	20.86	11.70	19.85	24.88
FeO	27.83	31.34	28.59	30.82	30.29	3.04	27.70	30.56	31.28	31.32
MnO	.58	.84	.70	.71	.65	.76	.64	.49	.77	.89
MgO	6.70	1.64	4.79	1.00	1.27	4.66	6.09	.60	.61	.34
CaO	.05	.09	.07	.10	.10	.08	.06	.08	.09	.08
Na <sub>2</sub> O	.05	.00	.21	.00	.00	.25	.19	.01	.00	.00
K <sub>2</sub> O	.03	.02	.03	.05	.06	.04	.03	.07	.07	.06
Total	98.29	97.92	96.62	98.95	99.86	96.76	97.27	98.56	97.89	99.71

Analysis No.	1-2	1-3	1-4	1-5	1-6	2-1	2-4	3-2	5-1	5-2
Si	.011	.066	.014	.018	.017	.013	.011	.017	.015	.013
Ti	.003	.020	.006	.025	.016	.004	.003	.020	.054	.060
Al	1.484	.249	1.228	.185	.152	1.250	1.402	.033	.046	.028
Cr	.461	.726	.544	.594	.538	.644	.509	.356	.603	.766
Fe <sup>3+</sup>	<u>.027</u>	<u>.855</u>	<u>.188</u>	<u>1.137</u>	<u>1.244</u>	<u>.073</u>	<u>.062</u>	<u>1.539</u>	<u>1.213</u>	<u>1.059</u>
Total	1.986	1.916	1.980	1.959	1.967	1.984	1.987	1.965	1.931	1.926
Mg	.300	.090	.230	.056	.070	.222	.280	.034	.035	.020
Fe <sup>2+</sup>	.699	.965	.769	.960	.939	.771	.715	.983	1.005	1.020
Mn	.015	.026	.019	.022	.020	.021	.017	.016	.025	.029
Ca	<u>.002</u>	<u>.004</u>	<u>.002</u>	<u>.004</u>	<u>.004</u>	<u>.003</u>	<u>.002</u>	<u>.003</u>	<u>.004</u>	<u>.003</u>
Total	1.016	1.085	1.020	1.042	1.033	1.017	1.014	1.036	1.069	1.072
Sp.	.750	.175	.622	.097	.081	.632	.708	.023	.023	.011
Chr.	.232	.365	.274	.297	.271	.325	.256	.178	.298	.378
Mag.	.014	.430	.095	.569	.624	.037	.031	.769	.599	.523
Usp.	.004	.030	.009	.037	.024	.006	.005	.030	.080	.088
$\frac{\text{Fe}+\text{Mn}}{\text{Fe}+\text{Mn}+\text{Mg}}$	.704	.917	.774	.946	.932	.781	.723	.967	.967	.981

\* Ferric iron adjustments made on the basis of 3 cation structural formula.

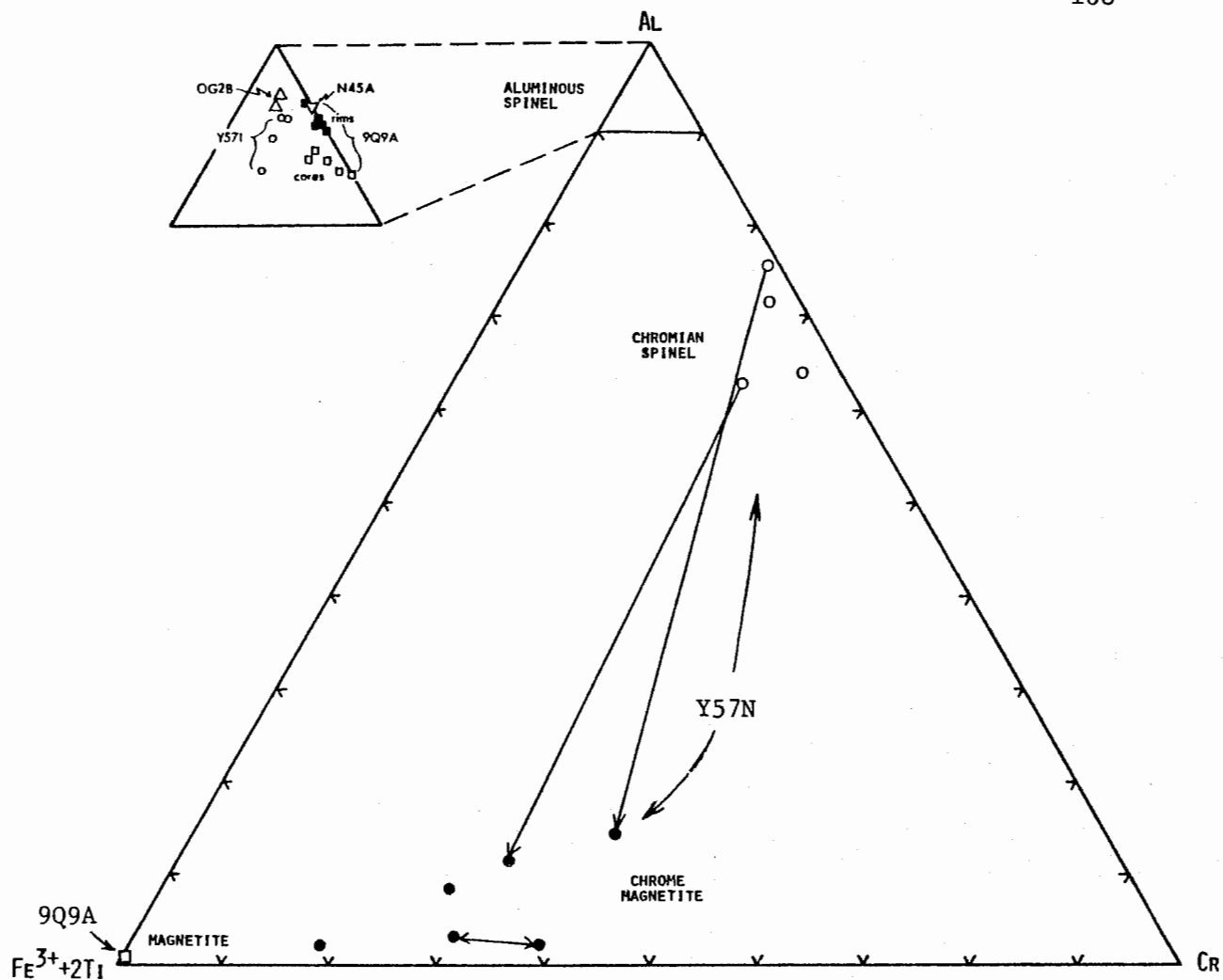


Figure 34. Spinel and magnetite analyses plotted in terms of Al, Cr, and ( $\text{Fe}^{3+} + 2\text{Ti}$ ). Chromian spinels rimmed by magnetite are from specimen Y57N. Arrows, pointing toward rims, connect analyses of single grains. Large square is 2 magnetite compositions from specimen 9Q9A.

rims of two grains are connected by tie lines; however, in most cases, very fine grain size prevented analysis of both of these regions within a single grain.

To show the relationship between ( $\text{Fe}/\text{Fe}+\text{Mg}$ ) ratio and  $\text{Fe}^{3+}$ , and between ( $\text{Fe}/\text{Fe}+\text{Mg}$ ) ratio and Al, the spinel analyses are projected on appropriate faces of a spinel composition prism as shown in Figure 35. Figure 35A

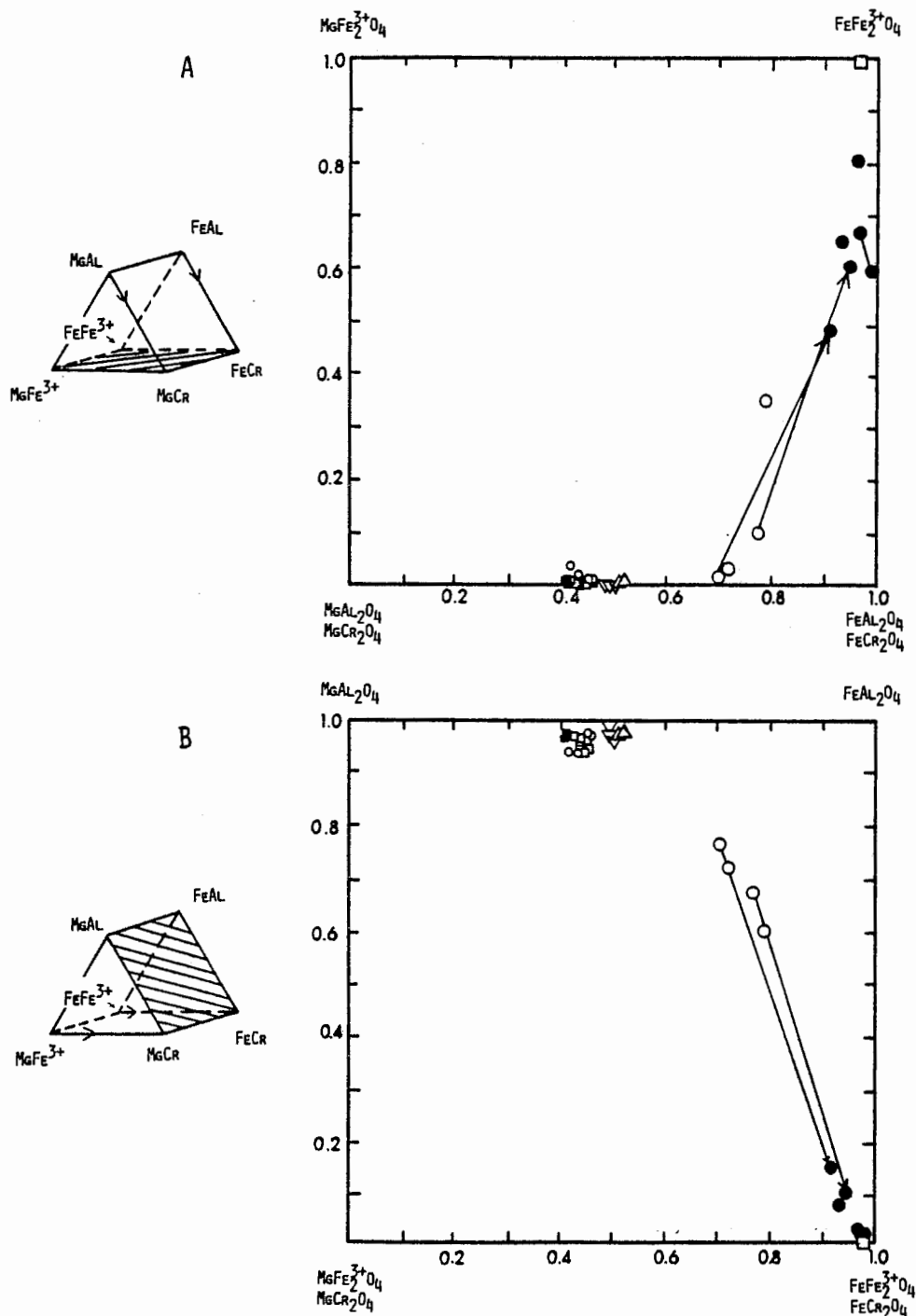


Figure 35. Ternary reciprocal systems showing faces of spinel composition prism. Symbols as in Figure 34.

- A. Base of prism with spinel and chromite edges combined.  $\text{Fe}/(\text{Fe}+\text{Mg})$  increases with  $\text{Fe}^{3+}$  in chromian spinel and chrome magnetite.
- B. Side of prism combining  $\text{Fe}^{3+}$  with chromite. Rims of spinels in 9Q9A (filled squares) are depleted in Cr with respect to cores. This is opposite to the zoning of the spinels in specimen Y57N (large circles).



represents the base of the prism with the spinel edge added to the chromite edge. The aluminous spinels show no significant change in  $\text{Fe}^{3+}$  content with increasing  $(\text{Fe}/\text{Fe}+\text{Mg})$  ratio. The  $\text{Fe}/(\text{Fe}+\text{Mg})$  ratio of the chromian spinels, however, increases with increasing  $\text{Fe}^{3+}$  outward. A similar trend is seen in Figure 35B in which the compositions are plotted in terms of spinel and chromite plus magnetite. The  $\text{Fe}/(\text{Fe}+\text{Mg})$  ratio increases outward with increasing  $\text{Fe}^{3+}$  and Cr. Most of the aluminous spinels generally show no significant relationship between  $(\text{Fe}/\text{Fe}+\text{Mg})$  ratio and Al content with the exception of the zoned spinels from 9Q9, in which a decrease in  $\text{Fe}/(\text{Fe}+\text{Mg})$  ratio is coupled with a slight decrease in chrome content outward. Magnetite, when plotted in Figure 35, shows a small Mg component and little or no Cr or Al.

If the rims of the chromian spinels are formed by oxidation, Al would be released which could contribute to the formation of chlorite from the surrounding Mg-silicates (Golding and Bayliss, 1968). There would be a corresponding decrease on Al and Mg with increasing  $\text{Fe}^{3+}$ , as observed in Y57N. During the oxidation process, some of the  $\text{Fe}^{2+}$  near the rim may go into octahedral position with a corresponding amount of  $\text{Fe}^{3+}$ , as observed in Y57N. During the oxidation process, some of the  $\text{Fe}^{2+}$  near the rim may go into octahedral position with a corresponding amount of  $\text{Fe}^{3+}$  into tetrahedral position (Mitra, 1972), similar to the structure of magnetite.

### Chlorite

Two prominent types of chlorite are observed within the orthopyroxene-olivine hornblendites: colorless, magnesian chlorite occurring as medium to coarse plates, considered a primary metamorphic phase; and pale green, very fine-grained chlorite, commonly as pseudomorphs after orthopyroxene (Fig. 26) and considered a retrograde product. A third type occurs as small, rounded blebs of fine-grained, colorless chlorite enclosing chromian spinel in specimen Y57N.

Primary chlorite ranges in abundance up to 13 modal percent (Table 1). Diagnostic optical properties of the prograde chlorite in thin section are given in Table 25. Sufficient quantities were not separated for oil immersion work to determine indices of refraction.

Table 25. Optical properties of chlorite.

Color: colorless  
 Estimated 2V:  $10-15^{\circ}(+)$ ;  $r < v$ , moderate.  
 Cleavage: basal.  
 Twinning: lamellar, very common.  
 Birefringence: first order gray (.004).  
 Texture: mottled, "bird's eye maple" surface.

---

Table 26 lists electron microprobe analyses and ionic ratios from specimens Y57N and OG2B, plus average analyses from Y57I, 9Q9A, and N45, and ionic ratios calculated from these averages. OG2B analyses were not averaged because of the relative spread in composition and difficulty in distinguishing primary from secondary chlorite.

Ideal clinochlore,  $\text{Mg}_5\text{Al}_2\text{Si}_3\text{O}_{10}(\text{OH})_8$ , is plotted as a large open circle in Figure 36. The diagonal line extending from clinochlore represents part of the ideal compositional range of chlorite with increasing Al content. Most of the analyses plot on or near this line. Retrograde chlorites, as well as those associated with chromian spinels (Y57N) fall within the cluster of primary chlorites. Fe/Mg ratios are shown in Figure 37. Chlorites from OG2B contain the most iron, and plot in two clusters. Pale green chlorites are more Fe-rich than the colorless variety.

Chlorite was separated from specimen Y57I to test for a correlation

Table 26. Electron probe analyses of chlorite.

Locality	Y57I	Y57N	9Q9A	OG2B									N45
Analysis No. #	Ave (8)	1-9	Ave (5)	1B <sup>†</sup>	2B	10B	12B	21B	24B	27B	4T	5T	Ave (4)
				gr	gr	gr	gr	cl	cl	cl	cl	cl	
SiO <sub>2</sub>	29.61	28.77	30.16	28.10	28.80	28.80	28.60	28.40	28.30	27.60	28.46	28.25	28.84
TiO <sub>2</sub>	.02	.02	.02	.04	.06	.03	.04	.00	.00	.00	.07	.06	.29
Al <sub>2</sub> O <sub>3</sub>	21.30	20.30	20.60	22.90	22.20	22.80	22.40	23.60	22.90	23.40	21.92	21.65	20.76
Cr <sub>2</sub> O <sub>3</sub>	.09	.97	.27								.18	.20	.24
FeO	7.52 <sup>6</sup>	6.70	6.28	8.57	8.19	8.14	8.09	8.12	8.18	7.92	7.54	7.38	7.30
MnO	.01	.04	.01	.00	.00	.00	.00				.05	.06	.00
MgO	29.35	29.50	30.21	27.70	27.80	27.70	27.10	27.70	28.00	28.50	28.70	28.61	28.18
CaO	.02	.02	.00	.02	.03	.03	.00	.00	.00	.00	.03	.02	.04
Na <sub>2</sub> O	.03	.00	.01	.00	.00	.00	.00	.00	.00	.04	.07	.09	.01
K <sub>2</sub> O	.00	.00	.00	--	--	--	--	--	--	--	.04	.03	.00
Total	87.95	86.34	87.56	87.33	87.18	87.77	86.22	87.82	87.38	87.46	87.06	86.35	85.66

Formulae calculated on the basis of 14 oxygens.

Locality	Y57I	Y57N	9Q9A	OG2B									N45
Analysis No.	Ave	1-9	Ave	1B	2B	10B	12B	21B	24B	27B	4T	5T	Ave
Si	2.818	2.793	2.865	2.709	2.744	2.756	2.780	2.712	2.726	2.652	2.743	2.745	2.808
Al	<u>1.182</u>	<u>1.207</u>	<u>1.135</u>	<u>1.291</u>	<u>1.226</u>	<u>1.244</u>	<u>1.220</u>	<u>1.288</u>	<u>1.274</u>	<u>1.348</u>	<u>1.257</u>	<u>1.255</u>	<u>1.192</u>
Total	4.000	4.000	4.000	4.000	4.000	4.000	4.000	4.000	4.000	4.000	4.000	4.000	4.000
Al	1.208	1.114	1.172	1.311	1.295	1.328	1.347	1.369	1.317	1.303	1.234	1.225	1.187
Ti	.001		.001	.003	.005	.002	.003				.005	.004	.020
Cr	.007	.074	.020								.014	.015	.017
Mg	4.163	4.267	4.276	3.980	3.990	3.950	3.926	3.942	4.005	4.081	4.123	4.142	4.087
Fe	.598	.539	.499	.691	.668	.673	.658	.648	.656	.636	.608	.600	.594
Mn			.001								.004	.005	.002
Ca	.002			.002	.003	.003					.003	.002	
Na	.005		.002								.013	.017	
K											.005	.004	
Total	5.984	5.994	5.971	5.984	5.961	5.956	5.934	5.959	5.978	6.027	6.009	6.014	5.907
<u>Fe+Mn</u>													
Fe+Mn+Mg	.126	.112	.105	.148	.143	.146	.144	.141	.141	.135	.129	.127	.127

# Ave indicates averaged analysis. The number of analyses averaged is given in parentheses.

† Letter following the analysis number indicates analyst: B = A.E. Bence; T = R.J. Tracy.

gr Pale green chlorite.

cl Colorless chlorite.

\* All Fe is taken as Fe<sup>2+</sup>.

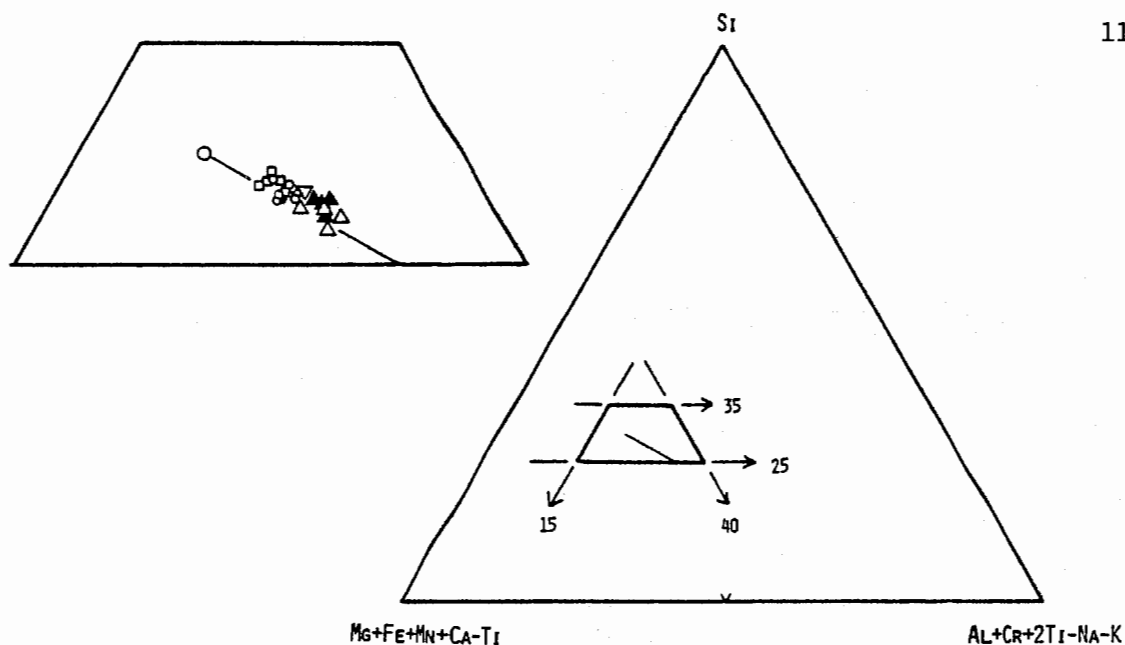


Figure 36. Electron microprobe analyses of chlorites plotted in terms of Si,  $(\text{Mg} + \text{Fe}^{2+} + \text{Mn} + \text{Ca-Ti})$ , and  $(\text{Al} + \text{Cr} + 2\text{Ti-Na-K})$ . Large circle = clinochlore, small open circles = Y57I, closed circle = Y57N, squares = 9Q9A, triangles = OG2B (open = colorless; filled = pale green), inverted triangle = N45A. The chlorite from Y57N is that enclosing a chromian spinel.

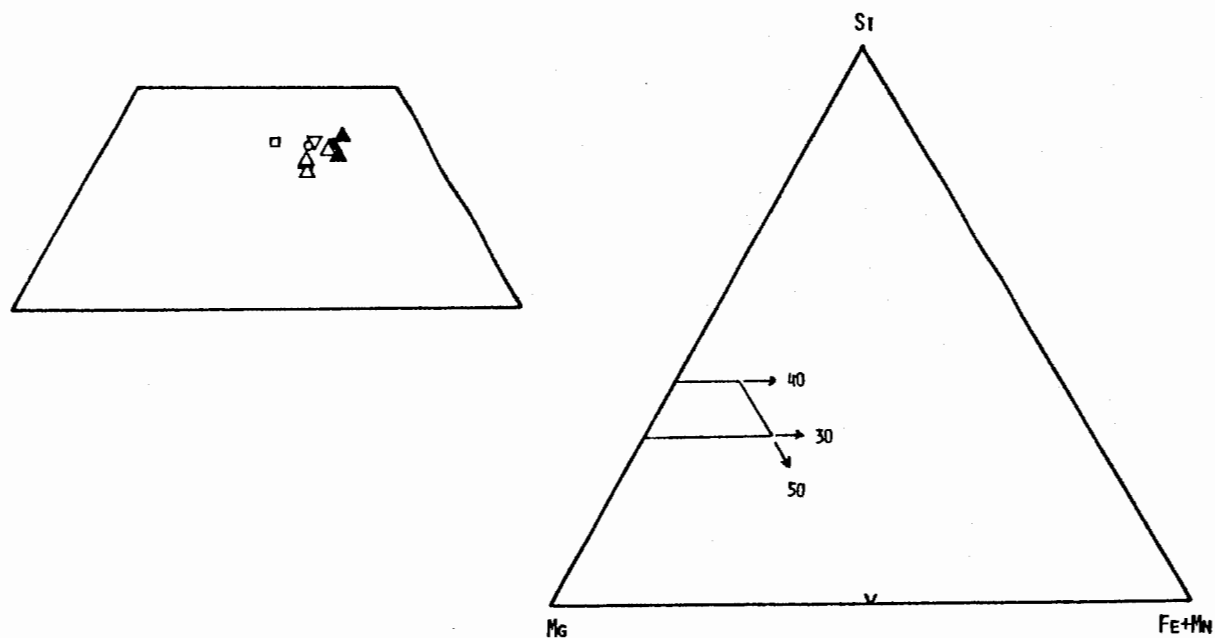


Figure 37. Microprobe analyses of chlorite plotted in terms of Si, Mg, and  $(\text{Fe} + \text{Mn})$ . Circles = Y57I, squares = 9Q9A, triangles = OG2B (open = colorless; filled = pale green), inverted triangle = N45A. All but OG2B analyses are averages.

between alumina content and lattice spacing. A plot of  $d_{(004)}$  against alumina content of chlorites from Nelson and Roy (1958) is employed by Chernosky (1974) to show that  $d_{(004)}$  decreases with increasing alumina content. An X-ray powder photograph of chlorite Y57I, run with silicon as an internal standard, indicates a  $d_{(004)}$  of  $3.525\text{\AA}$ . Chernosky's curve (1974, Fig. 3) predicts a  $d_{(004)}$  of  $3.575\text{\AA}$  for chlorite with the same alumina content. The difference in values may be due to the presence of Fe in Chlorite Y57I. In view of these facts, X-ray analysis of other chlorites to determine alumina content was not deemed worthwhile.

### Phlogopite and Biotite

Phlogopite occurs in trace amounts in some of the orthopyroxene-olivine hornblendites, either as discrete grains or intergrown with chlorite. It is optically negative with an estimated  $2V$  of  $0-5^\circ$  and very pale in color ( $X$  = colorless,  $Y=Z$  = pale tan). Phlogopite is distinguished from biotite solely on the basis of color. Biotite is dark red-brown.

Both minerals, occurring separately, are common in hybrid rocks, varying in abundance up to 24 modal percent (Table 3). Biotite occurs in a hornblendite (9Q9C) and coexists with quartz, plagioclase, hornblende, cummingtonite, and chlorite in a hornblende-cummingtonite-biotite schist (500AW). Specimen Y570, an anthophyllite-bearing hybridized ultramafic rock, contains phlogopite which is intergrown with chlorite. The chlorite has anomalous blue interference colors, indicating an iron-rich composition.

Electron microprobe analyses and calculated structural formulae of phlogopite from two localities (OG2 and N45) are given in Table 27. Phlogopite from OG2B has more iron than that from N45A, in agreement with the generally higher Fe values in other phases from locality OG2B. Phlogopite from OG2B also has less Al than that from N45A. Note that both formulae of N45 phlogopites are low in alkalis.

Table 27. Electron probe analyses of phlogopite.

Locality	OG2B				N45	
Analysis No.	6	8	9	10	1	2
SiO <sub>2</sub>	37.56	38.38	37.34	38.50	38.92	39.02
TiO <sub>2</sub>	.72	.68	.72	.66	.53	.55
Al <sub>2</sub> O <sub>3</sub>	17.38	18.29	17.19	18.03	19.12	18.92
Cr <sub>2</sub> O <sub>3</sub>	.13	.10	.17	.15	.20	.26
FeO*	7.46	6.94	6.82	7.56	5.85	6.10
MnO	.06	.05	.00	.06	.08	.01
MgO	21.02	21.61	21.02	22.09	23.12	22.84
CaO	.06	.05	.00	.05	.01	.01
BaO	.12	.21	.14	.18		
Na <sub>2</sub> O	.48	.64	.53	.45	.57	.31
K <sub>2</sub> O	6.50	7.77	8.00	6.95	6.36	6.05
Total	91.49	94.72	91.93	94.68	94.76	94.48

Formulae calculated on the basis of 11 oxygens.

Si	2.765	2.741	2.755	2.744	2.732	2.755
Al	<u>1.235</u>	<u>1.259</u>	<u>1.245</u>	<u>1.256</u>	<u>1.268</u>	<u>1.254</u>
Total	4.000	4.000	4.000	4.000	4.000	4.000
Al	.273	.281	.250	.259	.316	.326
Ti	.040	.037	.040	.035	.027	.029
Cr	.008	.006	.010	.008	.011	.014
Mg	2.306	2.300	2.312	2.346	2.418	2.398
Fe	.459	.415	.421	.451	.342	.359
Mn	<u>.004</u>	<u>.003</u>		<u>.004</u>	<u>.004</u>	<u>.000</u>
Total	3.090	3.042	3.033	3.103	3.118	3.126
Ca	.005	.004		.004	.000	.001
Na	.069	.089	.076	.062	.076	.042
K	.601	.708	.753	.632	.574	.544
Ba	<u>.003</u>	<u>.006</u>	<u>.004</u>	<u>.005</u>		
Total	.687	.807	.833	.703	.650	.587
<u>Fe+Mn</u>						
Fe+Mn+Mg	.167	.154	.154	.162	.125	.130

\* All Fe is taken as Fe<sup>2+</sup>.

## Plagioclase

Small quantities of plagioclase are present in many of the hybridized rocks, most notably as extensively sericitized, rounded, anhedral, interstitial grains coexisting with anthophyllite in specimens K34A and J98B. Twinning is generally absent. Plagioclase coexisting with quartz in specimen 500AW displays only poorly developed twinning. It contains intergrowths of two plagioclases formed by unmixing of bytownite (Smith, 1974). Similar intergrowths occur in plagioclase within the amphibolite adjacent to N01.

Sufficient plagioclase was separated from specimen J98B for oil immersion study. Plagioclases in specimens K34A and N01E were studied in thin section. Optical properties are given in Table 28. An electron microprobe analysis of plagioclase ( $An_{96}$ ) from specimen K34A is presented in Table 29. The plagioclases from within the hybridized ultramafic rocks are significantly more calcic than those from the adjacent amphibolite.

Table 28. Optical properties of plagioclase.

	J98B	K34A	N01E
Indices: $\alpha$	$1.574 \pm .002$		
$\beta$	$1.579 \pm .002$		
$\gamma$	$1.585 \pm .002$		
Estimated 2V:	$80^\circ$ (-)	$75-80^\circ$ (-)	$85^\circ$ (-)
Dispersion:	$r < v$ ; weak	$r < v$ ; weak	$r < v$ ; weak
Twinning:	none	none	Albite
Extinction angle:			$41^\circ$
Estimated composition:	An 90-93		An 75-80 <sup>#</sup> An 72-73 <sup>*</sup>

<sup>#</sup> Based upon optic angle and optic sign.

<sup>\*</sup> Based upon Michel-Levy method



Table 29. Electron probe analyses of plagioclase, garnet, and serpentine.

Locality		<u>Garnet</u>				<u>Plagioclase</u>	<u>Serpentine</u>
		K34A				K34A	9Q9A
Analysis No.	29	30	36	39		35	62
	core	rim	rim	core			
SiO <sub>2</sub>	39.62	38.98	38.66	38.04		43.46	41.19
TiO <sub>2</sub>	.01	.01	.05	.00		.00	.00
Al <sub>2</sub> O <sub>3</sub>	22.14	21.10	21.78	22.97		35.01	.24
Cr <sub>2</sub> O <sub>3</sub>	.07	.02	.03	.05		.00	.00
FeO*	23.62	23.93	24.09	24.51		.13	3.75
MnO	.91	.93	1.09	.85		.00	.00
MgO	10.08	9.55	9.35	10.31		.04	39.53
NiO	.02	.09	.01	.03		.00	.13
CaO	3.45	3.54	3.39	3.42		19.17	.00
Na <sub>2</sub> O	.00	.00	.08	.00		.44	.00
K <sub>2</sub> O	.00	.00	.00	.00		.00	.00
Total	99.92	98.15	98.53	100.18		98.25	84.84

\* All Fe is taken as Fe<sup>2+</sup>.

Garnet formulae calculated on the basis of 12 oxygens.

Locality	<u>Garnet</u>			
	K34A			
Analysis No.	29	30	36	39
Si	3.013	3.033	2.999	2.908
Al			<u>.001</u>	<u>.092</u>
Total	3.013	3.033	3.000	3.000
Al	1.984	1.936	1.989	1.977
Ti			.002	
Cr	<u>.002</u>			<u>.002</u>
Total	1.986	1.936	1.991	1.979
Mg	1.143	1.108	1.079	1.173
Ni		.005		
Fe	1.502	1.558	1.562	1.566
Mn	.058	.060	.071	.054
Ca	.281	.295	.280	.278
Na			<u>.011</u>	
Total	2.984	3.026	3.003	3.071
Pyr.	.383	.367	.361	.382
Alm.	.503	.516	.522	.510
Gros.	.094	.098	.094	.091
Spes.	.019	.020	.024	.018

Plagioclase formula on the basis of 8 oxygens.

<u>Plagioclase</u>	
K34A	
	35
Si	2.045
Al	<u>1.941</u>
Total	3.986
Mg	.001
Fe	.004
Ca	.966
Na	<u>.040</u>
Total	1.011
An	96.0
Ab	4.0
Or	0.0

Serpentine formula on the basis of 7 oxygens

<u>Serpentine</u>	
9Q9A	
	62
Si	1.987
Al	<u>.013</u>
Total	2.000
Al	
Ti	
Cr	
Mg	2.845
Ni	.004
Fe	.150
Mn	
Total	2.999
<u>Fe+Mn</u>	
Fe+Mn+Mg	.050

## Garnet

Very pale pink garnet was found in the hybrid rocks at locality K34. It occurs as subhedral to euhedral poikiloblasts up to 2mm across, making up to five modal percent of the rock where most abundant. It commonly contains inclusions of sericitized plagioclase, ilmenite, and very fine chlorite (Fig. 25). The index of refraction determined in oils is approximately 1.766. This is approximate because of the spread between different oils in the high index range.

Electron microprobe analyses and calculated structural formulae are given in Table 29 and illustrated in Figures 28 and 38. Figure 28 is a modified ACF diagram in which garnet K34A is plotted along with coexisting pargasite, anthophyllite, and plagioclase. Figure 38 is a ternary diagram in which garnet compositions are plotted in terms of Ca, Mg, and (Fe+Mn). The approximate compositions of the most and least magnesium garnets are  $\text{Py}_{38}, \text{Alm}_{51}, \text{Gr}_9, \text{Sp}_2$  and  $\text{Py}_{36}, \text{Alm}_{53}, \text{Gr}_9, \text{Sp}_2$  respectively. The limited data available indicate that the rims of the garnet are slightly depleted in Mg relative to the cores.

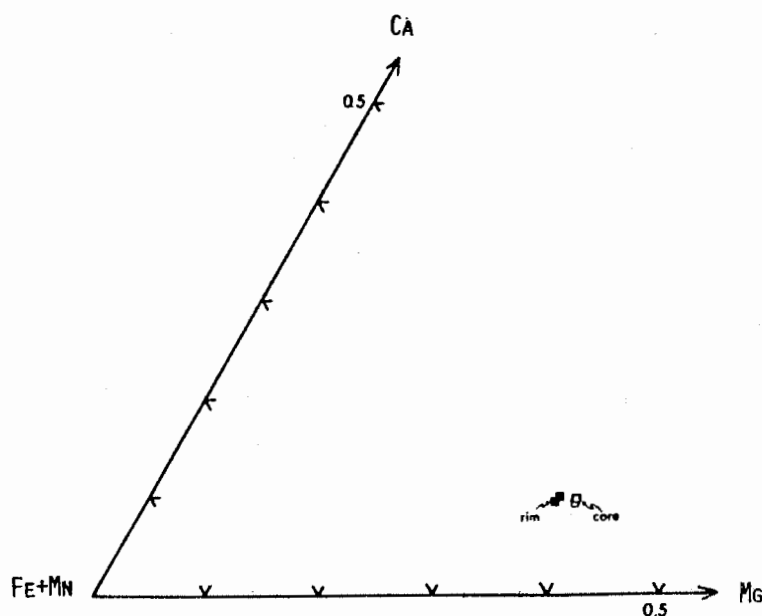


Figure 38. Electron microprobe analyses of garnet plotted in terms of Ca, Mg, and (Fe+Mn).

### Serpentine

Serpentine in the orthopyroxene-olivine hornblendites only occurs within serpentized cracks in olivine and coexists with magnetite. It is colorless and has low birefringence. An electron microprobe analysis and calculated formula of this serpentine is presented in Table 29. Note that there is just enough Al to fill the tetrahedral site and that there is no room for octahedral aluminum.

### Carbonate

Carbonate is most commonly observed as small, anhedral grains associated with nodules or fractures and is found only in minor abundance. Very commonly, the nodules which have been carbonated take on a tan color in hand specimen and appear to be made up of very fine, dark brown material when observed in thin section. The carbonate associated with fractures appears colorless in thin section. In specimen K28NA, colorless carbonate occurs evenly disseminated throughout the thin section making up approximately one percent of the slide. It is the only specimen studied in which the carbonate is neither associated with a nodule nor a fracture. No microprobe analyses are available of this phase and the composition cannot be determined in thin section.

### Ilmenite

Ilmenite typically makes up about 50% of the opaque minerals in the orthopyroxene-olivine hornblendites. It ranges in abundance from trace amounts to a few modal percent, occurring as fine, anhedral to subhedral homogeneous grains evenly disseminated throughout the specimens. It appears in a similar fashion in many hybrid rocks. Reflected light properties are given in Table 30.

Table 30. Reflected light optical properties of ilmenite.

Color: Pinkish brown to brown; very weak bireflectance.

Reflectivity: weak to moderate; 20%.

Anisotropy: strong; gray-brown to red-brown.

Electron microprobe analyses of ilmenite from four orthopyroxene-olivine hornblendites and one hybrid rock are given in Table 31. Structural formulae were calculated on the basis of 2 cations. Where oxygen summed to less than 3.00,  $\text{Fe}^{2+}$  was changed to  $\text{Fe}^{3+}$  to bring the sum to 3. These compositions are plotted in Figure 39, along with two magnetite compositions from serpentinized olivine. All of the ilmenite plots very close to end-member  $(\text{Fe,Mg,Mn})\text{TiO}_3$ , indicating very little hematite in solid solution. This reflects low values of  $f_{\text{O}_2}$  (Buddington and Lindsley, 1964). The substantial solid solution of  $\text{MgTiO}_3$  (Giekielite) presumably reflects the high temperature and high Mg content of the enclosing rock.

### Graphite

Graphite was observed in specimen Y57I. It is not very common and appears as brownish-yellow, anhedral material that does not take a good polish. It is weakly to moderately anisotropic from yellow to yellow-brown. A grain of graphite was plucked from a polished chip for the purpose of X-ray analysis. Debye-Sherrer powder photographs were taken using  $\text{FeK}_\alpha$  radiation and an Mn filter. The diffraction data indicate that this is crystalline graphite. The importance of the existence of crystalline graphite lies in its ability to act as an oxygen buffer in the presence of  $\text{CO}_2$ -CO fluid (French and Eugster, 1965) and to limit possible fluid compositions in the system C-O-H.

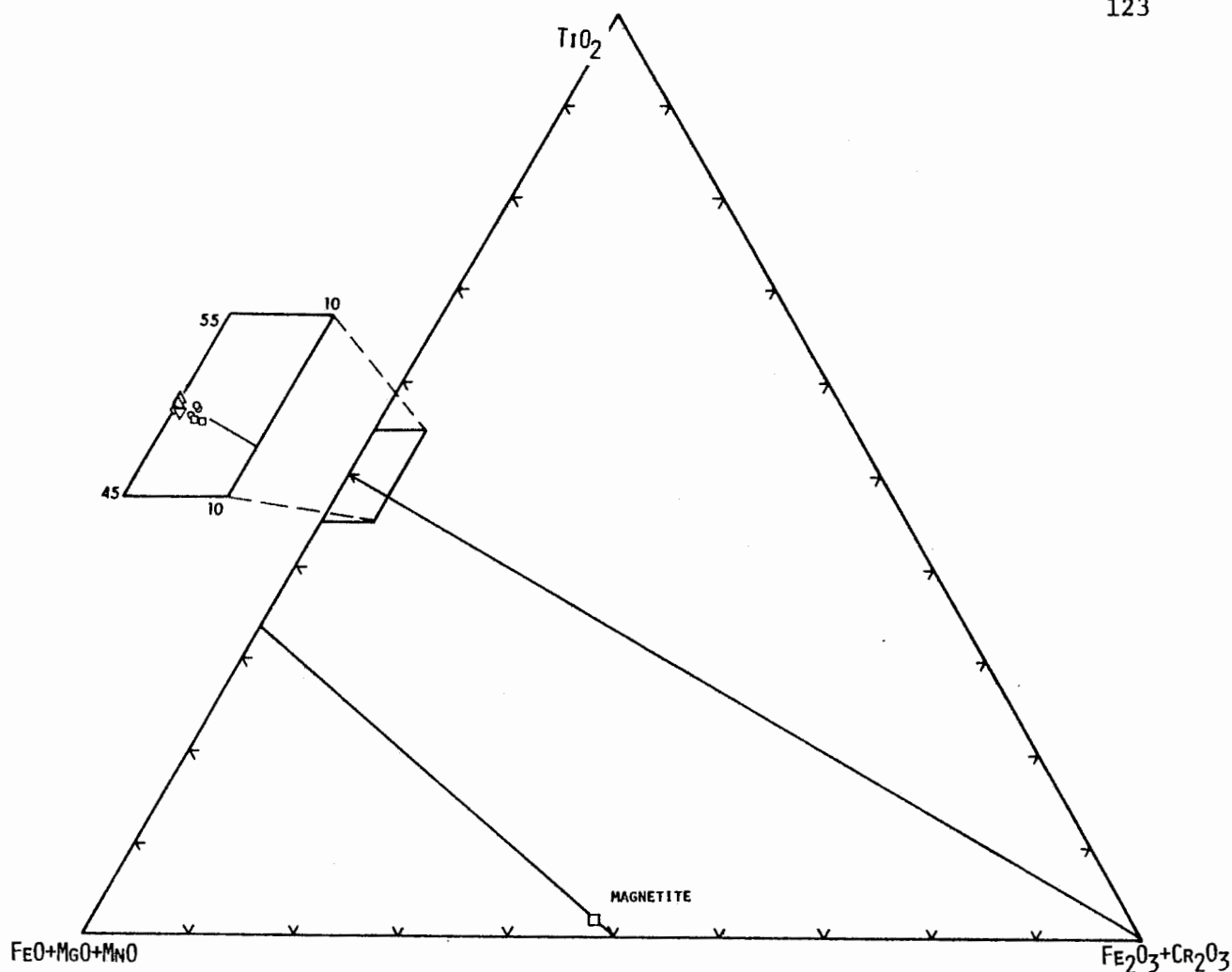


Figure 39. Ilmenite and magnetite compositions plotted in terms of  $\text{TiO}_2$ ,  $(\text{MgO} + \text{MnO})$ , and  $(\text{Fe}_2\text{O}_3 + \text{Cr}_2\text{O}_3)$ . Circles = Y57I, squares = 9Q9A, large square = 2 magnetites from 9Q9A, triangles = OG2B, inverted triangles = N45A, diamond = K34A.

### Sulfides

In many of the orthopyroxene-olivine hornblendites, sulfides make up a major percent of the opaque minerals. Pyrrhotite is the most commonly observed sulfide phase and is ubiquitous in the fresh specimens. Optical properties are given in Table 32. "Flame" lamellae are prevalent and are visible as areas of weakly contrasting color and reflectivity. The lamellae are visible in air but are best observed in oil under partially crossed nicols. They are probably due to a hexagonal-monoclinic inversion of pyrrhotite (Taylor, 1969).

Table 31. Electron probe analyses of ilmenite and sphene.

Locality	<u>Ilmenite</u>												<u>Sphene</u>
	Y57I			9Q9A			OG2B		N45	K34A			K34A
Analysis No.	7	12	11a	48	49	59	4B *	13B *	1	2a	3a	31	34
SiO <sub>2</sub>	.18	.18	.32	.13	.29	.28	.00	.00	.17	.19	.16	.22	29.70
TiO <sub>2</sub>	52.72	52.69	52.56	53.52	53.27	52.71	54.00	54.10	53.27	52.30	52.86	52.86	39.36
Al <sub>2</sub> O <sub>3</sub>	.18	.12	.19	.14	.13	.07	.00	.00	.05	.08	.07	.09	.95
Cr <sub>2</sub> O <sub>3</sub>	.18	.16	.04	.24	.21	.24	.07	.07	.32	.05	.12	.13	.02
FeO <sup>#</sup>	44.37	42.44	44.49	42.62	42.96	46.35	42.50	43.00	42.66	46.10	44.60	45.72	.87
MnO	.93	.80	.82	.91	.84	.80	.57	.63	.77	.61	.41	.76	.02
MgO	1.79	3.08	1.75	2.67	2.84	3.21	1.72	2.80	2.55	.21	1.52	.36	.07
NiO				.33	.22	.20						.33	.11
CaO	.11	.08	.08	.05	.13	.26	.03	.04	.07	.10	.05	.11	28.14
Na <sub>2</sub> O	.19	.13	.22	.06	.11	.18	.00	.00	.16	.00	.11	.02	.00
K <sub>2</sub> O	.03	.02	.00	.03	.02	.00			.00	.00	.00	.03	.00
Total	100.68	99.70	100.47	100.70	101.02	100.30	99.89	100.64	100.11	99.55	99.90	100.63	99.24

\* A. E. Bence, Analyst.

# All Fe is taken as Fe<sup>2+</sup>.

Ilmenite formulae calculated on the basis of 2 cations. Sphene formula calculated on the basis of 5 oxygens.

Locality	<u>Ilmenite</u>												<u>Sphene</u>
	Y57I			9Q9A				OG2B	N45		K34A		K34A
Analysis No.	7	12	11a	48	49	59	4B	13B	1	2a	3a	31	34
Si	.004	.004	.007	.003	.006	.007			.004	.004	.004	.005	.981
Ti	.978	.976	.977	.988	.961	.970	1.014	.999	.988	.996	.992	.999	.978
Al	.005	.003	.005	.004	.004	.001			.001	.002	.002	.002	.037
Cr	.003	.003	.001	.004	.004	.004	.001	.001	.006	.001	.002	.002	
Fe <sup>3+</sup>	.042	.050	.036	.012	.062	.048			.010				
Total	1.032	1.036	1.020	1.011	1.037		1.015	1.000	1.009	1.003	1.000	1.008	1.996
Mg	.065	.114	.064	.098	.135	.117	.064	.102	.094	.007	.056	.013	.003
Ni				.006	.004	.004							.002
Fe	.872	.823	.883	.863	.779	.817	.908	.883	.880	.974	.931	.960	.023
Mn	.019	.017	.017	.019	.017	.017	.012	.013	.016	.013	.008	.015	
Ca	.002	.001	.001	.001	.003	.007	.001	.001	.002	.002	.001	.002	.996
Na	.009	.009	.010	.002	.005	.008					.004	.001	
K	.001			.001									
Total	.968	.964	.975	.990	.943	.970	.985	.999	.992	.996	1.000	.991	1.024
<u>Fe+Mn</u>	.932	.881	.934	.900	.858	.877	.935	.898	.905	.993	.994	.987	
<u>Fe+Mn+Mg</u>													
FeTiO <sub>3</sub>	.902	.851	.908	.878	.823	.848	.923	.885	.886	.980	.936	.972	
MgTiO <sub>3</sub>	.067	.118	.066	.100	.143	.121	.065	.102	.095	.007	.056	.013	
MnTiO <sub>3</sub>	.020	.018	.017	.019	.018	.018	.012	.013	.016	.013	.008	.015	
Fe <sub>2</sub> O <sub>3</sub>	.011	.013	.009	.003	.016	.012	.000	.000	.003	.000	.000	.000	



Table 32. Reflected light optical properties of pyrrhotite.

Color: brownish-yellow.

Reflectivity: moderate to high; 30-40%.

Bireflectance: yellow to brownish-yellow; distinct.

Anisotropy: red-brown to gray-blue; strong.

Pentlandite was observed as a very minor phase in some of the pyrrhotite grains of specimen Y57I. It is lighter in color with respect to the pyrrhotite, and has a creamy appearance. It appears isotropic, however, colors may be masked by the strong anisotropy of the pyrrhotite. Pentlandite may have exsolved from pyrrhotite during the conversion of hexagonal into monoclinic pyrrhotite (Uytenbogaart and Burke, 1971), taking up the Ni which is displaced during the conversion (Haggerty, pers. comm.).

Pyrite is the second most common sulfide observed, most commonly appearing as euhedral grains within pyrrhotite. It is isotropic and has a lighter, more yellow color and a higher reflectivity (50%) than pyrrhotite. Pyrite is very commonly associated with chalcopyrite.

Chalcopyrite is easily distinguished from pyrrhotite and pyrite by its brassy color. It has high reflectivity (40-50%) and displays no bireflectance nor anisotropy. Chalcopyrite is most commonly observed as elongate or rounded blebs within pyrrhotite grains.

Sulfur within these lenses may have been present as a primary igneous phase or been introduced after emplacement of the lenses into the sulfidic schist member of the Partridge Formation. It is interesting to note the lack of sulfides in the samples from locality K34, situated in an area where amphibolite is the dominant country rock. The amphibolite might have prevented the influx of sulfur into the ultramafic rock from the sulfidic schist.

### Rutile and Sphene

Ilmenite is the dominant oxide in specimen K34A. However, it also contains small inclusions of what appear to be rutile rimmed by sphene (Fig. 40). These inclusions are invariably in contact with a grain edge. Electron microprobe analyses of an ilmenite of this type, together with a sphene rim, are given in Table 31. No analyses are available of rutile (lined area enclosed by sphene in Fig. 40) because of electron-beam overlap with sphene. Ilmenite grains containing rutile and sphene are also found in specimen 9Q9D.



Figure 40. Ilmenite grain from locality K34 as seen in reflected light (25x; oil). Numbers refer to locations of microprobe analyses given in Table 31. Lined area is rutile; stippled area is sphene.

## EMPLACEMENT OF BODIES

All of the orthopyroxene-olivine-spinel hornblendites described here lie within a rather narrow stratigraphic and structural domain and are considered to be of common origin. Present data are insufficient to establish irrefutably the mode of emplacement of these bodies. It is useful, therefore, to compare them with compositionally similar ultramafic rocks of known origin such as ultramafic lava flows and contact metamorphosed metasomatic margins of serpentinites. Also to be kept in mind are other occurrences of ultramafic rocks associated with Ordovician strata elsewhere in the northern Appalachians (Williams and Smyth, 1973) where emplacement is better understood. Contact relations and bulk chemistry are the most reasonable bases for comparison.

Contact Data

These bodies have a wide range of sizes and are all roughly lens shaped, elongated parallel to regional foliation. Planar and linear features within the bodies are generally conformable with regional trends except for where influenced by slight late stage rotation at locality Y57. Foliation of the country rock is folded around the northern end of the large outcrop at locality O18. This is indicative of the competence of these bodies relative to surrounding schists and amphibolites. The overall shape and structure of these bodies is suggestive of boudinage of once more continuous layers. However, if this were the case, one might expect a higher concentration of more closely-spaced outcrops along strike. It seems more likely that these are isolated inclusions deformed into lens-shaped bodies during the Devonian Acadian orogeny.

The outcrop at B65 lies entirely within the augen gneiss member of the Partridge Formation. The remaining bodies are within the sulfidic schist member, which is very rich in amphibolite throughout this region. Amphibolite is commonly in close proximity to the ultramafic lenses.

Mineral assemblages characteristic of hybridization occur at or near the margins of bodies at localities Y57, O18, K28N, K28S, 9Q9, and J98. Cumingtonite- or anthophyllite-hornblende-plagioclase gneisses are typical. The entire outcrop at locality K34 is hybridized, with plagioclase-garnet-anthophyllite-pargasite the dominant assemblage.

Biotite or phlogopite-rich rocks occur near the margins at localities 9Q9 and 500, respectively. The single best exposed contact is along the east side of N01 (Plate 3). The ultramafic body is in sharp contact with a hornblendite, which grades to a hornblende-plagioclase amphibolite away from the contact. Within the ultramafic body, a hornblende-chlorite-talc-cumingtonite rock grades inward to a hornblende-chlorite-cumingtonite rock with a sharp reduction in hornblende accompanied by a significant increase in chlorite (Table 5).

Metasomatic introduction of silica and alkalis during or soon after emplacement may have adjusted chemistry sufficiently for the formation of the present mineral assemblages in hybrid rocks during later metamorphism. Aside from the depletion in plagioclase toward the contact with N01, no other contact features, such as chill margins or contact hornfels, were observed that can be related to the emplacement of the bodies. In view of the very limited available contact data, however, this lack of evidence by itself is insufficient to rule out the possibility of high-temperature emplacement.

### Bulk Chemistry

Bulk chemical compositions calculated from microprobe and modal analyses are presented in Table 33. These compositions are plotted in ACF and ASF diagrams (Figure 41), modified from Irving and Ashley (1976). They trend along a line connecting the field of serpentinite compositions and plagioclase (Fig. 41A). 9Q9A is closest to the serpentinite field, and K34A, a hybridized rock containing the most Al and Si, plots closest to the plagioclase composition. As plotted in the Figure 41B, the orthopyroxene-olivine hornblendites at Y57 and 9Q9 project outside of the olivine-orthopyroxene-spinel field. The major amount of low-SiO<sub>2</sub> pargasite is probably responsible for displacing the projected bulk compositions toward higher SiO<sub>2</sub>.

The compositional trend of these bodies serves as an argument favoring a protolith of serpentinite, or its chemical equivalent. Bulk chemical changes could have occurred before or during emplacement into the Partridge Formation. Such changes, if they did occur, may have affected small bodies to a greater extent than the large bodies. Comparisons with other ultramafic rocks narrow the field of possible origins.

Ultramafic Lava Flows. Although available contact data do not support the idea that these bodies originated as ultramafic lava flows, comparison with such rocks is justified because of the general chemical consistency from outcrop to outcrop and the limited stratigraphic occurrence of the bodies being studied. An ultramafic lava flow deposited within the marine sediments and volcanics of the Partridge Formation would more than likely define a narrow stratigraphic horizon. Subsequent metamorphism and deformation of such a thin layer could result in the formation of lens-shaped bodies strung out parallel to regional structural trends.

Table 33. Analyzed and calculated bulk chemical compositions of selected ultramafic specimens.\*

	Orthopyroxene-Olivine Hornblendite							Hybridized Ultramafic Rock	
	Y57I		Y57E	9Q9A		OG2B	N45A	K34A	
	XRF	OXY	XRF	XRF	OXY	OXY	OXY	XRF	OXY
SiO <sub>2</sub>	43.49	42.47	45.07	42.36	41.54	43.98	46.08	45.65	46.15
TiO <sub>2</sub>	0.51	1.34	0.70	0.96	1.10	1.45	1.28	0.93	0.86
Al <sub>2</sub> O <sub>3</sub>	11.78	12.05	12.70	10.00	7.59	12.58	10.70	14.07	13.72
Cr <sub>2</sub> O <sub>3</sub>		0.21			0.33	0.20	0.33		0.01
Fe <sub>2</sub> O <sub>3</sub>						1.43			
FeO#	11.96	10.96	10.78	11.52	12.90	10.59	11.43	11.51	12.27
MnO	0.19	0.17	0.21	0.21	0.17	0.16	0.17	0.20	0.08
NiO						0.04			
MgO	23.11	21.66	18.14	25.39	28.44	19.52	21.43	15.19	15.83
CaO	7.22	7.19	9.60	5.52	4.74	7.36	6.39	8.52	7.50
Na <sub>2</sub> O		0.95			0.26	1.00	0.73		1.20
K <sub>2</sub> O	0.14	0.14	0.18	0.07	0.03	0.12	0.12	0.34	0.27
H <sub>2</sub> O		2.85			2.91	1.55	1.35		2.10
P <sub>2</sub> O <sub>5</sub>	0.09		0.09	0.15		0.03		0.16	

\* = Additional analyses and methods of calculation given in Appendix 1.

XRF = X-ray fluorescence analysis; M. Rhodes, University of Massachusetts, analyst.

OXY = Calculated analysis based upon ideal number of oxygens per unit formula (see Appendix 1).

# = All Fe as FeO except for specimen OG2B.

Figure 41A. Plot of molecular proportions of  $(\text{Al}_2\text{O}_3\text{-Na}_2\text{O-K}_2\text{O})$ ,  $\text{CaO}$ ,  $(\text{FeO+MnO+MgO})$  for bulk compositions of selected ultramafic rocks. Dashed fields are from Irving and Ashley (1976). A = Ca-Al silicate rich rocks from reaction zones; B = chlorite-tremolite-talc rich metasomatized serpentinite; C = harzburgite and serpentinite outside the Bogong Granite aureole.

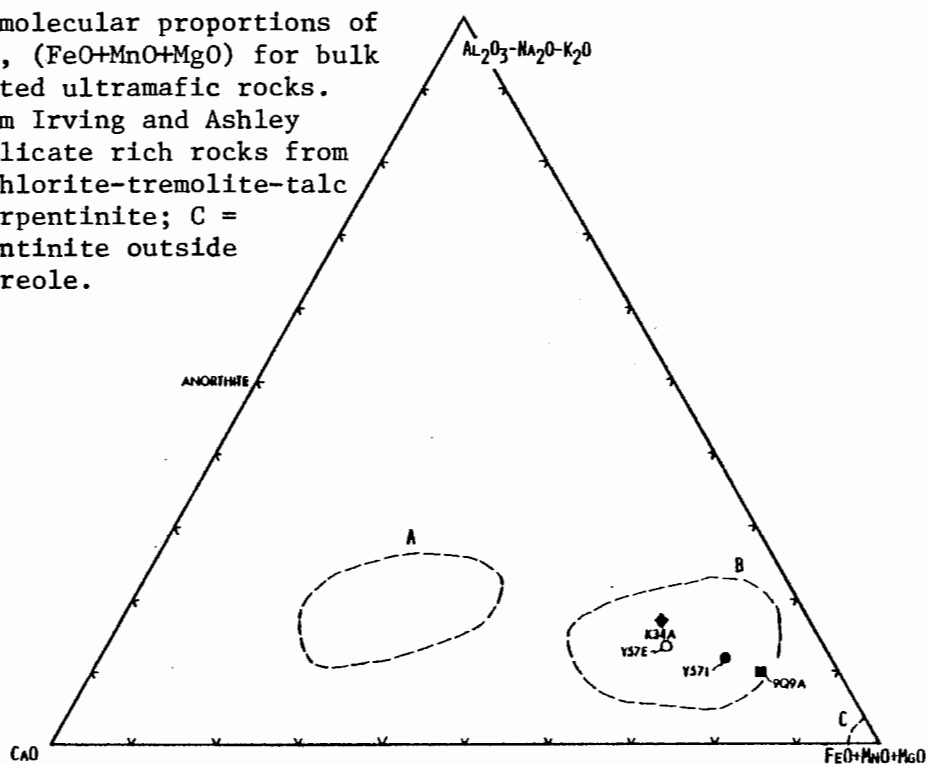
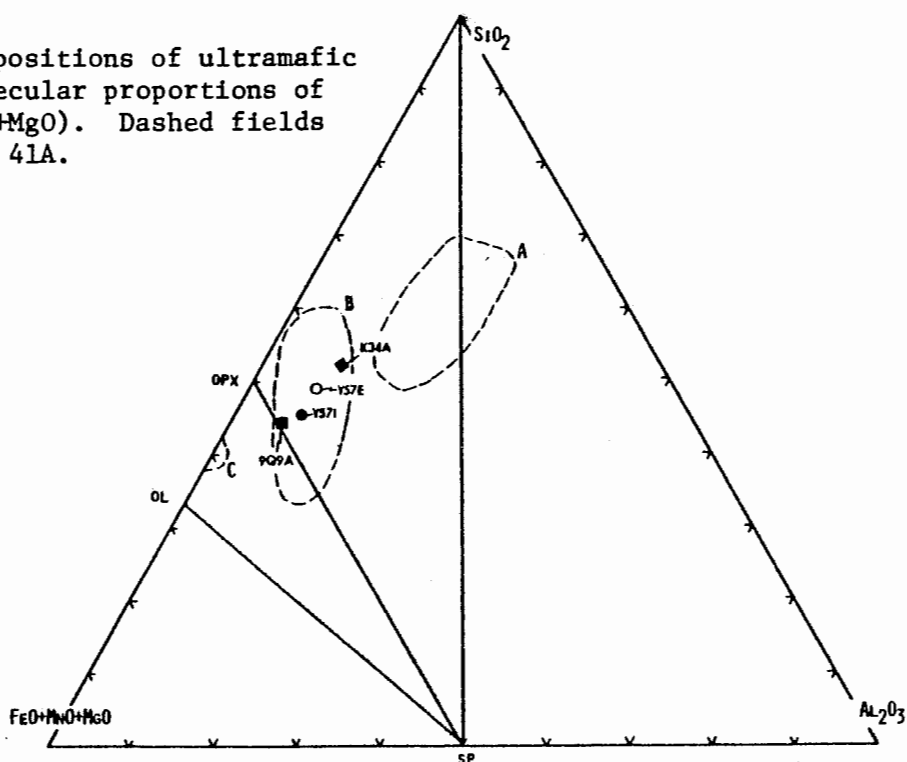


Figure 41B. Bulk compositions of ultramafic rocks in terms of molecular proportions of  $\text{SiO}_2$ ,  $\text{Al}_2\text{O}_3$ ,  $(\text{FeO+MnO+MgO})$ . Dashed fields are same as in Figure 41A.



Ultramafic lava flows were described and classified separately by Viljoen and Viljoen (1969 a and b) to characterize rocks from the Barberton Mountain Land, South Africa. These rocks were referred to as komatiites and have since been recognized within most of the Archean Shield areas (Arndt, Naldrett, and Pyke, 1977). Some komatiites are reported to occur in Proterozoic and lower Paleozoic terrains (Gale, 1973).

A combination of chemical and textural criteria are employed as diagnostic of komatiites. Quench textures must be present which establish the existence of a melt of komatiitic composition. This texture is usually distinguished by the presence of large skeletal crystals of olivine and, less commonly, skeletal pyroxene and/or plagioclase. In the absence of these textural features, chemical composition alone is insufficient to define a komatiite because of overlap with other ultramafic rock types (Brooks and Hart, 1974). Most komatiites have been subject to relatively low grade metamorphic conditions and quench textures are preserved. The ultramafics of this study, however, exist in the sillimanite-muscovite and sillimanite-K feldspar zones, and such textures would have been obliterated.

Komatiites are subdivided into peridotitic, pyroxenitic, and basaltic types on the bases of chemistry, texture, and stratigraphy (Arndt, et al., 1977). Peridotitic types have, thus far, only been found in Archean rocks. The Paleozoic komatiite is of the basaltic type. Depending upon type, MgO ranges from 40 down to 8 weight percent.  $\text{FeO}/(\text{FeO} + \text{MgO})$  ratios and  $\text{TiO}_2$  contents are low; NiO, and  $\text{Cr}_2\text{O}_3$  are high.  $\text{CaO}/\text{Al}_2\text{O}_3$  ratios greater than 1 were originally considered characteristic of these rocks (Viljoen and Viljoen, 1969a), however, komatiites with lower ratios have since been recognized (Arndt, et al., 1977).



Table 34 lists average compositions of each of the three types of komatiite. For comparative purposes, the average of Y57I and Y57E has been recalculated on an anhydrous basis. 9Q9A is listed separately (also on an anhydrous basis) because of the anomalous  $\text{Al}_2\text{O}_3$  and  $\text{MgO}$  values with respect to other analyses.

The average rocks of the present study do not compare well with either basaltic or pyroxenitic types. They are most similar to the peridotitic type, with  $\text{MgO} < 30\%$ , but  $\text{Al}_2\text{O}_3$  content is higher, and  $\text{CaO}/\text{Al}_2\text{O}_3$  ratio is lower. 9Q9A is closest in composition to the peridotitic komatiite. Considering that chemistry is not quite right, that textural features and proper associated rocks are absent, and that no peridotitic komatiites have been recognized in the Phanerozoic, it seems unlikely that these rocks represent ultramafic lava flows.

Contact Metamorphosed Metasomatic Margins of Serpentinities. Amphibole-orthopyroxene-olivine-spinel-chlorite assemblages have been reported where metasomatized margins of serpentinites are involved in contact aureoles of younger granites. Springer (1974) discusses the occurrence of magnesian-hornfels in aureoles associated with the contact metamorphism of serpentinite by the Jurassic Pine Hill Intrusive Complex in the western Sierras. In the central Cascades of Washington, a 2 km wide contact aureole is produced by the intrusion, during the late Cretaceous, of the Mount Stewart Batholith into serpentinite of the Ingalls Complex (Frost, 1975). Irving and Ashley (1976) refer to "aluminiferromagnesian hornfelses" in the contact aureole between the Coolac Serpentine and the Devonian Bogong Granite, in New South Wales, Australia. They also provide a list of other occurrences

Table 34. Bulk compositions of ultramafic rocks from central Massachusetts and averages of different types of komatiite; all cast on an anhydrous basis.

	Ave.*	9Q9A	Perid. Kom. <sup>+</sup> MgO >30%	Perid. Kom. <sup>+</sup> MgO <30%	Pyroxenitic <sup>+</sup> Komatiite	Basaltic <sup>+</sup> Komatiite
SiO <sub>2</sub>	44.28	42.36	44.90	46.00	50.20	51.60
TiO <sub>2</sub>	.61	.96	.19	.32	.61	.65
Al <sub>2</sub> O <sub>3</sub>	12.29	10.00	5.30	7.40	11.60	13.30
Cr <sub>2</sub> O <sub>3</sub>			.26	.39		
FeO	11.37	11.52	10.40	11.50	11.11	11.70
MnO	.21	.21	.18	.22	.19	.19
MgO	20.63	25.39	33.60	26.50	14.30	10.00
CaO	8.41	5.52	5.00	7.40	9.60	10.40
Na <sub>2</sub> O			.35	.45	2.34	2.16
K <sub>2</sub> O	.16	.07	.08	.10	.05	.11
<u>CaO</u> <u>Al<sub>2</sub>O<sub>3</sub></u>	.68	.55	.94	1.00	.83	.78

\* Averages of Y57I and Y57E.

+ Averages of classes as defined by Arndt et al. (1977, Table 7).

of similar rock types. The metamorphosed contact aureole of the Nain Complex in Labrador is reported by Berg (1976) to contain hornblende-orthopyroxene-olivine-spinel rocks which also contain anorthite, chlorite, ilmenite, cummingtonite, magnetite, and pyrrhotite.

Although these contact aureoles and serpentinites extend over a number of kilometers, the occurrence of rocks containing the hornblende-orthopyroxene-olivine-spinel assemblage is quite limited; commonly in layers a few meters or less in thickness. These layers are considered to have formed by complex processes involving early low temperature metasomatism and subsequent thermal metamorphism. At Paddy-Go-Easy Pass, for example (Frost, 1975), a chloritic blackwall exists between ultramafic rock comprising the serpentinite, and mafic inclusions within the body. The orthopyroxene-olivine-spinel assemblage was subsequently produced by the thermal effects associated with the

intrusion of the Mount Stewart Batholith. In a similar fashion, the Al-Fe-Mg hornfelses described by Irving and Ashley (1976), occur in reaction zones between serpentinite and tectonic inclusions.

Irving and Ashley have provided chemical analyses of sixteen Al-Fe-Mg hornfelses from within the thermal aureole of the Bogong Granite. In addition, they have tabulated analyses of fifteen serpentinitized harzburgites and reaction-zone rocks which lie outside the aureole (their Tables III and IV, respectively). Of these analyses, only two from within and one from outside of the aureole are reasonably close to the compositions of the rocks of this study (Table 35). The two analyses from within the aureole (SU37850; SU36560) are of samples taken a few hundred meters from each other in rock referred to as "patchily developed metaserpentinite." No detail is given concerning the third sample (MU3854). Rock analyses are not provided by Frost (1975), however, considering the similarities in regional setting and mineralogies between the rocks described by Frost and those of Irving and Ashley, it seems reasonable to assume that there would be similarities in chemical compositions.

In spite of some chemical similarities, however, the regional setting of the ultramafics in central Massachusetts does not correspond well with that of the ultramafics associated with the contact aureoles. No major serpentinite body or high grade equivalent occurs in the immediate vicinity of the ultramafics under consideration. If it is postulated that these lenses are remnants broken off of a reaction rim on a serpentinite body, it is difficult to explain why only rocks of this limited chemistry were broken off, unless the original reaction rims were very thick. Such a thick rim would have far exceeded the dimensions of the limited known serpentinite rims with which chemistry is comparable, and would also have required

Table 35. Bulk chemical compositions of ultramafic rocks from central Massachusetts and from New South Wales, Australia.

	Central Massachusetts*				New South Wales, Australia		
	Y57I XRF	Y57E XRF	OG2B OXY	9Q9A XRF	SU37850	SU36560	MU3854
SiO <sub>2</sub>	43.49	45.07	43.98 (44.67)#	42.36	41.10 (42.90)#	40.52 (41.89)	39.86 (42.18)
TiO <sub>2</sub>	0.51	0.70	1.45 ( 1.47)	0.96	1.20 ( 1.25)	1.89 ( 1.95)	0.83 ( 0.88)
Al <sub>2</sub> O <sub>3</sub>	11.88	12.70	12.58 (12.78)	10.00	11.36 (11.86)	13.26 (13.71)	13.32 (14.09)
Cr <sub>2</sub> O <sub>3</sub>			0.20				
Fe <sub>2</sub> O <sub>3</sub>			1.43 ( 1.45)		2.87 ( 3.00)	1.45 ( 1.50)	2.71 ( 2.87)
FeO	11.96 <sup>+</sup>	10.78 <sup>+</sup>	10.59 (10.76)	11.52 <sup>+</sup>	9.56 ( 9.98)	9.69 (10.02)	8.95 ( 9.47)
MnO	0.20	0.21	0.16 ( 0.16)	0.21	0.20 ( 0.21)	0.12 ( 0.12)	0.20 ( 0.21)
MgO	23.11	18.14	19.52 (19.83)	25.39	23.19 (24.21)	21.77 (22.51)	19.32 (20.44)
CaO	7.22	9.60	7.36 ( 7.48)	5.52	5.98 ( 6.24)	6.51 ( 6.73)	8.49 ( 8.98)
Na <sub>2</sub> O			1.00 ( 1.02)		0.93 ( 0.97)	0.88 ( 0.91)	0.56 ( 0.59)
K <sub>2</sub> O	0.14	0.18	0.12 ( 0.12)	0.07	0.06 ( 0.06)	0.08 ( 0.08)	0.16 ( 0.17)
P <sub>2</sub> O <sub>5</sub>	0.09	0.09	0.03 ( 0.03)	0.15	0.18 ( 0.19)	0.20 (0.21)	0.51 ( 0.54)
H <sub>2</sub> O <sup>+</sup>			1.55		4.11	3.11	5.43
H <sub>2</sub> O <sup>-</sup>					0.01		0.09
CO <sub>2</sub>					0.11	0.16	0.00

\* Analyses from Table A-1.

+ All Fe as FeO.

# Parentheses show analyses recalculated on an anhydrous basis.

SU37850 = Olivine-hornblende-pleonaste-magnetite-chlorite hornfels.

SU36560 = Cumingtonite-hornblende-olivine-pleonaste-magnetite-chlorite-(ilmenite) hornfels.

MU3854 = Hornblende-tremolite-chlorite-(prehnite-sphene-Cr-spinel) rock 20 km north of aureole.

metasomatic transport of components over large distances. An alternative proposal would be that the present bodies were once all serpentinite or chemically equivalent blocks that were metasomatically altered by low temperature processes, after emplacement in the Partridge Formation, but before Acadian regional metamorphism. In all these cases however, the question still remains as to the origin of the protoliths. Perhaps they represent mantle material that was emplaced through sialic crust into the eugeosynclinal sediments associated with the Paleozoic rift system, as proposed for the ultramafics in central Vermont along the Green Mountain Anticlinorium (Chidester and Cady, 1972). In the present case such rocks would have undergone complete metasomatic transformation during or following emplacement, leaving no pure remnant peridotite or serpentinite. An argument against this hypothesis is that no intrusive masses of the same ultramafic rock have yet been identified in underlying strata of the Ammonoosuc Volcanics or Monson Gneiss, although ultramafics of different mineralogy are known. An alternative hypothesis, suggested by serpentinite relations in Newfoundland, is that the original ultramafic fragments are "drop stones" from an overriding nappe containing ultramafic rocks that has since been eroded away. Although this hypothesis is troubled by lack of such a source nappe, it is quite consistent with the highly varied size of the bodies studied and with a number of Newfoundland melange deposits in which the matrix is black shale of Ordovician or older Paleozoic age. Should this fanciful hypothesis prove to be correct, then the ultramafic bodies studied here provide one of the first clues to important events of Ordovician tectonic history in the area, about which a great deal more has yet to be learned.

## METAMORPHISM

Interrelationship Between Bulk Chemistry and Mineralogy

The presently-observed metamorphic mineral assemblages in all but the retrograded rocks were formed during the Devonian Acadian Orogeny. Different assemblages probably formed under the same metamorphic conditions from different bulk compositions, imposed by earlier metasomatic processes that most probably took place during the Ordovician. Without knowledge of the mineral assemblages at the time of emplacement, it is not possible to trace a series of metamorphic reactions leading to the present assemblages. However, if it is assumed that the system became closed to non-volatile components following early metasomatism, certain isochemical reactions can be proposed which relate mineralogy to bulk chemistry.

Pargasite or hornblende is the dominant mineral in all of these rocks. It cannot be determined whether amphibole existed prior to emplacement. If, however, tremolitic amphibole and spinel were present following emplacement, and alkali activity were imposed during metasomatism, then the present assemblage can, in part, be explained by a metamorphic reaction of the type:

$\text{tremolite} + \text{spinel} + \text{Na}^+ = \text{pargasitic amphibole} + \text{forsterite} + \text{enstatite}$

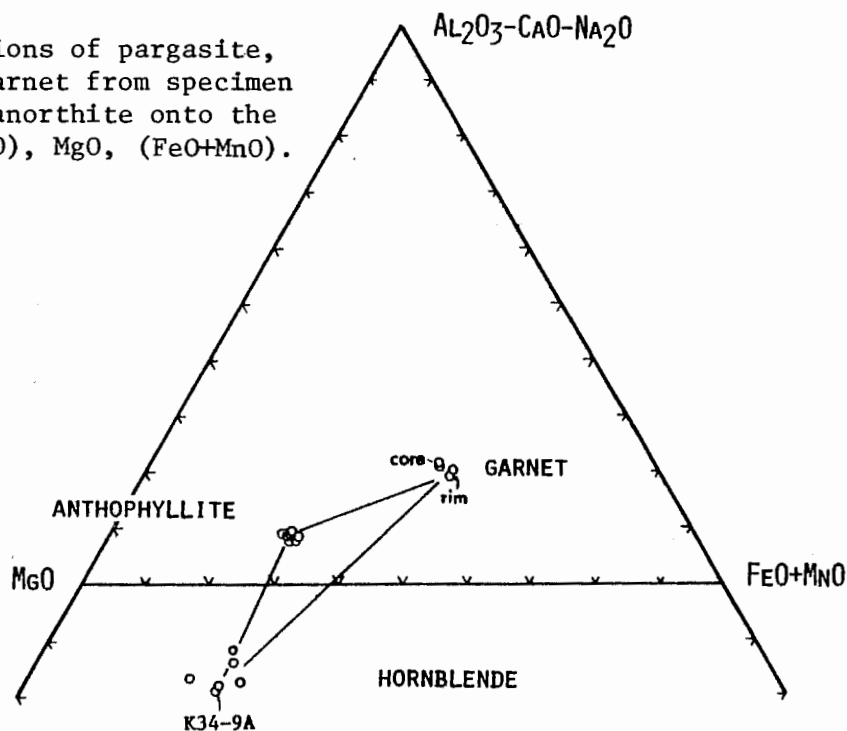
as proposed by Frost (1975, p. 292). This reaction suggests that Al content of an amphibole, coexisting with forsterite, enstatite, and spinel, is controlled by activities of alkalis. The lower Al content of the amphibole at 9Q9A (Table 15) is consistent with the lower alkali content of this specimen relative to those from the other localities (Table 33). Pargasite at locality N45 is zoned outward, toward the composition of actinolite. The rim contains less Al, Fe, Cr, and Na, and more Mg and Si than the core (Table 15). This is directly opposite to the amphibole zonation in 9Q9A, but its relation if any to the reaction cited above is uncertain.

The presence of aluminous anthophyllite in a rock is thought to be an indication that the rock underwent chemical adjustment by metasomatic influx of Si and Al, prior to metamorphism. It may be possible to generate low Al anthophyllite directly from a serpentinite composition; however, the Si- and Al-enriched bulk chemistry of the anthophyllite-bearing rock, K34A, and the fact that anthophyllite occurrence is restricted to olivine-free rocks in the margins of lenses or in small bodies, serve as arguments against such an origin.

Cummingtonite, like anthophyllite, is considered to have formed in rocks of hybrid bulk composition. It occurs in association with plagioclase along the outer edges of some lenses, while in at least two cases, it is associated with hornblende and disseminated throughout the lens. The only available analysis of this phase from any of these lenses is that of specimen N01A (Table 16), where it coexists with hornblende. This particular cummingtonite has an  $\text{Fe}/(\text{Fe}+\text{Mg})$  ratio of .32. It is suggested by Robinson and Jaffe (1969) that it would react to hornblende-anthophyllite in the presence of plagioclase. A cummingtonite-hornblende-plagioclase assemblage exists at locality K28N (Figure 12, Table 10), in a layer between the orthopyroxene-olivine-hornblende body and a hornblende-anthophyllite layer. Assuming both layers formed under identical metamorphic conditions, the differences in assemblage must be a function of an earlier-imposed chemical gradient. On the basis of observations by Robinson and Jaffe (1969), the hornblende-cummingtonite pair coexisting with plagioclase would be expected to have a higher  $\text{Fe}/(\text{Fe}+\text{Mg})$  ratio than the corresponding hornblende-anthophyllite pair. The hornblende-cummingtonite association at K28N should also be Fe-enriched with respect to the plagioclase-absent, hornblende-cummingtonite assemblage at N01A.

Although there is no quartz in these rocks, it is interesting to view the compositions of coexisting anthophyllite, hornblende, and garnet from K34A in an anorthite projection (Figure 42). In quartz-bearing rocks, cummingtonite-anthophyllite-garnet rather than hornblende-anthophyllite-garnet would be the stable assemblage (Robinson and Jaffe, 1969; Robinson, et al., 1971), suggesting that in the presence of excess  $\text{SiO}_2$ , hornblende at K34A would react with anthophyllite or garnet to form cummingtonite and plagioclase. Optical properties of hornblende and anthophyllite in specimen J98B, which contains no garnet, indicate that their compositions are close to the analogous minerals in specimen K34A. The absence of garnet in J98B may be caused by a slightly less aluminous or ferroan bulk chemistry or the compositions of coexisting hornblende and anthophyllite might have been affected by the concentration of a minor component, such as  $\text{MnO}$ .

Figure 42. Compositions of pargasite, anthophyllite, and garnet from specimen K34A projected from anorthite onto the plane ( $\text{Al}_2\text{O}_3$ - $\text{CaO}$ - $\text{Na}_2\text{O}$ ),  $\text{MgO}$ , ( $\text{FeO}+\text{MnO}$ ).

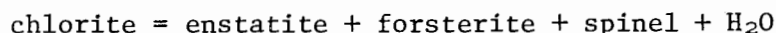




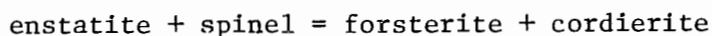
### Metamorphic Conditions

The metamorphic grade of the country rock associated with these ultramafic lenses has been established on the basis of phase relations in quartz-bearing pelitic rocks. Recent temperature and pressure estimates based on garnet-biotite equilibria and continuous Fe-Mg-Mn reactions (Tracy *et al.*, 1976) indicate a range of 605 to 675°C between zones II and V (Figure 2) at a pressure between 5 and 7 kbars. The metamorphic grade of the ultramafic rocks, themselves, is more difficult to ascertain because relations in the quartz-absent system,  $\text{MgO-Al}_2\text{O}_3\text{-SiO}_2$  (+ FeO, MnO, CaO, Na<sub>2</sub>O, K<sub>2</sub>O, Cr<sub>2</sub>O<sub>3</sub>, TiO<sub>2</sub>), are less well established. A reasonable estimate of temperature can be made on the basis of selected temperature-sensitive reactions, but pressure determinations at present are tenuous, at best.

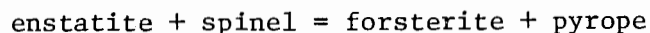
Chlorite breakdown. The primary metamorphic assemblage in these lenses is considered, in part, to represent the stable coexistence of chlorite and its breakdown products, enstatite + forsterite + spinel + vapor. Recent experimental studies involving the magnesian end-members (Fawcett and Yoder, 1966; Staudigel and Schreyer, 1977) have shown the terminal chlorite reaction:



to be a function of P, T, and  $a_{\text{H}_2\text{O}}$ . The reaction is temperature sensitive with a low pressure limitation defined by the fluid absent reaction:



and the upper pressure limited by the reaction:



There is some question as to the composition of the terminal chlorite. Experimental results of Fawcett and Yoder (1966) suggested that the Al content of Mg-chlorite increases with increasing pressure. However, Chernosky (1974) failed to find a similar correlation at pressures up to

2kb, and Staudigel and Schreyer (1977) found clinochlore to be the most thermally stable chlorite between the pressures of 10 and 35 kb  $P_{H_2O}$ .

The presence of iron in chlorite will lower its breakdown temperature (Turnock, 1960; Frost, 1975). Between 5 and 7 kbars  $P_{H_2O}$ , iron-bearing chlorite breaks down by continuous reaction to orthopyroxene, olivine, spinel, and a more magnesian chlorite, with increasing temperature. Iron in the system also affects the position of the low pressure-limiting, solid-solid reaction by expanding the field of enstatite + spinel as against forsterite + cordierite. It would also be expected that iron affects the position of the high pressure-limiting reaction but no confirming data are available.

If clinochlore is the terminal chlorite composition, as suggested by experimental work cited, then iron-bearing chlorites, with Al contents greater than that of clinochlore, should become less aluminous, as well as less Fe-rich, as the chlorite breakdown reaction progresses. Figure 43 shows chlorite and its breakdown products from these lenses plotted so as to illustrate the relationship between Al and Fe contents of the different chlorites. Figure 43A is expressed in terms of ionic ratios rather than oxides to expand the compositions towards Al. Figures 43A and B show a detectable relationship between Al and Fe contents of these chlorites, with both decreasing in the order, OG2B-N45A-Y57I-9Q9A.

The thermal metamorphic gradient across this region (Figure 2) would be expected to impose a systematic decrease in the Al and Fe contents of chlorites from north to south in the order, Y57I>9Q9A>OG2B>N45A. The disparity between the observed and the predicted progression can probably be explained by slight local variation in  $a_{H_2O}$  from lens to lens as discussed below.

Figure 43A. Si-(Al+Cr+2Ti-Na-K)-(Mg+Fe<sup>2+</sup>+Mn+Ni+Ca-Ti) ternary diagram showing compositions of chlorite and breakdown products. Closed circles represent overlap as indicated. Circles = Y57I; squares = 9Q9A; triangles = OG2B; inverted triangles = N45A.

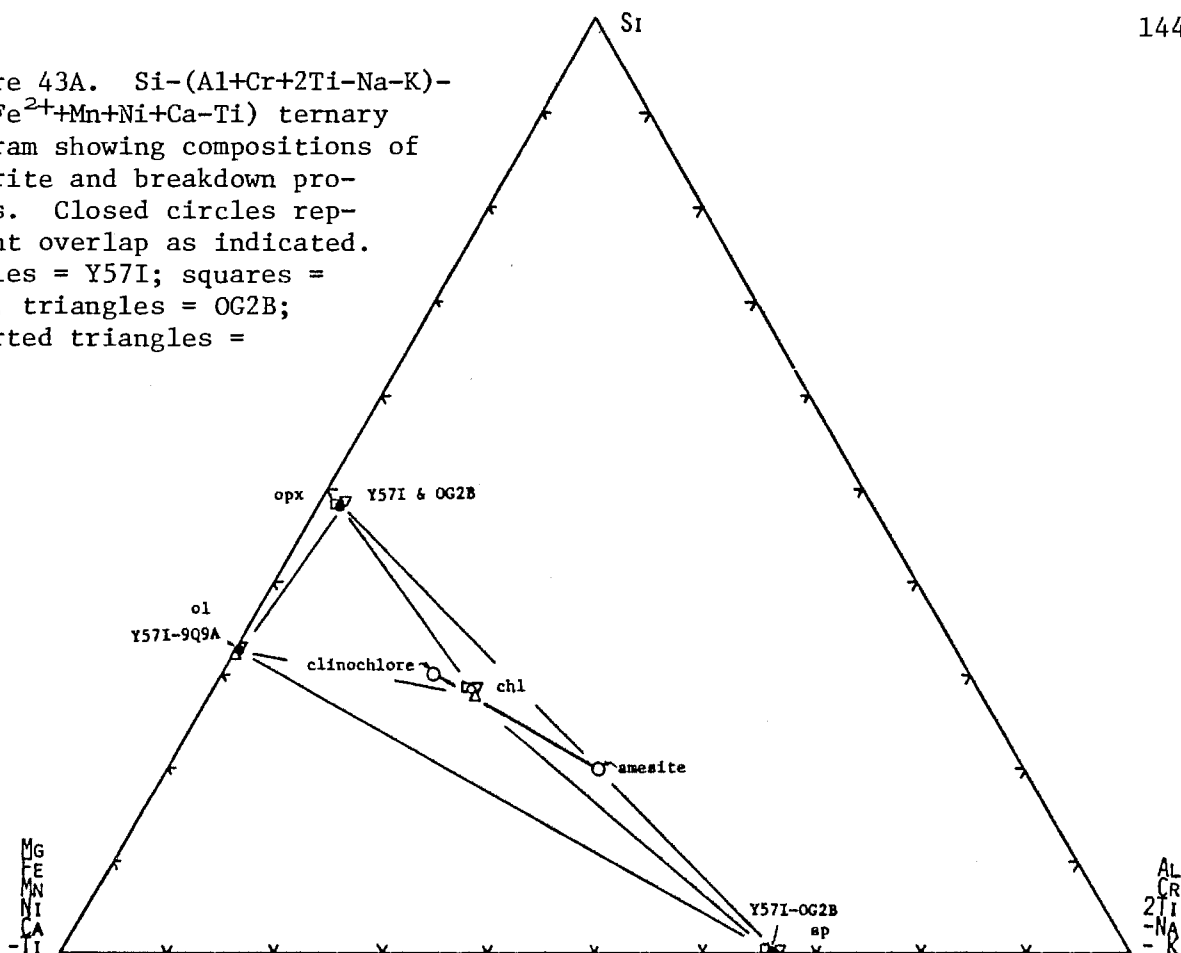
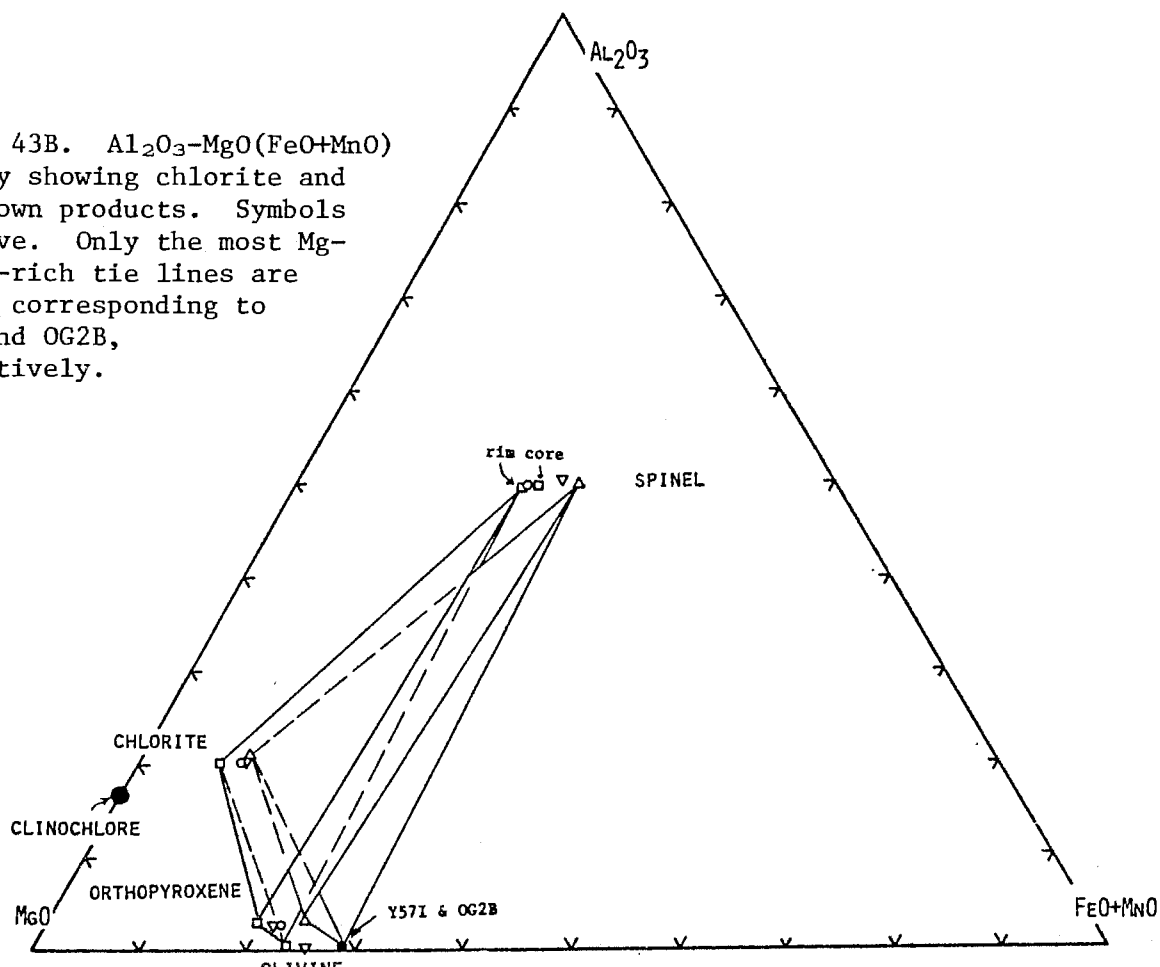


Figure 43B. Al<sub>2</sub>O<sub>3</sub>-MgO(FeO+MnO) ternary showing chlorite and breakdown products. Symbols as above. Only the most Mg- and Fe-rich tie lines are shown, corresponding to 9Q9A and OG2B, respectively.



Experimental and thermodynamic chlorite breakdown data considered above are for the case;  $P_{H_2O} = P_{Total}$ . In natural rocks however, it is more reasonable to assume conditions of  $P_{H_2O} < P_{Total}$ . Because chlorite breakdown involves dehydration, reducing  $P_{H_2O}$  with respect to  $P_{Total}$  will favor reaction products, thereby shifting the breakdown to a lower temperature. This has the effect of reducing the Fe/Mg ratio of the maximum stable chlorite at a given temperature. The implication is that  $a_{H_2O}$  was lower in the two large bodies, Y57 and 9Q9, off-setting the effects of the temperature gradient across the region on chlorite compositions. Retrograde metamorphism, however, could also contribute to iron-enrichment of a chlorite so that the observed composition is not only a function of  $a_{H_2O}$  and maximum temperature of metamorphism, but extent, if any, of retrograde metamorphism as well.

Because the complete chlorite equilibrium assemblage is in stable coexistence in these rocks, experimental and thermodynamic data can be applied to estimate conditions of metamorphism. All experiments and calculations are for  $P_{H_2O} = P_{Total}$  and yield only the maximum temperature of a given equilibrium.

Figure 44 depicts the invariant point generated by reactions involving forsterite, enstatite, spinel, cordierite, and chlorite in the system  $MgO-Al_2O_3-SiO_2-(H_2O)$ , showing the approximate orientation of these reactions in P-T space. The location of this invariant point as determined by Fawcett and Yoder (1966) is 3.25 kb at 750°C. Analogous iron-bearing reactions would occur at lower temperatures and pressures. Thermodynamic considerations of the effects of iron substitution into this system (Frost, 1975) are helpful in determining the amount of relative displacement of these reactions. Two diagrams presented by Frost (1975, Figures 12 and 13) are reproduced in Figure 45. The construction of these diagrams is based upon  $K_D$  values of

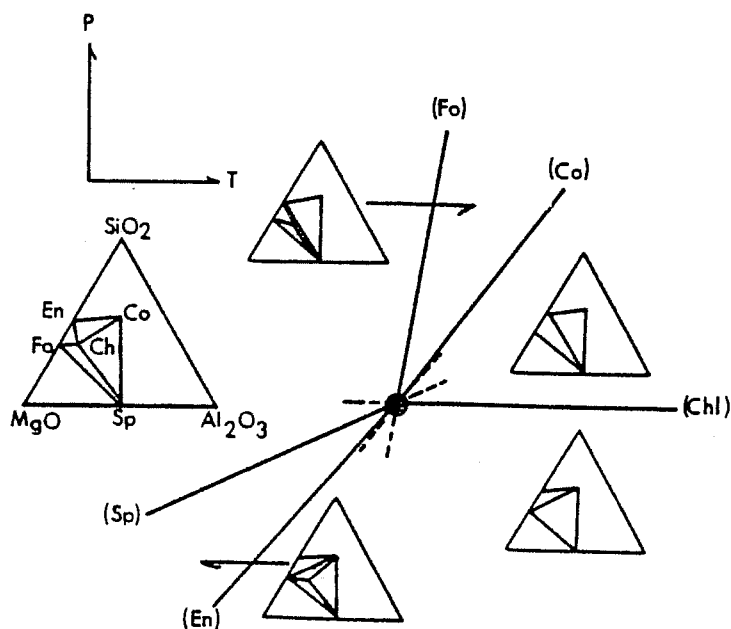


Figure 44. Chemographic relations among forsterite, cordierite, enstatite, spinel, clinocllore, and vapor in the system  $\text{MgO}-\text{Al}_2\text{O}_3-\text{SiO}_2-\text{H}_2\text{O}$ . The coordinates of the invariant point are 3.35kb, 765°C (Fawcett & Yoder, 1966).

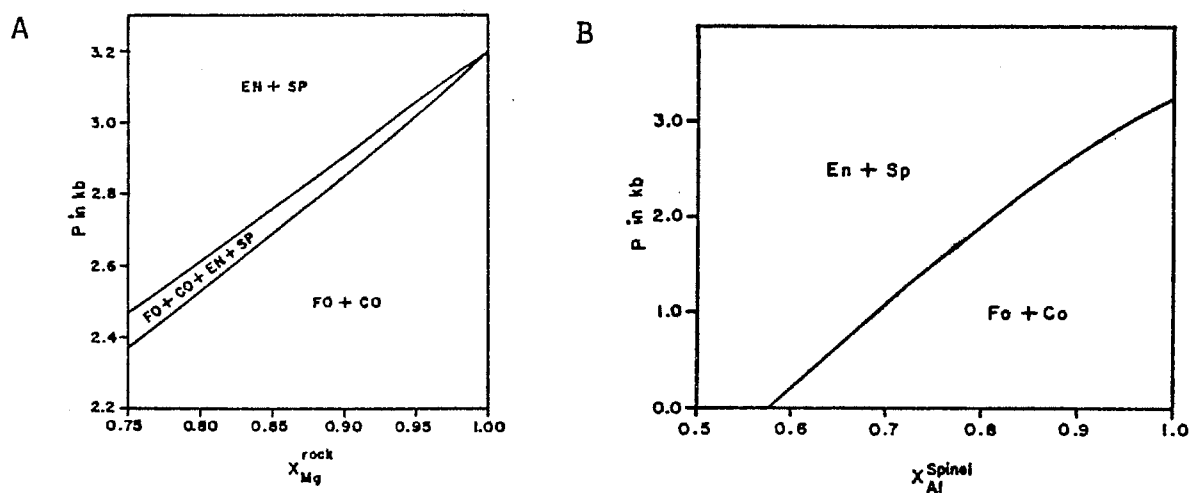


Figure 45. Effects on the reaction: 5 forsterite + cordierite = 10 enstatite + 2 spinel by:

- A. substitution for Mg.
- B. substitution of Cr for Al.

Both diagrams calculated by Frost (1975) for 730°C.

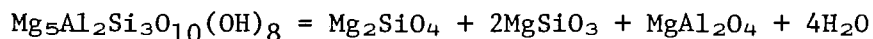
coexisting chlorite, orthopyroxene, olivine, and spinel in a metamorphic contact aureole (Frost, 1975, Figure 5), and equilibrium data amassed from various sources included Zen (1972), Chernosky (1973), and Robie and Waldbaum (1968).

Figure 45 is included to illustrate the sensitivity of the reaction:



to composition. Substitution of Fe for Mg or Cr for Al would cause a sharp decrease in the pressure at which this reaction occurs, thus making it less useful as a lower pressure-limiting reaction. Considering the compositions of the rocks of this study, this reaction probably could not occur above 2 kb.

Figure 46 is modified from Frost (1975, p. 306) to accommodate the chlorite, orthopyroxene, olivine and spinel compositions from this study, and to show the effects imposed by the condition,  $a_{\text{H}_2\text{O}} < 1$ . Frost's original diagram was based upon compositions of phases in a blackwall rock in which it was reasonable to approximate the bulk chemistry with that of a rock composed entirely of chlorite and/or its breakdown products. The compositions of rocks of the present study, however, do not fall into this category, as reflected by their high percentage of pargasite. If, however,  $X_{\text{Mg}}$  ( $X_{\text{Mg}} = \frac{\text{Mg}}{\text{Mg}+\text{Fe}+\text{Mn}}$ ) is calculated strictly upon the exact proportions of breakdown products according to the reaction:



then Figure 46 can be applied to roughly estimate the relative reduction in breakdown temperature associated with a given amount of iron in the chlorite. It can be seen that iron substitution causes a considerable reduction in breakdown temperature at a given pressure, and that a divariant field of stable coexistence of chlorite and breakdown products expands with increasing iron content. Thus, the likelihood of occurrence of this assemblage increases as iron is introduced into the system. Assuming that

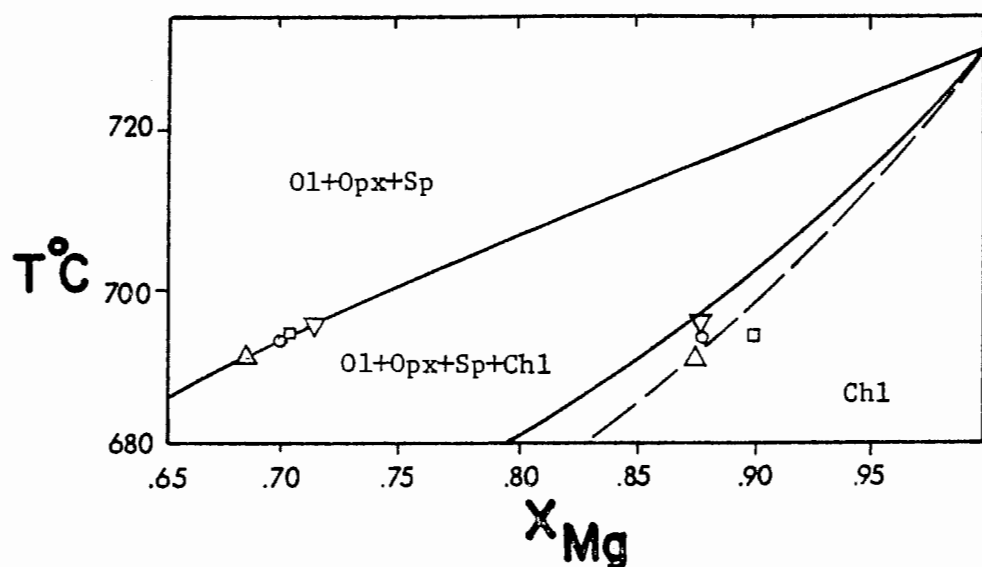


Figure 46. Temperature-composition diagram illustrating the relationship between iron content and breakdown temperature of chlorite according to the reaction:  $\text{Chl} = \text{Ol} + \text{Opx} + \text{Sp} + 4\text{H}_2\text{O}$ . Solid curves were calculated by Frost (1975) for a rock composed entirely of chlorite or its breakdown products at 3kb. Upper curve is the weighted mean composition of  $\text{Opx} + \text{Ol} + \text{Sp}$  (Appendix 2); lower curve is chlorite composition. Dashed curve shows displacement of the chlorite composition curve toward lower temperatures due to deviation from the pure system, as suggested by present data. Circles = Y57I, squares = 9Q9A, triangles = OG2B, inverted triangles = N45A.

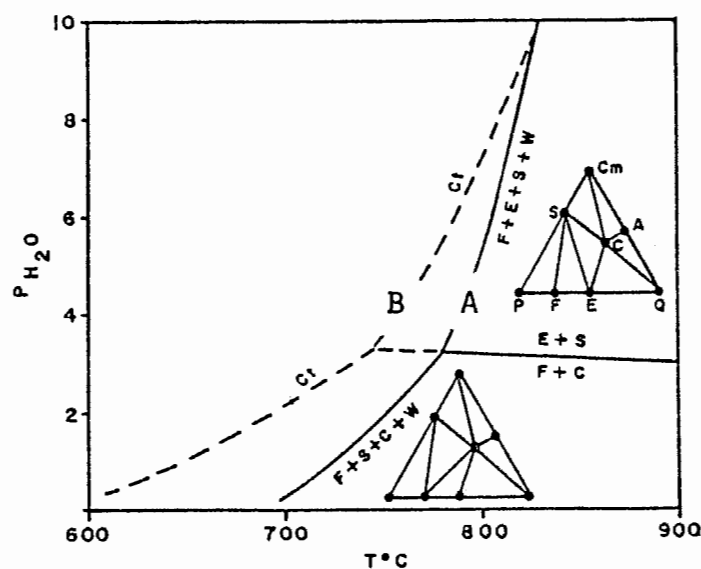


Figure 47. Breakdown of chlorite according to experimental work. Solid line indicates phase equilibria determined by Fawcett & Yoder (1966); dashed lines are derived from Chernosky (1973) and Zen (1972). Diagram is from Frost (1975).

equilibrium is maintained as the reaction proceeds, the maximum stable chlorite must contain iron and will break down at a temperature below that of its pure magnesian counterpart at a given pressure and  $a_{\text{H}_2\text{O}}$ . With increasing pressure, the position of the divariant field would shift to higher temperatures. Changing pressure would most likely affect the shape and slope of the divariant field; however, if such changes are considered to be negligible over a pressure range of a few kilobars, then Figure 46 can be used to estimate the relative displacement of breakdown temperature associated with chlorite of a given Fe/Mg ratio, at 5kb.

If it is assumed for convenience that the  $X_{\text{Mg}}$  of a given chlorite is more sensitive to  $a_{\text{H}_2\text{O}}$  than the  $X_{\text{Mg}}$  of its breakdown products, then the position of the upper curve of Figure 46 will remain relatively constant with changes in  $a_{\text{H}_2\text{O}}$ . If, then, the  $X_{\text{Mg}}$  of each breakdown assemblage is plotted on the upper curve, the associated chlorites are seen to fall on the low-temperature side of the lower curve calculated by Frost for  $a_{\text{H}_2\text{O}}=1$ . These are consistent with increased fractionation at lower temperature induced by lower  $a_{\text{H}_2\text{O}}$ . The maximum breakdown temperatures of chlorites plotted in Figure 46 are 35 - 45°C below their pure magnesian counterparts. Actual maximum temperatures can, therefore, be deduced from experimental or calculated Mg-chlorite breakdown curves.

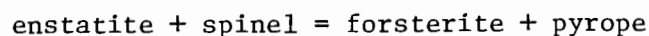
Figure 47 is a compilation of both experimentally and thermodynamically derived chlorite decomposition curves. Curve A is the most widely accepted experimentally derived univariant curve between 3 and 10 kb. Curve B has been calculated by Frost (1975) on the basis of thermodynamic data of Chernosky (1973) and Zen (1972). Frost's curve correlates well with the lower pressure experimental curve of Chernosky (1974). These curves show that at 5.5kb, Mg-chlorite would break down between 775 and 800°C.



Application of Figure 46 to account for iron content yielded a 35 - 45°C correction, as discussed. Thus, the maximum decomposition temperature of the chlorites in these bodies at  $a_{H_2O} = 1$  is between 730 and 765°C or about 100°C above the local temperature estimates based on garnet-biotite equilibria (Tracy, et al., 1976). The difference is attributed to an  $a_{H_2O}$  substantially below 1 within these bodies during peak regional metamorphism.

Aluminum content of orthopyroxene. Recent methods for estimating physical conditions of formation from the alumina content of orthopyroxene in spinel peridotite may be applied to the ultramafic rocks of the current study because of the stable coexistence of orthopyroxene, olivine, and spinel. Contradictory data, specifically with regard to the pressure sensitivity of this parameter, have recently been published. Pressure sensitive isopleths (at temperatures below 1000°C) derived from experimental data of MacGregor (1974), do not agree with the low pressure curves of Anastasiou and Seifert (1972) and are in direct conflict with calculated curves of Obata (1976). Obata's figures correspond with data of Anastasiou and Seifert and indicate that, below 1000°C, solubility of  $Al_2O_3$  in orthopyroxene coexisting with olivine and spinel is insensitive to pressure.

The upper pressure limit of the spinel-bearing assemblage in the Si-Al-Mg system is defined by the reaction:



The location and shape of this curve has been refined by high-pressure experimental data of Fujii (1976) and Danckwerth and Newton (1978). Both studies considered the locations and slopes of Al isopleths and also found them to be insensitive to pressure at low temperatures. The calculated isopleths of Danckwerth and Newton are displaced about 40-50°C below those of Obata (1976) and Fujii (1976).

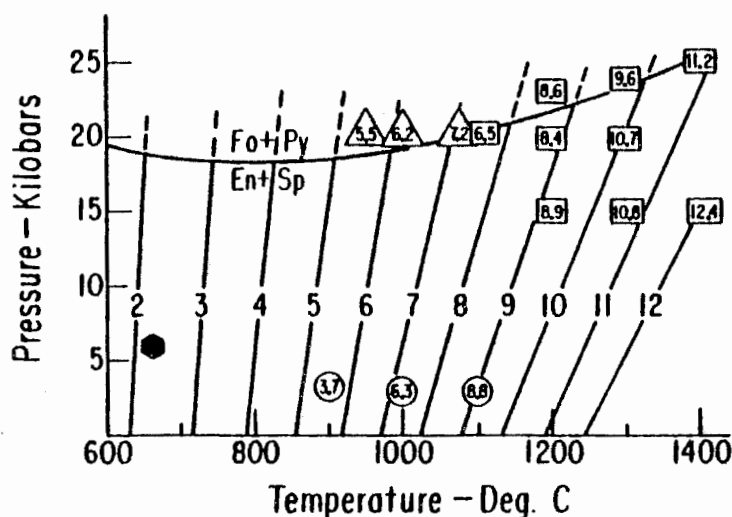


Figure 48. Calculated  $\text{Al}_2\text{O}_3$  isopleths of enstatite in weight %, in the presence of forsterite plus spinel. Figure is from Danckwerth and Newton (1978, Fig. 7, p 197). Triangles are experimental data of Danckwerth and Newton, rectangles are from Fujii (1976), and circles are from Anastasiou and Seifert (1972). The pyroxenes of the present study range from 2.17-2.27 weight %  $\text{Al}_2\text{O}_3$  and all plot within the solid hexagon.

Applying Danckwerth and Newton's curves to pyroxenes of the present study shows them to fall at about  $650^\circ\text{C}$  for a pressure just above 5 kb (Figure 48). Correction, however, for the composition of the natural assemblage as compared to the ternary  $\text{MgO}-\text{Al}_2\text{O}_3-\text{SiO}_2$  system, will cause a shift in temperature.

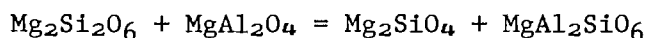
Danckwerth and Newton (1978) indicate that the equilibrium constant:

$$K = \frac{(X_{\text{Mg}})_{\text{Sp}} (X_{\text{Al}})_{\text{Sp}}^2 (X_{\text{Mg}}^{\text{M}})_{\text{En}}}{(X_{\text{Mg}})_{\text{Ol}}^2 (X_{\text{Al}}^{\text{M}})_{\text{En}}}$$

might be used to estimate the direction and magnitude of the temperature correction by assuming that additional components such as  $\text{FeO}$  and  $\text{Cr}_2\text{O}_3$  will be favored in spinel. This will effectively lower the value of  $K$  by reducing  $(X_{\text{Mg}})_{\text{Sp}}$  and  $(X_{\text{Al}})_{\text{Sp}}^2$ . According to Stroh (1976), the relative value

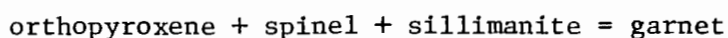
of K should be inversely proportional to temperature so that the correction applied to the pyroxenes in question would be toward higher temperature. Danckwerth and Newton (1978) caution against employment of Al content of orthopyroxene as a geothermometer unless it is in equilibrium with a spinel with a high molar content of  $\text{MgAl}_2\text{O}_4$ .

One further consideration is the fact that the isopleths of Obata (1976), Fujii (1976), and Danckwerth and Newton (1978) are all calculated assuming ideal solution by the reaction:



which requires that one half of the Al atoms be assigned to the  $M_1$  site. Structural formulae of the pyroxenes of this study, however, show that Al favors the tetrahedral position. A similar tendency was noted by Stroh (1976) for alpine-type peridotites (Figure 4, p. 181). Thus, this natural system is even further removed from the experimental situation, which should introduce additional uncertainty in determination of temperature by this method. In spite of these uncertainties, the temperature of  $650^\circ\text{C}$  is reasonably consistent with the temperatures reported by Tracy *et al.*, (1976) which were based on garnet-biotite equilibria.

Hypothetical application of garnet composition to estimate minimum pressure. The garnet in K34A is weakly zoned, with cores (pyrope = .383) slightly more magnesian than the rims (pyrope = .361) (Table 23). The reaction that produced the garnet is not obvious from the present assemblage. The garnet may have been produced at lower grade in some chlorite-rich assemblage and may now be on its way out by some continuous reaction such that pargasite and garnet react to produce anthophyllite and plagioclase. The composition of this garnet might be used to evaluate minimum pressure conditions by considering the hypothetical continuous Fe/Mg reaction:



by which such a garnet would begin to break down to its anhydrous products as illustrated in Figure 49. At a given temperature such a garnet would coexist with its breakdown products at only one pressure. More iron-rich garnets could exist in other assemblages at the same pressure whereas more magnesium-rich could not be stable at all. Thus, when appropriate garnet P-T isopleths for this reaction are determined or calculated, the garnet at K34A can be used as an indicator of minimum pressure for any temperature.

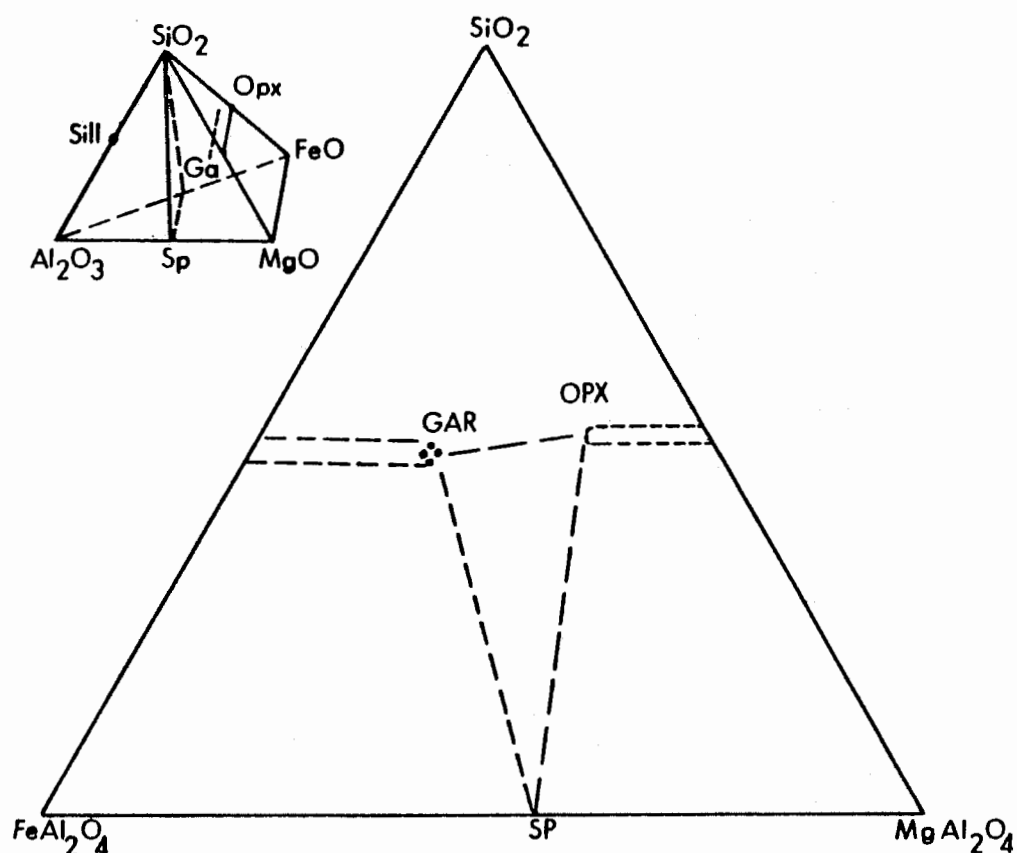


Figure 49. Projection from sillimanite onto the  $\text{SiO}_2\text{-MgAl}_2\text{O}_4\text{-FeAl}_2\text{O}_4$  plane of the  $\text{SiO}_2\text{-Al}_2\text{O}_3\text{-MgO-FeO}$  tetrahedron showing the hypothetical reaction:  $\text{Gar} = \text{Opx} + \text{Sp} + \text{Sill}$ .

## SUMMARY

Following is a list of major points covered in this study:

1. Maps have been constructed of 12 ultramafic bodies which occur within the Middle Ordovician Partridge Formation in central Massachusetts. The primary metamorphic assemblage is pargasite-orthopyroxene-olivine-spinel-chlorite-ilmenite.
2. The margins of some lenses have been chemically altered following emplacement but prior to peak regional, Devonian metamorphism; probably by metasomatic processes. Anthophyllite- or cummingtonite-plagioclase-hornblende assemblages characterize these hybridized rocks.
3. Secondary chlorite, talc, and carbonate were formed in many of the lenses by retrograde metamorphism.
4. Bulk chemical compositions have been calculated by two methods and are reasonably comparable with X-ray fluorescence analyses of the same samples. Some of these rocks are chemically similar to Archean peridotitic komatiites and to minor portions of metasomatized margins of serpentinites that were thermally metamorphosed following metasomatism.
5. Regional setting is probably most comparable with Newfoundland melange deposits into which "drop stones" were deposited from overriding ultramafic masses. A source nappe however, is missing from the regional setting in central Massachusetts.
6. Temperature of metamorphism has been estimated to be 730 - 765°C on the basis of the reaction, chlorite = orthopyroxene + olivine + spinel + 4H<sub>2</sub>O, and to be 650°C based upon the Al<sub>2</sub>O<sub>3</sub> content of orthopyroxene coexisting with

olivine and spinel. Other workers have made estimates of 605-675°C on the basis of assemblages in pelitic schists in the region. The high temperature estimated from the chlorite reaction is believed to be a function of  $a_{\text{H}_2\text{O}}$  being less than unity in the natural assemblage.

7. No estimate of pressure could be made from recently available data; however, a method is proposed by which garnet in ultramafic rock K34A could be used to estimate minimum pressure, should Fe/Mg isopleths become available for the appropriate equilibrium.

## REFERENCES

- ANASTASIOU, P. AND F. SEIFERT (1972) Solid solubility of  $\text{Al}_2\text{O}_3$  in enstatite at high temperatures and 1-5 kb water pressure. Contrib. Mineral. Petrol., 34, 272-287.
- ARNDT, N. T., A. J. NALDRETT, AND D. R. PYKE (1977) Komatiitic and iron-rich tholeiitic lavas of Munro Township, Northeast Ontario. J. Petrol. 18, 319-369.
- ASHWAL, L.D. (1974) Metamorphic Hydration of Augite-Orthopyroxene Monzodiorite to Hornblende Granodiorite Gneiss, Belchertown Batholith, West-Central Massachusetts. M.S. Thesis, University of Massachusetts, Amherst, Mass., 117 p.
- BENCE, A. E. AND A. L. ALBEE (1968) Empirical correction factors for the electron microanalysis of silicates and oxides. J. Geol., 76, 382-403.
- BERG, J. H. (1976) Metamorphosed mafic and ultramafic rocks in the contact aureoles of the Nain Complex, Labrador, and the miscibility gap between spinel and magnetite in natural  $\text{Cr-Al-Fe}^{3+}\text{-Ti}$  spinels. Geol. Soc. Am., Abstracts with Programs for 1976, 773-774.
- BILLINGS, M. P. (1956) The Geology of New Hampshire, Part II - Bedrock Geology. New Hampshire State Planning and Development Commission, 200 p.
- BØGGILD, O. B. (1905) Mineralogia Groenlandica. Medd. Gronland, 32, 400.
- BROOKS, C., AND S. R. HART (1974) On the significance of komatiite. Geology, 2, 107-110.
- BROWN, G. E., AND C. T. PREWITT (1973) High-temperature crystal chemistry of hortonolite. Am. Mineral., 58, 577-587.
- BUDDINGTON, A. F. AND D. H. LINDSLEY (1964) Iron-titanium oxide minerals and synthetic equivalents. J. Petrol., 5, 310-357.
- CHAYES, FELIX (1956) Petrographic Modal Analysis. John Wiley and Sons, New York, 113 p.
- CHERNOSKY, J. V. (1973) The stability of clinocllore and the free energy of Mg-cordierite. Trans. Am. Geophys. Un. 54, 79.
- \_\_\_\_\_ (1974) The upper stability of clinocllore at low pressure and the free energy of formation of Mg-cordierite. Am. Mineral. 59, 496-507.
- CHIDESTER, A. H. AND W. M. CADY (1972) Origin and emplacement of alpine-type ultramafic rocks. Nature Physical Science 240, No. 98, 27-31.

- DANCKWERTH, P. A. AND R. C. NEWTON (1978) Experimental determination of the spinel peridotite to garnet peridotite reaction in the system  $\text{MgO-Al}_2\text{O}_3\text{-SiO}_2$  in the range  $900^\circ\text{--}1100^\circ\text{C}$  and  $\text{Al}_2\text{O}_3$  isopleths of enstatite in the spinel field. Contr. Mineral. Petrol. 66, 189-201.
- DEER, W. A., R. A. HOWIE, AND J. ZUSSMAN (1966) An Introduction to the Rock Forming Minerals. John Wiley and Sons, Inc., New York.
- FAWCETT, J. J. AND H. S. YODER, JR. (1966) Phase relationships of chlorites in the system  $\text{MgO-Al}_2\text{O}_3\text{-SiO}_2\text{-H}_2\text{O}$ . Am. Mineral. 51, 353-378.
- FRENCE, B. M. AND H. P. EUGSTER (1965) Experimental control of oxygen fugacities by graphite gas equilibria. J. Geophys. Res. 70, 1529-1539.
- FROST, B. R. (1975) Contact metamorphism of serpentinite, chloritic blackwall and rodingite at Paddy-Go-Easy Pass, Central Cascades, Washington. J. Petrol. 16, 272-313.
- FUJII, T. (1976) Solubility of  $\text{Al}_2\text{O}_3$  in enstatite coexisting with forsterite and spinel. Carnegie Inst. Wash. Yearbook 75, 566-571.
- GALE, G. H. (1973) Palaeozoic basaltic komatiite and ocean-floor basalts from northeastern Newfoundland. Earth Planet. Sci. Lett. 18, 22-28.
- GOLDING, H. G. AND P. BAYLISS (1968) Altered chrome ores from the Coolac serpentinite belt, New South Wales, Australia. Am. Mineral. 53, 162-183.
- IRVING, A. J. AND P. M. ASHLEY (1976) Amphibole-olivine-spinel, cordierite-anthophyllite and related hornfels associated with metamorphosed serpentinites in the Goobarragandra District, near Tumut, New South Wales. J. Geol. Soc. Australia 23, 19-43.
- MORSE, S. A. AND BERG, J. H. (1971) Petrographic Methods In: S. A. Morse, Ed., The Nain Anorthosite Project, Labrador: Field Report 1971. Contrib. No. 9, Geology Dept., University of Massachusetts, Amherst, 69-71.
- NAYLOR, R. S. (1968) Origin and regional relationships of the core-rocks of the Oliverian Domes. In: E-an Zen, W. S. White, J. B. Hadley and J. B. Thompson, Jr., Eds., Studies of Appalachian Geology: Northern and Maritime. John Wiley and Sons, New York. 231-240.
- \_\_\_\_\_, G. M. BOONE, E. L. BOUDETTE, D. D. ASHENDEN, AND PETER ROBINSON (1973) Pre-Ordovician rocks in the Bronson Hill and Boundary Mountain anticlinoria, New England, U.S.A. Am. Geophys. Union Trans. 54, 495.
- OBATA, MASAOKI (1976) The solubility of  $\text{Al}_2\text{O}_3$  in orthopyroxenes in spinel and plagioclase peridotites and spinel pyroxenite. Am. Mineral. 61, 804-816.
- ROBIE, R. A. AND D. R. WALDBAUM (1968) Thermodynamic properties of minerals and related substances at 298.15 K (25.0 C) and one atmosphere (1.013 bars) pressure and higher temperatures. Bull. U.S. Geol. Surv. 1259.



- ROBINSON, PETER (1963) Gneiss domes of the Orange area, Mass. and N. H. Ph.D. thesis, Harvard University. 253 p.
- \_\_\_\_ (1967a) Gneiss domes and recumbent folds of the Orange area, west-central Massachusetts. In: New England Intercollegiate Geological Conference, 59th Ann. Mtg., Guidebook, 17-47.
- \_\_\_\_ (1967b) Geology of the Quabbin Reservoir area, central Massachusetts. In: New England Intercollegiate Geological Conference, 59th Ann. Mtg., Guidebook, 114-127.
- \_\_\_\_, H. W. JAFFE, AND P. W. WEIBLEN (1968) Exsolution in clinoamphiboles. Science 159, 1099.
- \_\_\_\_ AND H. W. JAFFE (1969) Chemographic exploration of amphibole assemblages from central Massachusetts and southwestern New Hampshire. Mineral. Soc. Am. Spec. Pap. 2, 251-274.
- \_\_\_\_, MALCOLM ROSS, AND H. W. JAFFE (1971) Composition of the anthophyllite-gedrite series, comparisons of gedrite and hornblende, and the anthophyllite-gedrite solvus. Am. Mineral. 56, 1005-1041.
- \_\_\_\_, R. J. TRACY, AND L. D. ASHWAL (1975) Relict sillimanite-orthoclase assemblage in kyanite-muscovite schist, Pelham dome, west-central Massachusetts. Trans. Am. Geophys. Union 56, 466.
- ROSS, MALCOLM, J. J. PAPIKE, AND K. W. SHAW (1969) Exsolution textures in amphiboles as indicators of subsolidus thermal histories. Mineral. Soc. Am. Spec. Pap. 2, 275-299.
- SAXENA, S. K. (1969) Silicate solid solutions and geothermometry; 2, distribution of  $\text{Fe}^{2+}$  and  $\text{Mg}^{2+}$  between coexisting olivine and pyroxene. Contrib. Mineral. and Petrol. 22, 147-156.
- SMITH, J. V. (1974) Feldspar Minerals Vol. 2. Springer Verlag, Berlin.
- SPRINGER, R. K. (1974) Contact metamorphosed ultramafic rocks in the western Sierra Nevada foothills, California. J. Petrol. 15, 160-195.
- STAUDIGEL, HUBERT AND WERNER SCHREYER (1977) The upper thermal stability of clinocllore,  $\text{Mg}_5\text{Al}(\text{AlSi}_3\text{O}_{10})(\text{OH})_8$ , at 10-35 kb  $\text{pH}_2\text{O}$ . Contrib. Mineral. Petrol. 61, 187-198.
- STROH, J. M. (1976) Solubility of alumina in orthopyroxene plus spinel as a geobarometer in complex systems. Applications to spinel-bearing alpine-type peridotites. Contrib. Mineral. Petrol. 54, 173-188.
- TAYLOR, L. A. (1969) Low temperature phase relations in the Fe-S system. Carnegie Inst. Wash. Yearbook 68, 259-270.
- THOMPSON, J. B., Jr., PETER ROBINSON, T. N. CLIFFORD, AND N. J. TRASK, Jr. (1968) Nappes and gneiss domes in west-central New England. In: E-an Zen, W. S. White, J. B. Hadley, and J. B. Thompson, Jr., Eds., Studies of Appalachian Geology: Northern and Maritime. John Wiley and Sons, New York. 811-838.

- TRACY, R. J. (1975) High Grade Metamorphic Reactions and Partial Melting in Pelitic Schist, Quabbin Reservoir Area, Massachusetts. Ph.D. Thesis, Contribution No. 20, Geology Dept., University of Massachusetts, Amherst, 127 p.
- \_\_\_\_\_, PETER ROBINSON, AND A. B. THOMPSON (1976) Garnet composition and zoning in the determination of temperature and pressure of metamorphism, central Massachusetts. Am. Mineral. 61, 762-775.
- TURNOCK, A. C. (1960) The stability of iron chlorites. Carnegie Inst. Wash. Yearbook 59, 98-103.
- UYTENBOGAARDT, W. AND E. A. J. BURKE (1971) Tables for Microscopic Identification of Ore Minerals. Elsevier Publishing Co., Amsterdam, 430 p.
- VILJOEN, M. J. AND R. P. VILJOEN (1969a) The geology and geochemistry of the lower ultramafic unit of the Onverwacht Group and a proposed new class of igneous rock. Upper Mantle Project. Spec. Publs. Geol. Soc. S. Afr. 2, 221-244.
- \_\_\_\_\_. (1969b) Evidence for the existence of a mobile extrusive peridotite magma from the komate formation of Onverwacht Group. Geol. Soc. S. Afr. Spec. Pub. 2, Upper Mantle Project, 87-112.
- WILLIAMS, HAROLD AND W. R. SMYTH (1973) Metamorphic aureoles beneath ophiolite suites and Alpine peridotites: tectonic implications with west Newfoundland examples. Am. J. Sci. 273, 594-621.
- ZEN, E-An (1972) Gibbs free energy, enthalpy, and entropy of ten rock-forming minerals; calculations, discrepancies, implications. Am. Mineral. 57, 524-553.

## APPENDIX 1

Bulk chemical compositions of selected samples were established through X-ray techniques and calculations based on modal and electron microprobe analyses (Table A-1). Two methods of calculation were employed; each serving as a check upon the other. Both methods are extremely simplified and should be regarded only as approximations.

The first method is based upon the ideal number of oxygen atoms per formula. The assumption is made that the volume of each phase is proportional to the number of oxygens in its formula, thus establishing a relationship between modal and microprobe analyses. This will be referred to as the oxygen-volume method. To begin with, each cation in the formula of a given mineral is multiplied by a factor equal to the modal abundance of that mineral divided by its total number of oxygens. When this operation is completed for every mineral, addition proceeds as follows: Adjusted Si values from all minerals are added together and the sum is listed. Similarly, all other adjusted cations are separately added and listed. These individual totals show the contribution of each cation to the total chemistry of the rock. These adjusted cations are then listed as oxides, being sure to first divide the monovalent and trivalent ions by two. Each oxide is then multiplied by its molecular weight and products are listed. The total of all of these products is divided into each individual product and the answer is multiplied by 100, yielding the weight percent of each oxide.  $\text{H}_2\text{O}$  is calculated on the ideal  $\text{H}^+$  contents of the hydrous phases.

The second method involves the use of the densities, electron microprobe analyses, and modal analysis of each phase. The modal percent of each phase is multiplied by the density of that phase (Deer, Howie, and Zussman, 1966),

Table A-1. Whole rock chemistries as determined by calculated and X-ray fluorescence techniques.

Orthopyroxene-Olivine Hornblendites												Hybrid Rock		
Y57I			Y57E	909A			OG2B		N45A		K34A			
OXY	DEN	XRF	XRF	OXY	DEN	XRF	OXY	DEN	OXY	DEN	OXY	DEN	XRF	
SiO <sub>2</sub>	42.47	42.43	43.49	45.07	41.54	42.33	42.36	43.98	43.86	46.08	45.86	46.15	45.70	45.65
TiO <sub>2</sub>	1.34	1.42	.51	.70	1.10	1.17	.96	1.45	1.72	1.28	1.30	.86	.87	.93
Al <sub>2</sub> O <sub>3</sub>	12.05	12.25	11.88	12.70	7.59	7.71	10.00	12.58	12.82	10.70	10.75	13.72	13.60	14.07
Cr <sub>2</sub> O <sub>3</sub>	.21	.22			.33	.35		.20	.20	.33	.35	.01	.03	
Fe <sub>2</sub> O <sub>3</sub>			13.29	11.98			12.80	1.43	1.45					12.79
FeO	10.96	11.16	(11.96)	(10.78)	12.90	12.82	(11.52)	10.59	10.80	11.43	11.56	12.27	12.13	(11.51)
MnO	.17	.17	.20	.21	.17	.17	.21	.16	.17	.17	.17	.08	.11	.20
NiO								.04	.01					
MgO	21.66	21.69	23.11	18.14	28.44	27.69	25.39	19.52	19.63	21.43	21.43	15.83	15.61	15.19
CaO	7.19	7.13	7.22	9.60	4.74	4.68	5.52	7.36	7.20	6.39	6.17	7.50	7.39	8.52
Na <sub>2</sub> O	.95	.95	(.95)	"1.00" <sup>+</sup>	.26	.25	(.26)	1.00	.98	.73	.70	1.20	1.18	(1.20)
K <sub>2</sub> O	.14	.14	.14	.18	.03	.03	.07	.12	.12	.12	.12	.27	.27	.34
H <sub>2</sub> O	2.85				2.91			1.55		1.35		2.10		
P <sub>2</sub> O <sub>5</sub>			.09	.09			.14	.03						.16
Total	99.99	97.56	100.88	99.67	100.01	97.15	97.72	100.01	98.96	100.01	98.41	99.99	96.89	99.05

OXY = Oxygen-volume method.

DEN = Density method.

XRF = X-ray fluorescence analyses; Michael Rhodes, University of Massachusetts, analyst.

\* = Calculated by oxygen-volume method.

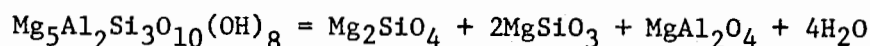
+ = Estimated.

yielding a factor which is in units of mass. The weight percent of each oxide of a phase as determined by microprobe analysis is then multiplied by this factor. This is done for all phases and then each oxide is totaled.

Actual chemical analyses were run by X-ray fluorescence. Sodium was not analyzed. The calculated value is listed for summation purposes. Iron was analyzed as  $\text{Fe}_2\text{O}_3$ ; however, iron calculated as  $\text{FeO}$  is shown in parentheses (not included in the total). These analyses are on an anhydrous basis.

## APPENDIX 2

The combined  $X_{\text{Mg}}$  of olivine, orthopyroxene, and spinel in equilibrium with chlorite is calculated from the  $X_{\text{Mg}}$  of each phase (Tables 17, 18, 19) and weighted in the proper proportions to make chlorite according to the reaction:

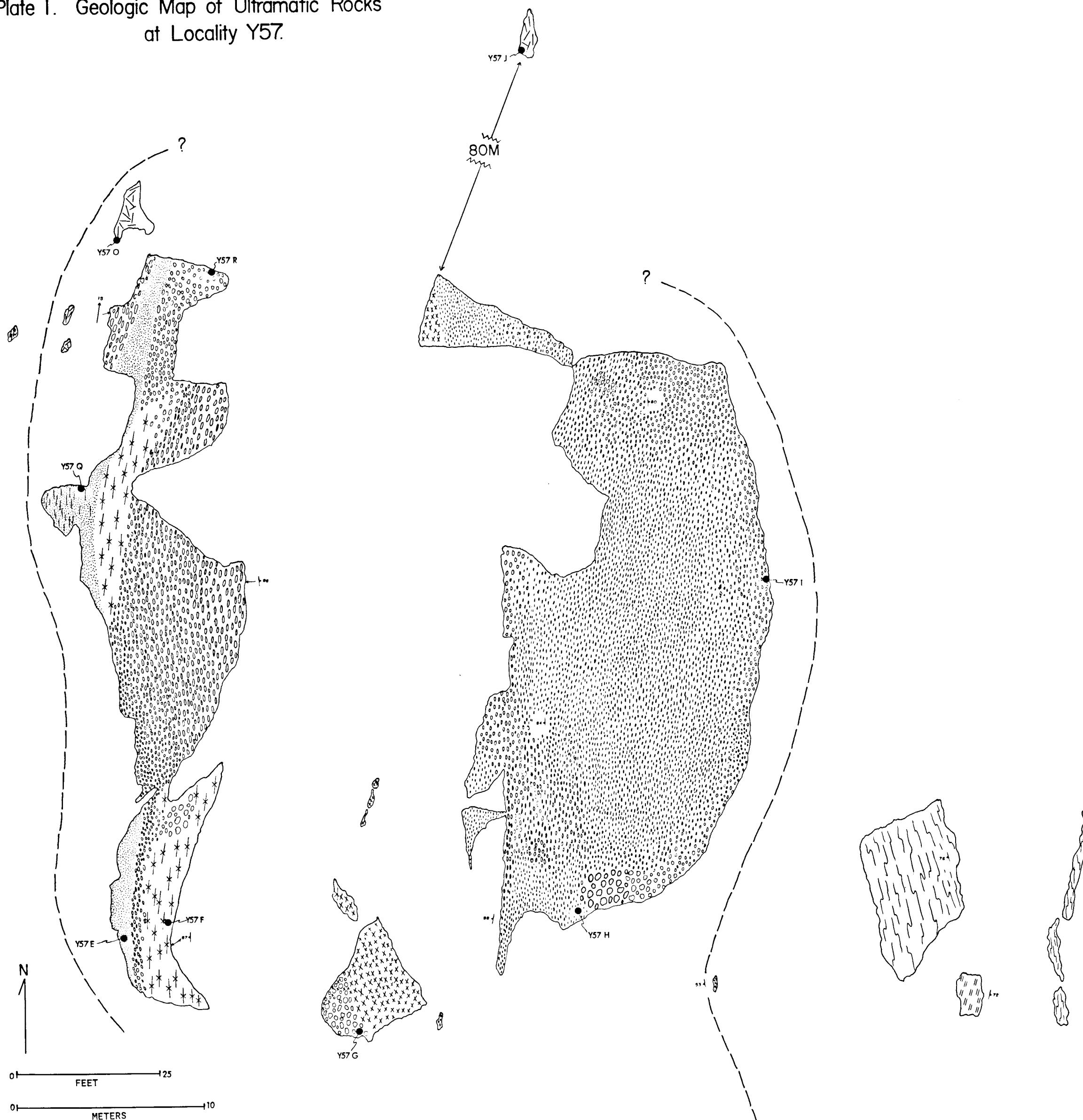


Calculations are shown in Table A-2.





Table A-2

	Y57I	9Q9A	OG2B	N45A
	$X_{\text{Mg}}$	$X_{\text{Mg}}$	$X_{\text{Mg}}$	$X_{\text{Mg}}$
Ol	.711 x 2=1.422	.754 x 2=1.508	.709 x 2=1.418	.747 x 2=1.494
Opx	.769 x 2=1.538	.789 x 2=1.578	.745 x 2=1.490	.777 x 2=1.554
Sp	.547 x 1= .547	.440 x 1= .440	.524 x 1= .524	.507 x 1= .507
Total	3.507	3.526	3.432	3.555
$X_{\text{Mg}}$ (Total/5)	.701	.705	.686	.711

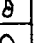
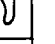
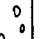
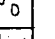
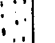
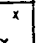
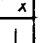
Plate 1. Geologic Map of Ultramafic Rocks  
at Locality Y57.





HYBRIDIZED ROCKS: Related to metasomatism or vein filling.




	Surface characterized by broken rind of coarse hornblende related to late vein filling.
	Well-foliated, medium-grained, phlogopite-talc-chlorite-hornblende schist.
	Fine-grained hornblende with a weak lineation defined by cummingtonite.
	Medium-grained hornblende characterized by randomly oriented anthophyllite needles.

**METAMORPHOSED ULTRAMAFIC ROCKS:** Include both primary prograde orthopyroxene-olivine hornblende (with spinel, chlorite, and ilmenite) and rocks affected by extensive retrograde hydration and carbonation.

	<p>Pitted coarse nodules composed of orthopyroxene and olivine.</p>
	<p>Coarse nodules of various sizes up to 2.5cm. Commonly characterized by extensive hydration and carbonation.</p>
	<p>Flat nodules of various sizes; if pink, they are orthopyroxene megacrysts; if brown or tan, they are retrograded and composed of carbonate, chlorite and talc.</p>
	<p>Surface characterized by pits of various sizes. Secondary pale green chlorite is the most common retrograde product.</p>
	<p>Medium-grained, dark-gray, massive orthopyroxene-olivine hornblende.</p>
	<p>Medium-grained, moderately foliated, orthopyroxene-olivine hornblende.</p>
	<p>Fine-grained, massive orthopyroxene-olivine hornblende.</p>

PARTRIDGE FORMATION: Sulfidic schist member.

	Rusty weathering, sillimanite-bearing sulfidic schist.
	Foliated, hornblende-plagioclase amphibolite.

-  Inferred contact.  
 Strike and dip of foliation.  
 Trend and plunge of mineral lineation.  
Y57 E  Specimen locality.

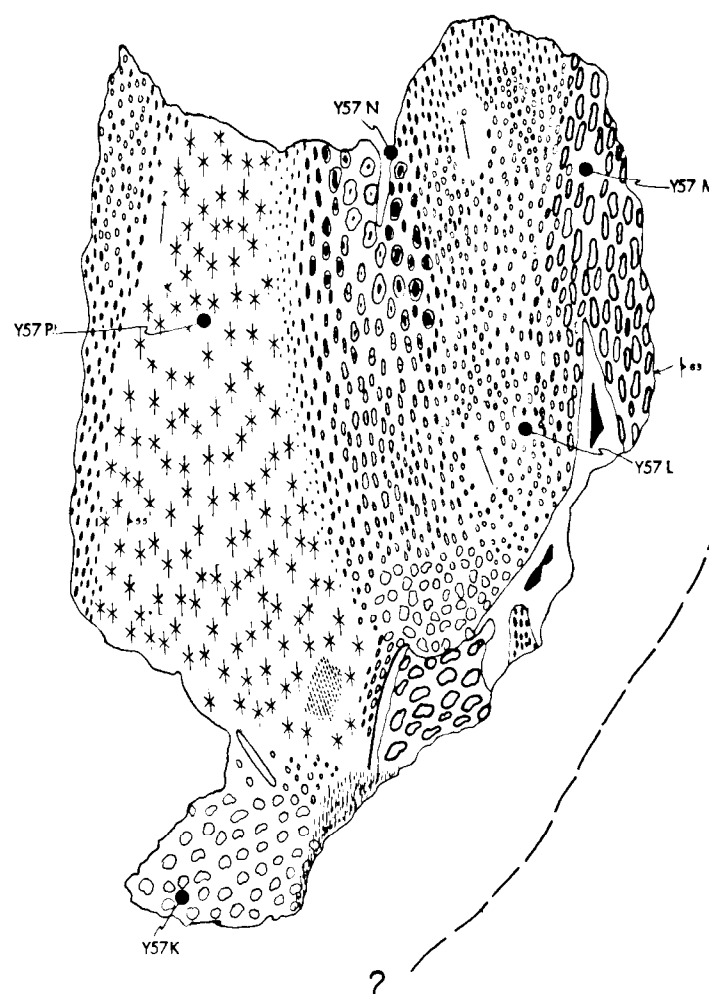


# Plate 2. Geologic Map of Ultramafic Rocks at Locality O18.

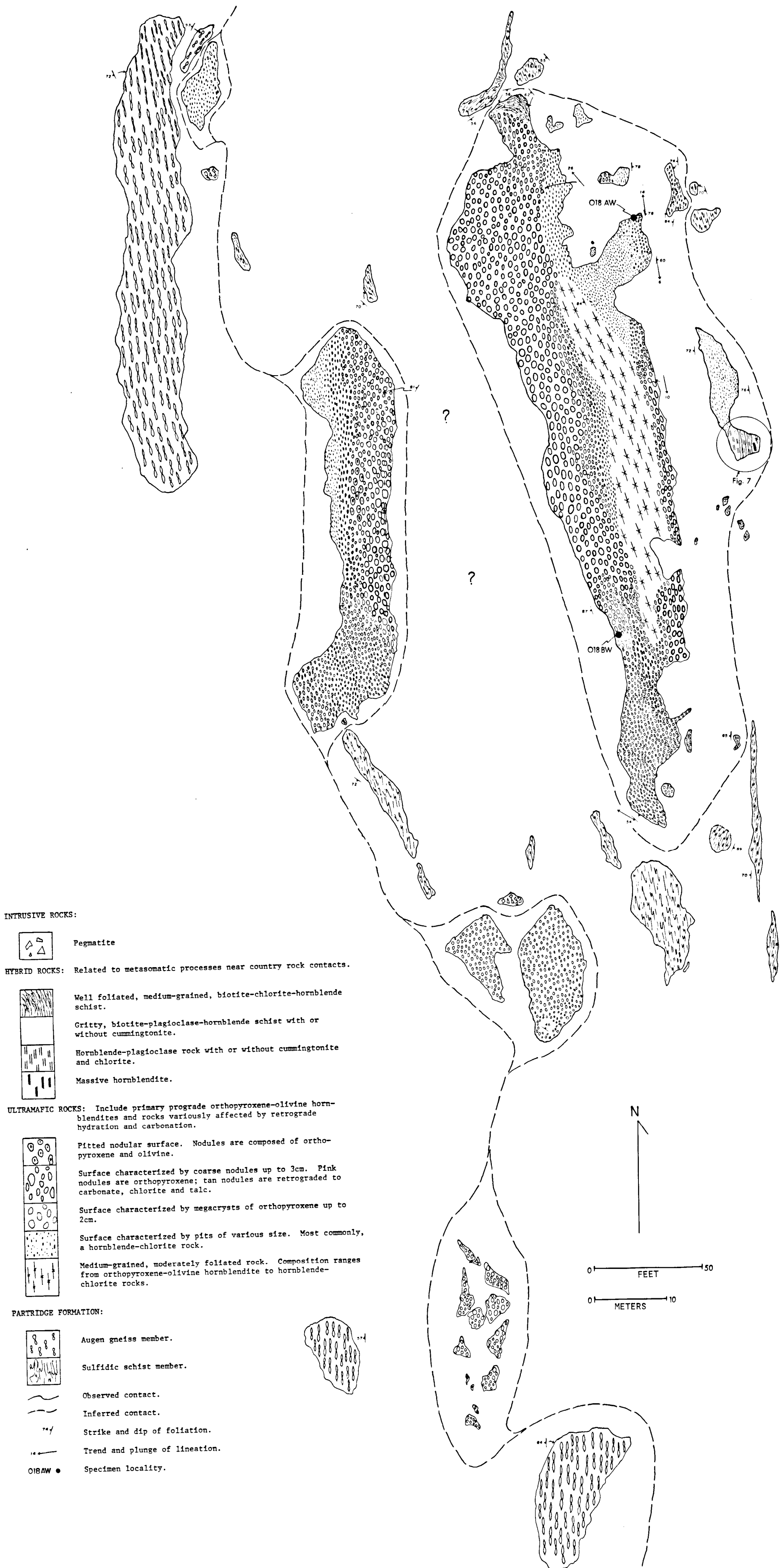
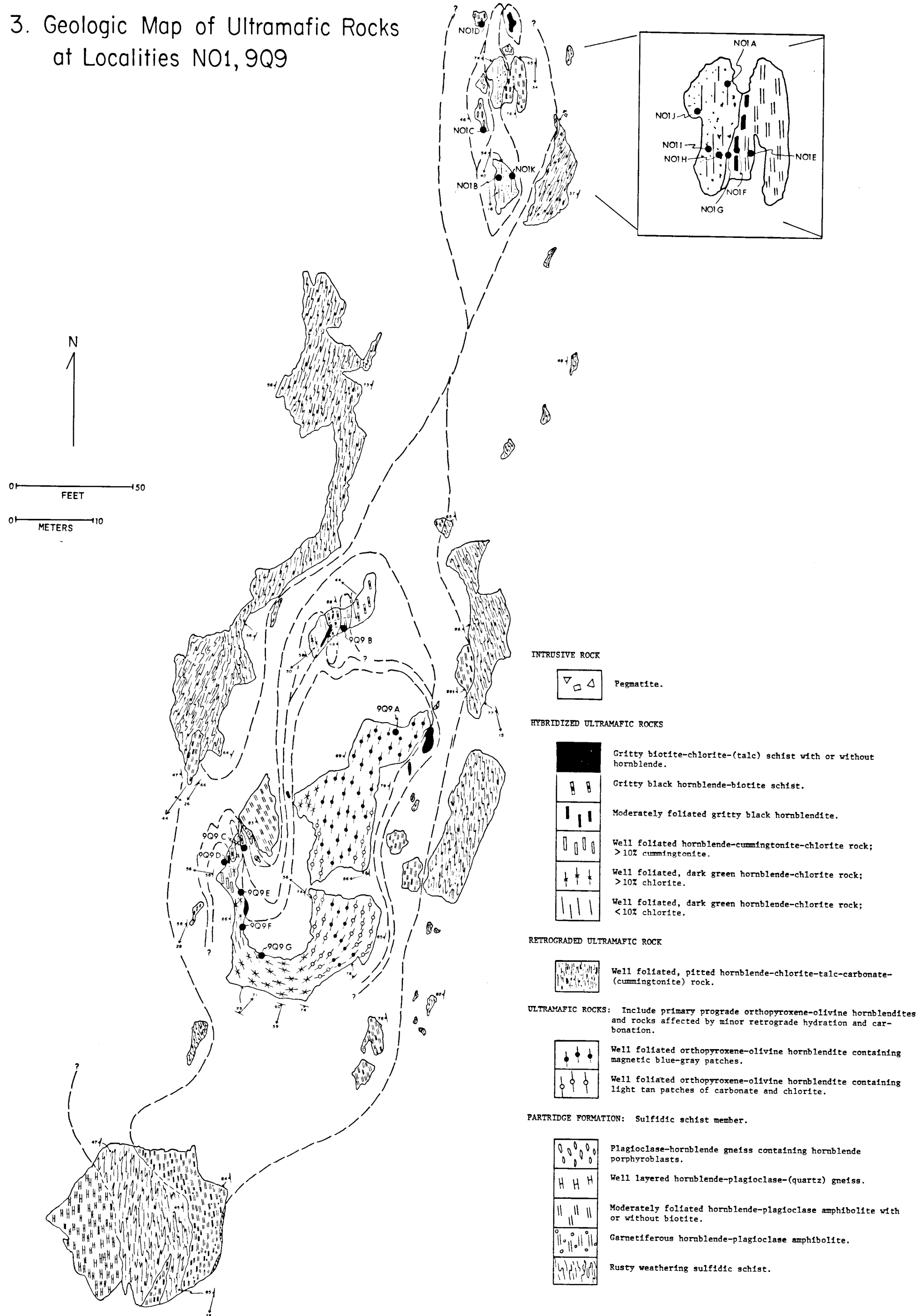


Plate 3. Geologic Map of Ultramafic Rocks at Localities NO1, 9Q9

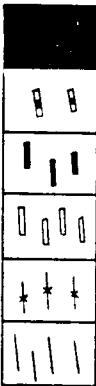


INTRUSIVE ROCK



Pegmatite.

HYBRIDIZED ULTRAMAFIC ROCKS



Gritty biotite-chlorite-(talc) schist with or without hornblende.  
Gritty black hornblende-biotite schist.  
Moderately foliated gritty black hornblendite.  
Well foliated hornblende-cummingtonite-chlorite rock; >10% cummingtonite.  
Well foliated, dark green hornblende-chlorite rock; >10% chlorite.  
Well foliated, dark green hornblende-chlorite rock; <10% chlorite.

RETROGRADED ULTRAMAFIC ROCK



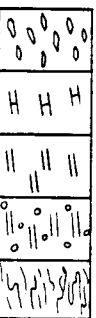
Well foliated, pitted hornblende-chlorite-talc-carbonate-(cummingtonite) rock.

ULTRAMAFIC ROCKS: Include primary prograde orthopyroxene-olivine hornblendites and rocks affected by minor retrograde hydration and carbonation.



Well foliated orthopyroxene-olivine hornblendite containing magnetic blue-gray patches.  
Well foliated orthopyroxene-olivine hornblendite containing light tan patches of carbonate and chlorite.

PARTRIDGE FORMATION: Sulfidic schist member.



Plagioclase-hornblende gneiss containing hornblende porphyroblasts.  
Well layered hornblende-plagioclase-(quartz) gneiss.  
Moderately foliated hornblende-plagioclase amphibolite with or without biotite.  
Garnetiferous hornblende-plagioclase amphibolite.  
Rusty weathering sulfidic schist.



